

Distribution Agreement

In presenting this thesis or dissertation as a partial fulfillment of the requirements for an advanced degree from Emory University, I hereby grant to Emory University and its agents the non-exclusive license to archive, make accessible, and display my thesis or dissertation in whole or in part in all forms of media, now or hereafter known, including display on the world wide web. I understand that I may select some access restrictions as part of the online submission of this thesis or dissertation. I retain all ownership rights to the copyright of the thesis or dissertation. I also retain the right to use in future works (such as articles or books) all or part of this thesis or dissertation.

Signature:

Alexandra Manta

Date

Econometrics Modeling with Multilayer and Induced Network Data

By

Alexandra Manta
Doctor of Philosophy
Economics

David T. Jacho-Chavez, Ph.D.
Advisor

Elena Pesavento, Ph.D.
Advisor

Weihua An, Ph.D.
Committee Member

Kim P. Huynh, Ph.D.
Committee Member

Accepted:

Kimberly Jacob Arriola, Ph.D., MPH
Dean of the James T. Laney School of Graduate Studies

Date

Econometrics Modeling with Multilayer and Induced Network Data

By

Alexandra Manta

M.A. in Economics, Emory University, 2021

B.A. in Economics, National and Kapodistrian University of Athens, 2017

Advisor:

David T. Jacho-Chavez, Ph.D.

Elena Pesavento, Ph.D.

An abstract of

A dissertation submitted to the Faculty of the
James T. Laney School of Graduate Studies of Emory University
in partial fulfillment of the requirements for the degree of
Doctor of Philosophy in Economics

2023

Abstract

Econometrics Modeling with Multilayer and Induced Network Data

By Alexandra Manta

Data abundance and complexity necessitate the identification of a system's operations mechanisms. In an economy, one of the most important driving forces of its mechanisms is related to economic entities interactions. The study of interactions can uncover multiple types of relationships and complicated patterns. Multilayer networks literature offers the mathematical and topological bases to represent interactions in network structures and evaluate their characteristics and diagnostics. On the other hand, Econometrics offers the flexibility to construct models able to incorporate networks and provide insights for causal inference.

Network connections can be utilized for inference when incorporated in economic models but they can also act as post-estimation instruments towards understanding estimated effects across entities and over time. Economic interactions are also dynamic and their evolution can be depicted in network formations. Network representations can reveal information such as the centrality of entities in the entire system, the entities' incoming and outgoing connections ratio, the distance and clustering among entities and the strength of the connections.

Economic crisis periods can be better diagnosed and possibly prevented with systemic risk monitoring. To evaluate risk transmission and study estimated spillover effects among economic entities, one can employ a network framework which can report on the economic situation. More specifically, on how shocks originating from the system's entities affect others and how these interactions have formulated the entire network.

The first chapter proposes the identification and estimation of social parameters, under a Multilayered Linear-in-Means model, when there are more than one types of social ties among economic agents. The second chapter replicates the code of an empirical paper and provides new findings using an extended version of the original dataset. The third chapter proposes the estimation of block specific spillover effects for credit risk monitoring.

Econometrics Modeling with Multilayer and Induced Network Data

By

Alexandra Manta

M.A. in Economics, Emory University, 2021

B.A. in Economics, National and Kapodistrian University of Athens, 2017

Advisor:

David T. Jacho-Chavez, Ph.D.

Elena Pesavento, Ph.D.

A dissertation submitted to the Faculty of the
James T. Laney School of Graduate Studies of Emory University
in partial fulfillment of the requirements for the degree of
Doctor of Philosophy in Economics
2023

Acknowledgements

Completing my dissertation would not have been the same without the guidance, mentoring, trust, and support I received from specific people. These people are mainly my advisors and mentors, my family and friends.

First, I would like to thank my advisors and committee members. Their contribution to my research progress and to me as a professional was of major significance.

Thank you to Professor Jacho for his academic advising and mentoring. He taught me the principles of professionalism, hard-work, dedication and how research is done. The fact that he was always there as a constant source of support and reference helped me complete my research tasks with confidence and made me a better researcher and professional overall. I am grateful to Professor Jacho for teaching me how important it is to ‘trust but verify’, deliver quality on-time and work in teams. It is with great pleasure and honor that I am at the position to say ‘thank you’ as a student under his supervision.

Thank you to Professor Pesavento for her academic dedication and guidance. Her knowledge and intuition on Time Series were very influential to my work and development as a researcher. She taught me how to communicate my ideas better, how fundamental it is to be able to view the bigger picture and, most importantly, how to approach and think about research ideas. I would also like to thank Professor Pesavento for all the times she was stepping in for help, being there available for me and being approachable. It is with great appreciation and delightfulness that I had the opportunity to be one of her students.

Thanks to Dr. Kim P. Huynh for his valuable guidance, suggestions, comments, and availability when his intuition was important. I learned how to think out of the box about research projects and how to be best prepared in interviews from him, which I appreciate a lot. Thanks to Professor Weihua An for his useful comments, suggestions and resources.

Secondly, I would like to express my gratitude to my family and my friends to whom I owe a lot for their continuous support, care, love and the work-life balance they helped me maintain.

A huge ‘thank you’ to one of my biggest supporters during my Ph.D., Thanos, my husband. Thank you for being there for me, supporting me, motivating me, believing in me. Your selfless advice and effective guidance helped me in each and every step of my Ph.D. studies.

Next, I would like to thank my parents Konstantinos and Anastasia, and my brother Dimitris. Mom and dad, thank you for your endless love and care during my graduate studies. Making you happy and proud of my accomplishments is my only way to repay you for everything

you have done for me. Dimitris, thank you for believing in me, this gave me strength to keep going. Many thanks to the rest members of my family, because the interaction with them helped me thrive, grow and achieve my professional goals.

Thanks to all my friends, supporters and mentors in the US and in Greece. Specifically, thanks to Professor Alexopoulos, his wife Alexandra and Professor Reveliotis for the fruitful discussions and all their care and support. Thanks to Jezamin, the wife of Professor Jacho for being approachable, giving me valuable professional advice, comments, tips based on her experience and for dedicating time to help me in my preparation for the job market.

Also, a huge thank you to my networks study group classmates: Juan, Pablo, Santiago, Linh and Diego. Thank you very much to each and every one of you for our discussions, the useful feedback we have given each other which helped us become better and the happy hour moments we have had fun! Thanks to all the rest Economics graduate students that entered between 2016 - 2022 for the ideas and thoughts we have exchanged. Thanks to the Economics Department staff for working on creating for us a friendly, unifying and bonding spirit through event organizing, resources and smiley faces.

Contents

1	Estimating Social Effects in a Multilayered Linear-in-Means Model with Network Data	1
1.1	Introduction	2
1.2	Identification	3
1.3	Estimation	4
1.4	Monte Carlo Experiments	7
1.5	Empirical Application	8
1.6	Appendix: Constrained Estimation	14
1.7	Appendix: Proofs of Main Results	15
1.8	Appendix: Auxiliary Results	18
1.9	Appendix: Monte Carlo Results	27
1.9.1	Supplementary Monte Carlo	38
1.10	Appendix: Empirical Application	39
1.10.1	Data Description	39
1.10.2	Supplementary Estimation Results	40
2	Risk Transmission across European entities using Networks: A Wide Replication of Gross and Siklos (2020)	47
2.1	Introduction	48
2.2	Replication Static results	49
2.3	Replication Dynamic results	74
2.4	Conclusion	86
3	Estimated spillover effects of block factors	87
3.1	Introduction	88
3.2	Motivation	90
3.3	Methodology	92

3.3.1	The Dynamic Hierarchical Factor Model (DHF M)	93
3.3.2	A Vector Autoregressive (VAR) model with block factors	96
3.4	Empirical Results	98
3.4.1	Full-sample Results	100
3.4.2	Sub-sample Results	122
3.5	Conclusion	144
3.6	Appendix: Assumed zero correlations under the DHFM	145

List of Figures

1.1	Monte Carlo Plots	13
1.2	Monte Carlo Box Plots in S1 with M1	30
1.3	Monte Carlo Q-Q Plots in S1 with M1	31
1.4	Monte Carlo Box Plots in S1 with M2	32
1.5	Monte Carlo Q-Q Plots in S1 with M2	33
1.6	Monte Carlo Box Plots in S2 with M1	34
1.7	Monte Carlo Q-Q Plots in S2 with M1	35
1.8	Monte Carlo Box Plots in S2 with M2	36
1.9	Monte Carlo Q-Q Plots in S2 with M2	37
1.10	Estimated Interactive Terms for Credit Card	44
1.11	Estimated Interactive Terms for Auto Loan	45
2.1	Hallin and Liska (2007) IC_2 criterion	54
2.2	Evolution of the common factor over the full-sample period ranging from October 23, 2006 up to May 19, 2022. The common factor is estimated using the Generalized dynamic factor model of Barigozzi and Hallin (2016)	58
2.3	Static Granger-causality cross-sectoral network connectedness	62
2.4	CDS network plot for the full-sample period (2006-2022) under forecast horizon $h = 10$	63
2.5	CDS network plot for the full-sample period (2006-2022) under forecast horizon $h = 5$	64
2.6	CDS network plot for the full-sample period (2006-2022) under forecast horizon $h = 15$	65
2.7	CDS network plot for the full-sample period (2006-2022) under forecast horizon $h = 20$	66

2.8	CDS network plot for the full-sample period (2006-2022) under forecast horizon $h = 10$ when imposing two common factors	67
2.9	Individual senders of financial risk for the full-sample period (2006-2022) . .	70
2.10	Aggregate cross-sectoral connectedness	71
2.11	Geographical connectedness	72
2.12	Distribution of elastic net parameters for different window sizes	76
2.13	CDS network before and after Lehman Brother’s bankruptcy	77
2.14	CDS network before and after the onset of the sovereign debt crisis	78
2.15	Dynamic system-wide connectedness	79
2.16	Dynamic system-wide connectedness for different window sizes	80
2.17	Dynamic cross-sectoral connectedness	81
2.18	Dynamic cross-sectoral connectedness, net distribution	82
2.19	Dynamic cross-sectoral connectedness, sub-sectors	83
2.20	Dynamic network connectedness across country groups	84
2.21	Dynamic Granger-causality connectedness	85
3.1	Hallin and Liska (2007) IC_2 criterion	108
3.2	Evolution of the <i>global</i> common factor over the full-sample period ranging from October 23, 2006 up to May 19, 2022. The global common factor X_t is estimated using the Dynamic Hierarchical Factor model by Moench, Ng and Potter (2013)	112
3.3	Evolution of the <i>block-specific</i> common factors over the full-sample period ranging from October 23, 2006 up to May 19, 2022. The block-specific common factors are estimated using the Dynamic Hierarchical Factor model by Moench, Ng and Potter (2013)	113
3.4	Individual senders of financial risk for the full-sample period (2006-2022) . .	118
3.5	CDS network graph for the full-sample period (2006-2022)	119
3.6	CDS network graph for the full-sample period (2006-2022) with only the idiosyncratic component in the estimated VAR, i.e. no block-specific factors are included in the panel VAR	120
3.7	CDS variance decomposition heatmap for the full-sample period (2006-2022)	121
3.8	Global common factor evolution in periods 1, 2, and 3	126

3.9	Evolution of the block-specific common factors over period 1 ranging from October 23, 2006 up to December 31, 2009. The block-specific common factors are estimated using the Dynamic Hierarchical Factor model by Moench, Ng and Potter (2013)	127
3.10	Evolution of the block-specific common factors over period 2 ranging from January 1, 2010 up to December 31, 2015. The block-specific common factors are estimated using the Dynamic Hierarchical Factor model by Moench, Ng and Potter (2013)	128
3.11	Evolution of the block-specific common factors over period 3 ranging from January 1, 2016 up to May 19, 2022. The block-specific common factors are estimated using the Dynamic Hierarchical Factor model by Moench, Ng and Potter (2013)	129
3.12	CDS heatmap for the sample period 1: 10/23/2006 - 12/31/2009	130
3.13	CDS heatmap for the sample period 2: 01/01/2010 - 12/31/2015	131
3.14	CDS heatmap for the sample period 3: 01.01.2016 - 05.19.2022	132
3.15	CDS network graph for the sample period 1: 10/23/2006 - 12/31/2009 . . .	133
3.16	CDS network graph for the sample period 2: 01.01.2010 - 12.31.2015	134
3.17	CDS network graph for the sample period 3: 01.01.2016 - 05.19.2022	135
3.18	CDS heatmap for the sample period I: 10/23/2006 - 08/08/2007	136
3.19	CDS heatmap for the sample period II: 08/09/2007 - 09/14/2008	137
3.20	CDS heatmap for the sample period III: 09/15/2008 - 04/01/2009	138
3.21	CDS heatmap for the sample period IV: 04/02/2009 - 05/08/2010	139
3.22	CDS network graph for the sample period I: 10/23/2006- 08/08/2007	140
3.23	CDS network graph for the sample period II: 08/09/2007 - 09/14/2008	141
3.24	CDS network graph for the sample period III: 09/15/2008 - 04/01/2009	142
3.25	CDS network graph for the sample period IV: 04/02/2009 - 05/08/2010	143

List of Tables

1.1	Estimation Results	12
1.2	Monte Carlo Results of SD1	42
1.3	Monte Carlo Results of SD2	42
1.4	Descriptive Statistics	43
2.1	List of CDS entities in the panel dataset	55
2.2	Properties of the estimated common factor	59
2.3	Summary statistics of CDS data by country and by sector	60
2.4	Out-of-sample forecast results	61
2.5	Rank correlation coefficients between the baseline model (1 factor, 10 days forecast horizon) and alternative specifications	68
2.6	Ranking of largest senders and receivers of credit risk	69
2.7	Geographical connectedness and financial linkages	73
3.1	List of CDS entities in the panel dataset	109
3.2	Explanatory power R^2 of the estimated common factors	114
3.3	Summary statistics of CDS data by country and by sector	115
3.4	Out-of-sample forecast results	116
3.5	Ranking of largest senders and receivers of credit risk for the full-sample period 2006-2022	117
3.6	Summarizing the assumed zero correlations of the DHFM model	147

Chapter 1

Estimating Social Effects in a Multilayered Linear-in-Means Model with Network Data

Note: This chapter is the product of collaborative research and has been published, see [Manta, Ho, Huynh and Jacho-Chávez \(2022\)](#), with title “Estimating social effects in a multilayered Linear-in-Means model with network data”, in *Statistics & Probability letters*. The views expressed in this chapter are solely those of the authors and may differ from Transunion and Bank of Canada views.

This paper studies the identification and estimation of social parameters in a general version of the Linear-in-Means model commonly fitted in the Social Sciences with multilayered network data. A Monte Carlo exercise showcases its good small-sample properties while an empirical application to Canadian consumers’ credit usage demonstrates its applicability.

Our estimates show that one's credit-card balance increases by \$0.31 for an extra \$1 owed by surrounding neighbors.

1.1 Introduction

Let the outcome variable of interest for observation i , y_i , be determined by $y_i = \alpha + \sum_{\ell=1}^L \beta_{\ell} \sum_{j \neq i} w_{\ell;i,j} y_j + \sum_{\ell=1}^L \sum_{j \neq i} w_{\ell;i,j} \mathbf{x}_j^{\top} \boldsymbol{\delta}_{\ell} + \mathbf{x}_i^{\top} \boldsymbol{\gamma} + e_i$, where $i, j \in \{1, \dots, n\}$ are also known as *nodes*, \mathbf{x} is a vector of attributes that characterizes the observations i and j , $w_{\ell;i,j} = w_{\ell;i,j}^* / \sum_{j=1}^n w_{\ell;i,j}^*$ with $w_{\ell;i,j}^*$ equals 1 if j is connected with i through a type- ℓ social tie (an *edge*), and 0 otherwise, e_i represents an unobserved latent error, n is the number of observations or nodes in the sample, and L is the total number of observed networks (layers). The structure of these $\ell = 1, \dots, L$ *social* networks is fully characterized by the square $n \times n$ matrices, \mathbf{W}_{ℓ} , the *adjacency matrices*, with each (i, j) entry given by $w_{\ell;i,j}$. In matrix form, this model can be written as

$$\mathbf{y} = \alpha \mathbf{1} + \sum_{\ell=1}^L \beta_{\ell} \mathbf{W}_{\ell} \mathbf{y} + \mathbf{X} \boldsymbol{\gamma} + \sum_{\ell=1}^L \mathbf{W}_{\ell} \mathbf{X} \boldsymbol{\delta}_{\ell} + \mathbf{e}, \quad E_{\mathbf{X}, \mathbf{W}_1, \mathbf{W}_2, \dots, \mathbf{W}_L}[\mathbf{e}] = \mathbf{0}, \quad (1.1)$$

where α and β_{ℓ} are scalars, $\boldsymbol{\gamma}$ and $\boldsymbol{\delta}_{\ell}$ are $K \times 1$ vectors of direct and contextual effects, respectively, $\mathbf{1}$ is a $n \times 1$ vector of ones, \mathbf{y} is an $n \times 1$ vector of outcomes, \mathbf{X} is a $n \times K$ matrix of exogenous covariates, and \mathbf{e} is a $n \times 1$ vector of unobservables such that $E_{\mathbf{X}, \mathbf{W}_1, \mathbf{W}_2, \dots, \mathbf{W}_L}[\mathbf{e}] \equiv E[\mathbf{e} | \mathbf{X}, \mathbf{W}_1, \mathbf{W}_2, \dots, \mathbf{W}_L] = \vec{\mathbf{0}}$, where $\vec{\mathbf{0}}$ represents a $n \times 1$ vector of zeroes. \mathbf{I} represents an identity matrix of order n in what follows.

Setting $L = 1$ in (1.1) yields the so-called *Linear-in-Means* model (see Section 3.1 in [de Paula, 2017](#), pp. 275-289) which is the workhorse model to estimate social effects in the

Social Sciences. The specific case when $L = 2$ and \mathbf{W}_2 being the row-normalized version of \mathbf{W}_1 was studied in Liu et al. (2014), while the special case where $\boldsymbol{\delta}_1 = \dots = \boldsymbol{\delta}_L = \vec{0}$ (higher-order Spatial Autoregressive model) was presented by Badinger and Egger (2011). The results here can be understood as a generalization of these, when the researcher observes different types of social ties among observations, e.g., geographical neighbours ($\ell = 1$), same race ($\ell = 2$), same age group ($\ell = 3$), etc., instead.

1.2 Identification

Assumption 1. *The parameters β_ℓ, γ , and $\boldsymbol{\delta}_\ell$ in (1.1) are such that (a) $\beta_1 \neq 0$, (b) $\sum_{\ell=1}^L |\beta_\ell| < 1$, and (c) $\max(|\gamma\beta_1 + \boldsymbol{\delta}_1|, |\gamma\beta_2 + \boldsymbol{\delta}_2|, \dots, |\gamma\beta_L + \boldsymbol{\delta}_L|) \neq 0$ hold, for all $\ell \neq \ell'$ where $\ell, \ell' \in \{1, 2, \dots, L\}$.*

Assumption 2. *The matrices, \mathbf{W}_ℓ in (1.1), are $n \times n$ adjacency matrices such that the sum of the elements in each row equals to 1 or 0, and $\mathbf{W}_\ell \neq \mathbf{W}_{\ell'}$, for all $\ell \neq \ell'$ where $\ell, \ell' \in \{1, 2, \dots, L\}$.*

Assumption 1(a) is simply a normalization and is made without loss of generality, while Assumption 1(b) ensures the invertibility of a matrix in the proof, and 1(c) guarantees that social effects are not zero or cancelled each other out in the reduced form version of (1.1). Assumption 2 rules out perfect collinearity in (1.1).

Theorem 1. *Let Assumptions 1 and 2 hold in the structural model (1.1). If the matrices \mathbf{X} , $\mathbf{W}_\ell \mathbf{X}$, $\mathbf{W}_{\ell'} \mathbf{X}$, $\mathbf{W}_\ell \mathbf{W}_{\ell'} \mathbf{X}$, $\mathbf{W}_{\ell'} \mathbf{W}_\ell \mathbf{X}$, $\mathbf{W}_\ell^2 \mathbf{X}$, and $\mathbf{W}_{\ell'}^2 \mathbf{X}$ are linearly independent for all $\ell \neq \ell'$ where $\ell, \ell' \in \{1, 2, \dots, L\}$, then the social parameters $\alpha, \beta_\ell, \gamma$, and $\boldsymbol{\delta}_\ell$ in (1.1) are identified.*

This result guarantees that the social parameters can be uniquely recovered from the estimating sample $\{y_i, \mathbf{x}_i^\top, \{w_{1;i,j}\}_{j=1,j \neq i}^n, \dots, \{w_{L;i,j}\}_{j=1,j \neq i}^n\}_{i=1}^n$. Notice that the required linear independence can be numerically verified, and it requires that at least one pair of nodes shares more than one type of social ties among them.

1.3 Estimation

First, notice that (1.1) can be rewritten as

$$\mathbf{y} = \alpha \iota + \sum_{\ell=1}^L \mathbf{W}_\ell \mathbf{S} \boldsymbol{\theta}_\ell + \mathbf{X} \boldsymbol{\gamma} + \mathbf{e}, \quad E_{\mathbf{X}, \mathbf{w}_1, \mathbf{w}_2, \dots, \mathbf{w}_L}[\mathbf{e}] = 0, \quad (1.2)$$

where \mathbf{S} is a $n \times (K + 1)$ matrix defined as $\mathbf{S} \equiv [\mathbf{y} \quad \mathbf{X}]$, and $\boldsymbol{\theta}_\ell \equiv (\beta_\ell, \boldsymbol{\delta}_\ell^\top)^\top$ is a $(K + 1) \times 1$ vector of parameters such that $\mathbf{W}_\ell \mathbf{y} \mathbf{f}_\ell + \mathbf{W}_\ell \mathbf{X} \boldsymbol{\delta}_\ell = \mathbf{W}_\ell \mathbf{S} \boldsymbol{\theta}_\ell$, for all $\ell = 1, 2, \dots, L$. Note that (1.2) cannot be directly estimated by ordinary least squares because of the simultaneity among the $\mathbf{W}_\ell \mathbf{y}$ terms. Therefore, following [Kelejian and Prucha \(1998\)](#), a Generalized Two-Stage Least Squares (G2SLS) estimator of $(\alpha, \boldsymbol{\gamma}, \boldsymbol{\theta}_1^\top, \boldsymbol{\theta}_2^\top, \dots, \boldsymbol{\theta}_L^\top)$ is as follows:

Step One: Rewrite (1.2) as

$$\mathbf{y} = \mathbf{D} \boldsymbol{\psi} + \mathbf{e}, \quad (1.3)$$

where $\mathbf{D} = [\iota, \mathbf{X}, \mathbf{W}_1 \mathbf{y}, \mathbf{W}_1 \mathbf{X}, \mathbf{W}_2 \mathbf{y}, \mathbf{W}_2 \mathbf{X}, \dots, \mathbf{W}_L \mathbf{y}, \mathbf{W}_L \mathbf{X}]$ is a matrix of variables with dimensions $n \times [(L + 1)(K + 1)]$ and $\boldsymbol{\psi} = (\alpha, \boldsymbol{\gamma}, \boldsymbol{\theta}_1^\top, \boldsymbol{\theta}_2^\top, \dots, \boldsymbol{\theta}_L^\top)^\top$ is a $[(L + 1)(K + 1)] \times 1$ vector of parameters. From (1.3), the parameters $\boldsymbol{\psi}$ can be estimated by Two-Stage Least

Squares (2SLS). Let

$$\mathbf{Z} = [\iota, \mathbf{X}, \mathbf{W}_1\mathbf{X}, \mathbf{W}_2\mathbf{X}, \dots, \mathbf{W}_L\mathbf{X}, \mathbf{W}_1^2\mathbf{X}, \mathbf{W}_2^2\mathbf{X}, \dots, \mathbf{W}_L^2\mathbf{X}, \mathbf{W}_1\mathbf{W}_2\mathbf{X}, \\ \mathbf{W}_1\mathbf{W}_3\mathbf{X}, \dots, \mathbf{W}_1\mathbf{W}_L\mathbf{X}, \mathbf{W}_2\mathbf{W}_1\mathbf{X}, \mathbf{W}_2\mathbf{W}_3\mathbf{X}, \dots, \mathbf{W}_2\mathbf{W}_L\mathbf{X}, \dots, \\ \mathbf{W}_L\mathbf{W}_1\mathbf{X}, \mathbf{W}_L\mathbf{W}_2\mathbf{X}, \dots, \mathbf{W}_L\mathbf{W}_{L-1}\mathbf{X}]$$

be the $n \times \{1 + K(L^2 + L + 1)\}$ matrix of instruments (IV) for the variables in \mathbf{D} . For the general case where $K > 1$, the model is overidentified and the 2SLS estimator is

$$\widehat{\boldsymbol{\psi}}_{2\text{SLS}} = [\mathbf{D}^\top \mathbf{Z} (\mathbf{Z}^\top \mathbf{Z})^{-1} \mathbf{Z}^\top \mathbf{D}]^{-1} \mathbf{D}^\top \mathbf{Z} (\mathbf{Z}^\top \mathbf{Z})^{-1} \mathbf{Z}^\top \mathbf{y}. \quad (1.4)$$

Step Two: This step consists of constructing the optimal instruments for the regressors $\mathbf{W}_\ell \mathbf{y}$. The optimal instruments are given by $E_{\mathbf{X}, \mathbf{w}_1, \mathbf{w}_2, \dots, \mathbf{w}_L}[\mathbf{W}_\ell \mathbf{y}]$, $\forall \ell$. Note that from $\mathbf{y} = \alpha(\mathbf{I} - \sum_{\ell=1}^L \beta_\ell \mathbf{W}_\ell)^{-1} \iota + (\mathbf{I} - \sum_{\ell=1}^L \beta_\ell \mathbf{W}_\ell)^{-1} (\mathbf{X}\boldsymbol{\gamma} + \sum_{\ell=1}^L \mathbf{W}_\ell \mathbf{X} \boldsymbol{\delta}_\ell) + (\mathbf{I} - \sum_{\ell=1}^L \beta_\ell \mathbf{W}_\ell)^{-1} \mathbf{e}$, one has

$$E_{\mathbf{X}, \mathbf{w}_1, \mathbf{w}_2, \dots, \mathbf{w}_L}[\mathbf{W}_\ell \mathbf{y}] = \mathbf{W}_\ell \alpha \left(\mathbf{I} - \sum_{\ell=1}^L \beta_\ell \mathbf{W}_\ell \right)^{-1} \iota \\ + \mathbf{W}_\ell \left(\mathbf{I} - \sum_{\ell=1}^L \beta_\ell \mathbf{W}_\ell \right)^{-1} \left(\mathbf{X}\boldsymbol{\gamma} + \sum_{\ell=1}^L \mathbf{W}_\ell \mathbf{X} \boldsymbol{\delta}_\ell \right), \quad (1.5)$$

for all $\ell = 1, \dots, L$. Valid estimators of equation (1.5) are then given by $E_{\mathbf{X}, \mathbf{w}_1, \mathbf{w}_2, \dots, \mathbf{w}_L}[\mathbf{W}_\ell \mathbf{y}]$ ($\widehat{\boldsymbol{\psi}}_{2\text{SLS}}$), where $\widehat{\boldsymbol{\psi}}_{2\text{SLS}} = (\widehat{\alpha}_{2\text{SLS}}, \widehat{\boldsymbol{\gamma}}_{2\text{SLS}}, \widehat{\boldsymbol{\theta}}_{1;2\text{SLS}}^\top, \widehat{\boldsymbol{\theta}}_{2;2\text{SLS}}^\top, \dots, \widehat{\boldsymbol{\theta}}_{L;2\text{SLS}}^\top)^\top$ from the first step. Now, rewriting (1.1) as (1.3), one has that the estimator of the $n \times [(L + 1)K + (L + 1)]$ matrix

of optimal instruments is given by

$$\begin{aligned} \widehat{\mathbf{Z}} = & [\iota, \mathbf{X}, E_{\mathbf{X}, \mathbf{W}_1, \mathbf{W}_2, \dots, \mathbf{W}_L}[\mathbf{W}_1 \mathbf{y}](\widehat{\boldsymbol{\psi}}), E_{\mathbf{X}, \mathbf{W}_1, \mathbf{W}_2, \dots, \mathbf{W}_L}[\mathbf{W}_2 \mathbf{y}](\widehat{\boldsymbol{\psi}}), \dots, \\ & E_{\mathbf{X}, \mathbf{W}_1, \mathbf{W}_2, \dots, \mathbf{W}_L}[\mathbf{W}_L \mathbf{y}](\widehat{\boldsymbol{\psi}}), \mathbf{W}_1 \mathbf{X}, \mathbf{W}_2 \mathbf{X}, \dots, \mathbf{W}_L \mathbf{X}]. \end{aligned} \quad (1.6)$$

Therefore, the G2SLS estimator of $\boldsymbol{\psi} = (\alpha, \boldsymbol{\gamma}, \boldsymbol{\theta}_1^\top, \boldsymbol{\theta}_2^\top, \dots, \boldsymbol{\theta}_L^\top)^\top$, is

$$\widehat{\boldsymbol{\psi}}_{\text{G2SLS}} = (\widehat{\mathbf{Z}}^\top \mathbf{D})^{-1} \widehat{\mathbf{Z}}^\top \mathbf{y}. \quad (1.7)$$

The supplemental materials points out how one can go about adapting Steps One and Two above to incorporate the identifying restrictions in Assumption 1.

Assumption 3. *The matrix \mathbf{Z} is such that $\mathbf{Q}_{\mathbf{Z}\mathbf{Z}} = \lim_{n \rightarrow \infty} n^{-1} \sum_{i=1}^n \mathbf{z}_i \mathbf{z}_i^\top$ is finite and non-singular. In addition, $\mathbf{Q}_{\mathbf{Z}\mathbf{D}} = \lim_{n \rightarrow \infty} n^{-1} \sum_{i=1}^n \mathbf{z}_i \mathbf{d}_i^\top$ is finite and non-singular.*

Assumption 4. *The matrix $\boldsymbol{\Omega}$ is positive definite and it is such that $\boldsymbol{\Omega} = \lim_{n \rightarrow \infty} n^{-1} \sum_{i=1}^n \mathbf{z}_i \mathbf{z}_i^\top E_{\mathbf{Z}}[e_i^2]$.*

Assumption 5. *The structural innovations $\{e_i\}$ are independently jointly distributed with expectations $E_{\mathbf{X}, \mathbf{W}_1, \mathbf{W}_2, \dots, \mathbf{W}_L}[e_i] = 0$ and $E_{\mathbf{X}, \mathbf{W}_1, \mathbf{W}_2, \dots, \mathbf{W}_L}[e_i^2] = \sigma_{e_i}^2 < \infty, \forall i = 1, \dots, n$. In addition, they are uniformly bounded in absolute value, and satisfy $\lim_{n \rightarrow \infty} n^{-1} \sum_{i=1}^n \sigma_{e_i}^2 < \infty, \liminf_{n \rightarrow \infty} n^{-1} \sum_{i=1}^n \sigma_{e_i}^2 > 0$, and for some $\xi > 0$, $\sup_{n,i} E|e_i|^{2+\xi} < \infty$.*

Assumption 6. *The column sums of each $\mathbf{W}_\ell, \forall \ell$, and all elements in the matrix $[\mathbf{X}, \mathbf{e}]$ are uniformly bounded in absolute value, for all n .*

Assumptions 3 and 4 use the notation \mathbf{z}_i^\top to represent the i th row of \mathbf{Z} and e_i to

denote the i th element of the $n \times 1$ vector of the structural error term. These assumptions are standard in IV estimation as they guarantee the existence of the asymptotic variance-covariance matrix, while Assumptions 5 and 6 requires summability conditions of conditional variances and random variables.

Theorem 2. *Let Assumptions 1 – 6 hold for model (1.1), then $\widehat{\boldsymbol{\psi}}_{\text{G2SLS}} = \boldsymbol{\psi} + o_p(1)$ and $n^{1/2}(\widehat{\boldsymbol{\psi}}_{\text{G2SLS}} - \boldsymbol{\psi}) \xrightarrow{d} N(\mathbf{0}, V_\psi)$, where $V_\psi = \mathbf{Q}_{\mathbf{ZD}}^{-1} \boldsymbol{\Omega} \mathbf{Q}_{\mathbf{DZ}}^{-1}$ and $\mathbf{Q}_{\mathbf{DZ}} = \mathbf{Q}_{\mathbf{ZD}}^\top$.*

Theorem 2 demonstrates that the resulting G2SLS estimator is asymptotically unbiased, root- n consistent, and asymptotically normal. The corresponding standard errors can be calculated as the square root of the main diagonal elements divided by n of the following consistent estimator $\widehat{V}_\psi = (n^{-1} \widehat{\mathbf{Z}}^\top \widehat{\mathbf{D}})^{-1} (n^{-1} \sum_{i=1}^n \widehat{\mathbf{z}}_i \widehat{\mathbf{z}}_i^\top \widehat{e}_i^2) (n^{-1} \widehat{\mathbf{D}}^\top \widehat{\mathbf{Z}})^{-1}$ of V_ψ , where $\widehat{\mathbf{z}}_i^\top$ is defined as the i th row of the matrix $\widehat{\mathbf{Z}}$, $\widehat{\mathbf{e}}_i$ is defined as $\widehat{\mathbf{e}}_i = \mathbf{y} - \widehat{\alpha}_{\text{G2SLS}} \boldsymbol{\iota} - \mathbf{W}_1 \mathbf{S} \widehat{\boldsymbol{\theta}}_{1;\text{G2SLS}} - \mathbf{W}_2 \mathbf{S} \widehat{\boldsymbol{\theta}}_{2;\text{G2SLS}} - \dots - \mathbf{W}_L \mathbf{S} \widehat{\boldsymbol{\theta}}_{L;\text{G2SLS}} - \mathbf{X} \widehat{\boldsymbol{\gamma}}_{\text{G2SLS}}$ and $\widehat{\boldsymbol{\psi}}_{\text{G2SLS}} = (\widehat{\alpha}_{\text{G2SLS}}, \widehat{\boldsymbol{\gamma}}_{\text{G2SLS}}^\top, \widehat{\boldsymbol{\theta}}_{1;\text{G2SLS}}^\top, \widehat{\boldsymbol{\theta}}_{2;\text{G2SLS}}^\top, \dots, \widehat{\boldsymbol{\theta}}_{L;\text{G2SLS}}^\top)^\top$.

1.4 Monte Carlo Experiments

The small sample performance of the proposed G2SLS estimator in Section ?? is analyzed here where $L = 3$ and $K = 1$ in (1.1), where $\{x_i\}_{i=1}^n$ and $\{e_i\}_{i=1}^n$ are drawn from independent standard normal distributions. A total of 1,100 data sets, $\{y_i, x_i\}_{i=1}^n$ and $\{\{w_{\ell;i,j}\}_{i=1}^n\}_{j=1}^n$, with $w_{\ell;i,j} = w_{\ell;i,j}^* / \sum_{j=1}^n w_{\ell;i,j}^*$, $\forall \ell \in \{1, 2, 3\}$, for $n \in \{50, 100, 200\}$ are generated from a combination of a model specification and a network formation model as follows:

Model Specification: The parameter values of $\boldsymbol{\psi}$ are set to be all positive, i.e., $\alpha = 0.15$, $\gamma = 0.8$, $\beta_\ell = \frac{\phi}{3}$, where $\phi = 0.9$ and $\delta_\ell = \frac{1}{3}$.

Networks Formation Model: The $n \times n$ adjacency matrices $\mathbf{W}_\ell^* = [w_{\ell;i,j}^*]$ are such that \mathbf{W}_1^* is generated as an [Erdős and Rényi's \(1959\)](#) random graph with density 0.01, while the remaining adjacency matrices are defined as $w_{\ell;i,j}^* = w_{\ell-1;i,j}^* c_{1,\ell;i,j} + (1 - w_{\ell-1;i,j}^*) c_{2,\ell;i,j}$, for $i \neq j$, $\ell \in \{2, 3\}$, where $c_{1,\ell;i,j}$, and $c_{2,\ell;i,j}$ are drawn independently from an independent Bernoulli distribution with parameters 0.5, and 0.99 respectively in each replication.

Figure 1.1 displays the Box and Q-Q plots. Overall, the small sample properties of the proposed G2SLS estimator of all parameters of interest seem to be as expected, with little to no bias as sample size increases and shrinking dispersion. The asymptotic normal approximation in Theorem 2 seems adequate even with a sample size of 50 observations.

1.5 Empirical Application

Economics literature suggests that consumers are subject to the influence of conspicuous consumption made by their network peers, see, e.g., [Bertrand and Morse \(2016\)](#) and consequently adjust their debt-taking behaviors accordingly [Agarwal et al. \(2019\)](#). Existing evidence is mainly based on the variation of neighbor's income in a geographic network of residential locations, i.e. the contextual effect in a mono-layered network.

Using anonymized Canadian consumer credit data from TransUnion®[®], the proposed method here is applied to empirically estimate the effect of social influence on consumers' use of credit. We focus on consumers residing in a remote urban service area where has a single economic focus. Our analysis is based on cross-sectional data of 47,593 individuals at the end of 2018. A detailed data description and summary statistics are provided in the supplemental materials.

The outcome of interest is the outstanding loan balance. We consider 2 common consumer loan types – credit cards and auto loans. Network layers ($L = 2$) are constructed conditional on individuals living in the same *census dissemination area (DA)*, a small geographic unit bounded by roads or other natural boundaries and comprised of many smaller neighborhoods. On average, a DA is about 0.2 km² in size with 1,322 adults. Within a DA, consumers are connected if they are in the same age group (\mathbf{W}_1) or if they live in the same neighborhood (\mathbf{W}_2). In other words, $w_{1;i,j}^* = 1$ if individual i and j are in the same age group *within* the same DA; 0 otherwise. Similarly, $w_{2;i,j}^* = 1$ if individual i and j live in the same neighborhood *within* the same DA; 0 otherwise. Our setup follows a common assumption in the urban economics literature that, while individuals can choose which DA to live in, the actual residing neighborhood within the DA is exogenous and random depending on housing availability.

Our contextual effects are based on consumer’s credit scores in the previous quarter, normalized with zero mean and unit variance. It reflects one’s credit worthiness and correlates with individual income levels. Direct effects considered in this model includes and individual’s credit score, total non-residential debts in the previous quarter, and the total credit-card limit. Fixed effects for age group \times homeowner and DA \times homeowner interactions are also included in the model. Specifically, our estimation model for individual i ’s balance in loan type $k \in \{\text{credit card, auto loan}\}$ is specified as

$$loan_i^k = \alpha + \sum_{\ell=1}^2 \beta_{\ell} \sum_{j \neq i} w_{\ell;i,j} loan_j^k + \sum_{\ell=1}^2 \delta_{\ell} \sum_{j \neq i} w_{\ell;i,j} crsc_j + \mathbf{X}_i \gamma + e_i \quad (1.8)$$

where $w_{\ell;i,j} = w_{\ell;i,j}^* / \sum_{j=1}^n w_{\ell;i,j}^*$ is the weight, $crsc_j$ is the credit score of individual j , and

$\mathbf{X}_i = \{crsc_i, \text{total non-residential debt, total credit-card limit, age group} \times \text{homeowner, DA} \times \text{homeowner}\}$ is a vector of regressors for the direct effects.

Estimation results are reported in Table 1.1. For credit-card balances, there is significant peer effect in both network layers. When one's age-group peers on average have \$1 extra dollar of credit-card balance, the individual has \$0.38 more; when one's neighbors on average have \$1 extra dollar in balance, the individual has \$0.31 more, *ceteris paribus*. The age-group contextual effect also shows that one's credit-card balance is \$992.7 higher when the peer's average credit score is a standard-deviation higher. Our results are consistent with the explanation of status-maintaining in the presence of conspicuous consumption.

For auto loans, only the neighborhood peer effect is significant. An individual has \$0.11 more auto loan when one's neighbors on average have \$1 more in auto loan. This is a non-trivial amount, given that an average individual owes \$15,091 in this category. The neighborhood peer effect follows the intuition that car consumption is quite visible. We do not observe significant age-group peer effect nor significant contextual effects as in the case of credit cards, because cars are expensive durable goods that consumers do not adjust frequently. Indeed, the data shows that less than 50% of consumers have auto loans.

The direct effects have the expected signs and give intuitive results. Credit-worthy individuals with high credit scores have less in credit card balances. For each dollar of consumer loan an individual owes, \$0.05 is attributed to credit card. Also, the coefficient for credit card limit is 0.265, meaning that the conditional average credit card utilization is 26.5%. Results for auto loans are in similar direction, except the coefficient estimate for credit card limit is of the opposite sign, suggesting that individuals with higher credit-card

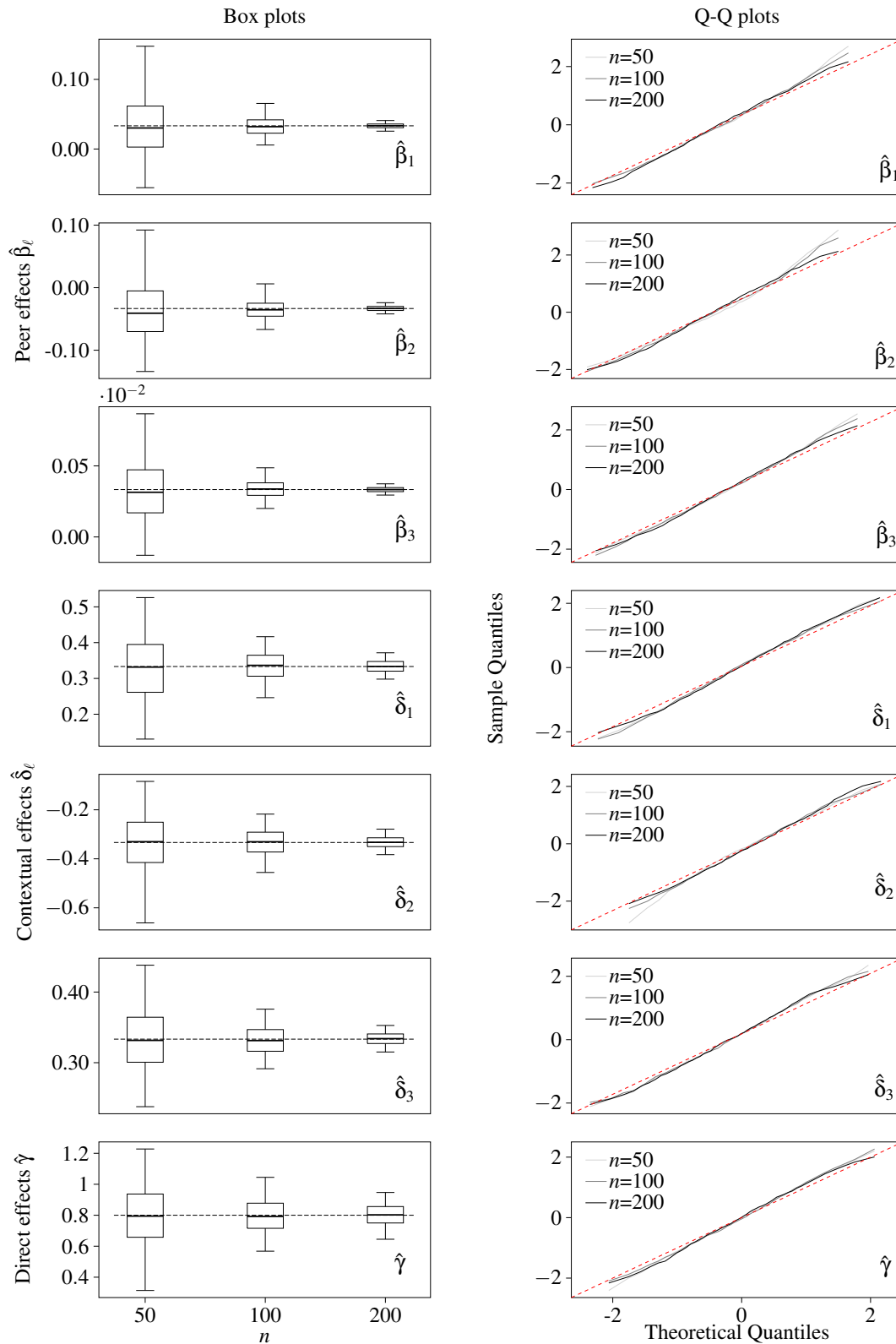
limits are those with higher income and smaller amount of auto loans after controlling for peer and contextual effects.

Table 1.1: Estimation Results

Variables	Credit card	Auto loan
Peer effects (β_ℓ)		
Age group	0.384*** (0.069)	0.067 (0.059)
Neighbor	0.306** (0.124)	0.107*** (0.032)
Contextual effects (δ_ℓ)		
Credit scores (age group)	992.684*** (274.950)	492.260 (790.325)
Credit scores (neighbor)	311.816 (201.002)	-450.795 (487.897)
Direct effects (γ)		
Credit scores	-2445.794*** (63.412)	-610.996*** (134.909)
Consumer loans	0.054*** (0.002)	0.313*** (0.012)
Credit card limit	0.265*** (0.007)	-0.092*** (0.009)
Adjusted R^2	0.424	0.385

Note: ***, **, * denotes 10%, 5% and 1% significance, respectively. Interaction terms for age-group \times home-ownership and DA \times home-ownership, as well as a constant term are included. Estimation results for the interaction terms are reported in the supplementary materials.

Figure 1.1: Monte Carlo Plots



Note: The plots are for each sample size $n \in \{50, 100, 200\}$, based on 1, 100 replications using the networks formation model for $L = 3$ layers.

1.6 Appendix: Constrained Estimation

Steps One and Two in the main text are performed without imposing restrictions on the parameters in (1.1). However, they can easily be modified to accommodate inequality constraints instead. For example, take $L = 3$ and $K = 1$, then a set of sufficient restrictions for Assumption 1 to hold takes the form $\mathbf{R}\boldsymbol{\psi} < \mathbf{c}$, i.e.,

$$\begin{bmatrix} 0 & -1 & 0 & 0 & 0 & 0 & 0 & 0 \\ 0 & 0 & -1 & 0 & 0 & 0 & 0 & 0 \\ 0 & 0 & 0 & -1 & 0 & 0 & 0 & 0 \\ 0 & 0 & 1 & 0 & 1 & 0 & 1 & 0 \\ 0 & 0 & 1 & 0 & 1 & 0 & -1 & 0 \\ 0 & 0 & 1 & 0 & -1 & 0 & 1 & 0 \\ 0 & 0 & 1 & 0 & -1 & 0 & -1 & 0 \\ 0 & 0 & -1 & 0 & 1 & 0 & 1 & 0 \\ 0 & 0 & -1 & 0 & 1 & 0 & -1 & 0 \\ 0 & 0 & -1 & 0 & -1 & 0 & 1 & 0 \\ 0 & 0 & -1 & 0 & -1 & 0 & -1 & 0 \end{bmatrix} \begin{bmatrix} \alpha \\ \gamma \\ \beta_1 \\ \delta_1 \\ \beta_2 \\ \delta_2 \\ \beta_3 \\ \delta_3 \end{bmatrix} < \begin{bmatrix} 0 \\ 0 \\ 0 \\ 1 \\ 1 \\ 1 \\ 1 \\ 1 \\ 1 \\ 1 \\ 1 \end{bmatrix},$$

when $\beta_1 > 0$, $\gamma > 0$, and $\delta_1 > 0$ without loss of generality. Then one can replace the standard least squares projection in Step One by the quadratic programming problem in [Judge and Takayama \(1966\)](#) and [Liew \(1976\)](#). Similarly, the IV estimation in Step Two can also be adapted to account for these inequality constraints as in [Giles \(1982a,b\)](#). Results in Theorem 2 can then be modified accordingly at the expense of more complicated derivations.

1.7 Appendix: Proofs of Main Results

Proof of Theorem 1: First by Assumption 1 it follows by Lemma 1 in 1.8 that $\mathbf{I} - \sum_{\ell=1}^L \beta_\ell \mathbf{W}_\ell$ is invertible, so one can write (1.1) as

$$\mathbf{y} = \alpha \left(\mathbf{I} - \sum_{\ell=1}^L \beta_\ell \mathbf{W}_\ell \right)^{-1} \iota + \left(\mathbf{I} - \sum_{\ell=1}^L \beta_\ell \mathbf{W}_\ell \right)^{-1} \left(\mathbf{X}\boldsymbol{\gamma} + \sum_{\ell=1}^L \mathbf{W}_\ell \mathbf{X} \boldsymbol{\delta}_\ell \right) + \left(\mathbf{I} - \sum_{\ell=1}^L \beta_\ell \mathbf{W}_\ell \right)^{-1} \mathbf{e}. \quad (1.9)$$

Consider two sets of structural parameters $(\alpha, \beta_\ell, \boldsymbol{\gamma}, \boldsymbol{\delta}_\ell)$ and $(\alpha', \beta'_\ell, \boldsymbol{\gamma}', \boldsymbol{\delta}'_\ell)$, $\forall \ell = 1, \dots, L$, leading to the same reduced form (1.9), where $\sum_{\ell=1}^L |\beta'_\ell| < 1$ and $\mathbf{I} - \sum_{\ell=1}^L \beta'_\ell \mathbf{W}_\ell$ is invertible as well (see Lemma 1 in 1.8). Then, one has

$$\begin{aligned} \alpha \left(\mathbf{I} - \sum_{\ell=1}^L \beta_\ell \mathbf{W}_\ell \right)^{-1} \iota &= \alpha' \left(\mathbf{I} - \sum_{\ell=1}^L \beta'_\ell \mathbf{W}_\ell \right)^{-1} \iota \\ \left(\mathbf{I} - \sum_{\ell=1}^L \beta_\ell \mathbf{W}_\ell \right)^{-1} \left(\mathbf{X}\boldsymbol{\gamma} + \sum_{\ell=1}^L \mathbf{W}_\ell \mathbf{X} \boldsymbol{\delta}_\ell \right) &= \left(\mathbf{I} - \sum_{\ell=1}^L \beta'_\ell \mathbf{W}_\ell \right)^{-1} \\ &\quad \left(\mathbf{X}\boldsymbol{\gamma}' + \sum_{\ell=1}^L \mathbf{W}_\ell \mathbf{X} \boldsymbol{\delta}'_\ell \right). \end{aligned}$$

Now, pre-multiplying both sides of the last equality by $\left(\mathbf{I} - \sum_{\ell=1}^L \beta_\ell \mathbf{W}_\ell \right) \cdot \left(\mathbf{I} - \sum_{\ell=1}^L \beta'_\ell \mathbf{W}_\ell \right)$. By Assumptions 1(a) and 2(b), one has $\beta_1 \neq 0$ and $\beta_\ell = c_\ell \beta_1$, for any $|c_\ell| < +\infty$, $\forall \ell \in \{2, 3, \dots, L\}$, (see Lemma 2 in 1.8), and along with Assumption 2 one could further

rewrite

$$\begin{aligned} \mathbf{X}(\gamma - \gamma') + \sum_{\ell=1}^L \mathbf{W}_\ell \mathbf{X} [(\boldsymbol{\delta}_\ell + \gamma' \beta_\ell) - (\boldsymbol{\delta}'_\ell + \gamma \beta'_\ell)] + \sum_{\ell=1}^L \mathbf{W}_\ell^2 \mathbf{X} (\beta_\ell \boldsymbol{\delta}'_\ell - \beta'_\ell \boldsymbol{\delta}_\ell) \\ + \sum_{\ell=1}^L \sum_{\ell'=1, \ell' \neq \ell}^L \mathbf{W}_\ell \mathbf{W}_{\ell'} \mathbf{X} (\beta_\ell \boldsymbol{\delta}'_{\ell'} - \beta'_{\ell'} \boldsymbol{\delta}_\ell) = 0. \end{aligned} \quad (1.10)$$

Since \mathbf{X} , $\mathbf{W}_\ell \mathbf{X}$, $\mathbf{W}_{\ell'} \mathbf{X}$, $\mathbf{W}_\ell \mathbf{W}_{\ell'} \mathbf{X}$, $\mathbf{W}_\ell^2 \mathbf{X}$, and $\mathbf{W}_{\ell'}^2 \mathbf{X}$ are linearly independent for all $\ell \neq \ell' \in \{1, 2, \dots, L\}$, then it follows

$$\begin{aligned} \gamma &= \gamma', \\ \boldsymbol{\delta}_\ell + \gamma' \beta_\ell &= \boldsymbol{\delta}'_\ell + \gamma \beta'_\ell, \\ \beta_\ell \boldsymbol{\delta}'_\ell &= \beta'_\ell \boldsymbol{\delta}_\ell, \text{ and} \\ \beta_\ell \boldsymbol{\delta}'_{\ell'} &= \beta'_{\ell'} \boldsymbol{\delta}_{\ell'} \end{aligned}$$

for all ℓ, ℓ' such that $\ell \neq \ell' \in \{1, 2, \dots, L\}$.

Assume first that $\beta_\ell \boldsymbol{\delta}'_\ell \neq \vec{0}$ for all $\ell = 1, 2, \dots, L$. Then, there must exist a $\lambda \neq 0$ such that $\beta'_\ell = \lambda \beta_\ell$, $\boldsymbol{\delta}'_\ell = \lambda \boldsymbol{\delta}_\ell$. Substituting yields $\boldsymbol{\delta}'_\ell + \gamma \beta'_\ell = \lambda(\boldsymbol{\delta}_\ell + \gamma \beta_\ell) = \boldsymbol{\delta}_\ell + \gamma \beta_\ell$, which implies that $\lambda = 1$. Hence, by Assumption 1, one has $\beta'_\ell = \beta_\ell$ and $\boldsymbol{\delta}'_\ell = \boldsymbol{\delta}_\ell$, for all $\ell = 1, 2, \dots, L$.

Second, suppose that $\beta_{\ell'} \boldsymbol{\delta}'_{\ell'} = \vec{0}$ and $\beta_\ell \boldsymbol{\delta}'_\ell \neq \vec{0}$ for ℓ, ℓ' such that $\ell \neq \ell' = 1, 2, \dots, L$. By Assumption 1, this implies that it has to be the case that $\beta_{\ell'} = \beta'_{\ell'} = 0$, or $\boldsymbol{\delta}_{\ell'} = \boldsymbol{\delta}'_{\ell'} = \vec{0}$, or both. In case that $\beta_{\ell'} = \beta'_{\ell'} = 0$, then it comes that $\boldsymbol{\delta}_{\ell'} = \boldsymbol{\delta}'_{\ell'}$. In case that $\boldsymbol{\delta}_{\ell'} = \boldsymbol{\delta}'_{\ell'} = \vec{0}$, then it follows that $\beta_{\ell'} = \beta'_{\ell'}$. If both hold, then this means that $\beta_{\ell'} = \beta'_{\ell'} = 0$ and $\boldsymbol{\delta}_{\ell'} = \boldsymbol{\delta}'_{\ell'} = \vec{0}$. For the parameters $\beta_\ell, \beta'_\ell, \boldsymbol{\delta}_\ell, \boldsymbol{\delta}'_\ell$ one has that there must exist a $\lambda \neq 0$ such

that $\beta'_\ell = \lambda\beta_\ell, \delta'_\ell = \lambda\delta_\ell$. Substituting yields $\delta'_\ell + \gamma\beta'_\ell = \lambda(\delta_\ell + \gamma\beta_\ell) = \delta_\ell + \gamma\beta_\ell$, which implies that $\lambda = 1$. Hence, one has $\beta'_\ell = \beta_\ell$ and $\delta'_\ell = \delta_\ell$.

Third, assume $\beta_\ell\delta'_\ell = \vec{0}$ for all $\ell = 1, 2, \dots, L$. Then, by Assumption 1 one has $\delta_\ell = \delta'_\ell = \vec{0}, \forall \ell$, or $\beta_\ell = \beta'_\ell = 0, \forall \ell$, or both for some (but not all) ℓ . In the case where $\delta_\ell = \delta'_\ell = \vec{0} \forall \ell$, then by Assumption 1, one has $\beta_\ell = \beta'_\ell, \forall \ell$. Next, in case where $\beta_\ell = \beta'_\ell = 0 \forall \ell$, then by Assumption 1, one has $\delta_\ell = \delta'_\ell, \forall \ell$. Finally, in case where both $\beta_{\ell'} = \beta'_{\ell'} = 0$ and $\delta_{\ell'} = \delta'_{\ell'} = \vec{0}$ for some ℓ' (but not all layers $1, 2, \dots, L$) and given Assumption 1, one has that there must exist a $\lambda \neq 0$ such that $\beta'_\ell = \lambda\beta_\ell, \delta'_\ell = \lambda\delta_\ell$. Substituting yields $\delta'_\ell + \gamma\beta'_\ell = \lambda(\delta_\ell + \gamma\beta_\ell) = \delta_\ell + \gamma\beta_\ell \forall \ell$, which implies that $\lambda = 1$. Hence, one has $\beta'_\ell = \beta_\ell$ and $\delta'_\ell = \delta_\ell$, for all $\ell = 1, 2, \dots, L$.

Therefore, from the above one gets that $\beta'_\ell = \beta_\ell, \gamma' = \gamma$ and $\delta'_\ell = \delta_\ell, \forall \ell$. Now, consider that $\alpha(\mathbf{I} - \sum_{\ell=1}^L \beta_\ell \mathbf{W}_\ell)^{-1}\iota = \alpha'(\mathbf{I} - \sum_{\ell=1}^L \beta_\ell \mathbf{W}_\ell)^{-1}\iota$ implies that $\alpha = \alpha'$. Hence, the social effects $\alpha, \beta_\ell, \gamma$, and δ_ℓ in (1.1) are identified for all $\ell \in \{1, 2, \dots, L\}$. \square

Proof of Theorem 2: Recall that by equation (1.7) in the main text, the Generalized Two-Stage Least Squares (G2SLS) estimator of the structural parameters is $\widehat{\boldsymbol{\psi}}_{\text{G2SLS}} = (\widehat{\mathbf{Z}}^\top \mathbf{D})^{-1} \widehat{\mathbf{Z}}^\top \mathbf{y}$. This can be rewritten as $\widehat{\boldsymbol{\psi}}_{\text{G2SLS}} - \boldsymbol{\psi} = (\widehat{\mathbf{Z}}^\top \mathbf{D})^{-1} \widehat{\mathbf{Z}}^\top \mathbf{e}$, where $\mathbf{D} = [\iota, \mathbf{X}, \mathbf{W}_1\mathbf{y}, \mathbf{W}_1\mathbf{X}, \mathbf{W}_2\mathbf{y}, \mathbf{W}_2\mathbf{X}, \dots, \mathbf{W}_L\mathbf{y}, \mathbf{W}_L\mathbf{X}]$ and $\widehat{\mathbf{Z}}$ is defined as in equation (1.6) in the main text. Now, under the Assumptions 3–6 in the main text, Lemmas 4, 5, and 6 it follows that $n^{-1} \widehat{\mathbf{Z}}^\top \mathbf{e} \xrightarrow{p} \mathbf{0}$. Similarly, by Lemma 4 and the continuous mapping theorem one also has $n^{-1} \widehat{\mathbf{Z}}^\top \mathbf{D} = O_p(1)$. Therefore $\widehat{\boldsymbol{\psi}}_{\text{G2SLS}} \xrightarrow{p} \boldsymbol{\psi}$.

Next, applying the same arguments as in the proof of Lemma 6, one has

$$n^{-1/2} \mathbf{Z}^\top \mathbf{e} \xrightarrow{d} N(\mathbf{0}, \mathbf{\Omega}) \quad (1.11)$$

where $\mathbf{\Omega} = \lim_{n \rightarrow \infty} n^{-1} \sum_{i=1}^n \mathbf{z}_i \mathbf{z}_i^\top E_{\mathbf{Z}}[e_i^2]$, which can be written equivalently as $\mathbf{\Omega} = \lim_{n \rightarrow \infty} n^{-1} \sum_{i=1}^n \mathbf{z}_i \mathbf{z}_i^\top E_{\mathbf{X}, \mathbf{W}_1, \mathbf{W}_2, \dots, \mathbf{W}_L}[e_i^2]$, and consequently

$$n^{-1/2} (\widehat{\boldsymbol{\psi}}_{\text{G2SLS}} - \boldsymbol{\psi}) \xrightarrow{d} \mathbf{Q}_{\text{ZD}}^{-1} \times N(\mathbf{0}, \mathbf{\Omega}) \\ N(\mathbf{0}, \mathbf{Q}_{\text{ZD}}^{-1} \mathbf{\Omega} \mathbf{Q}_{\text{DZ}}^{-1}).$$

□

1.8 Appendix: Auxiliary Results

Lemma 1. *The $n \times n$ matrix, $\mathbf{I} - \sum_{\ell=1}^L \beta_\ell \mathbf{W}_\ell$, is invertible for any scalar $\beta_\ell, \forall \ell$, such that $\sum_{\ell=1}^L |\beta_\ell| < 1$, where \mathbf{I} represents an identity matrix of order n .*

Proof of Lemma 1: First note that in the case where $\beta_1 = \beta_2 = \dots = \beta_L = 0$, one is left with \mathbf{I} which is invertible. Second, consider setting $\lambda = \sum_{\ell=1}^L |\beta_\ell|$, where if $\lambda = 0$ one has $\sum_{\ell=1}^{L-1} |\beta_\ell| = -|\beta_L|$ which implies $\beta_1 = \beta_2 = \dots = \beta_L = 0$, so clearly $\lambda \neq 0$. Hence, one can write

$$\mathbf{I} - \sum_{\ell=1}^L \beta_\ell \mathbf{W}_\ell = \mathbf{I} - \lambda \sum_{\ell=1}^L \frac{\beta_\ell}{\sum_{\ell=1}^L |\beta_\ell|} \mathbf{W}_\ell,$$

where one can show that $\mathbf{W} \equiv \sum_{\ell=1}^L \frac{\beta_\ell}{\sum_{\ell=1}^L |\beta_\ell|} \mathbf{W}_\ell$ has $\sum_{j=1, i \neq j}^n |\omega_{ij}| \leq 1$ of each row. Note that

\mathbf{W} is not necessarily a stochastic matrix, since it is not guaranteed that it has non-negative entries. Therefore, using [Gerschgorin's \(1931\) Circle Theorem](#) for the eigenvalues of \mathbf{W} , e_j , it holds that $|e_j| \leq 1$. Also, it might be the case that some eigenvalues are complex numbers. In that case, in order for $\mathbf{I} - \sum_{\ell=1}^L \beta_\ell \mathbf{W}_\ell$ to be invertible (regarding the complex eigenvalues) one needs that $1 - \alpha_j \lambda \neq 0$, where α_j is the real part of the complex e_j . Therefore since $|e_j| \leq 1$ one has that $|e'_j| \leq 1$, where e'_j are the real eigenvalues or the real parts of the complex eigenvalues. Now, given that

$$\det(\mathbf{I} - \lambda \mathbf{W}) \neq 0 \text{ when } \prod_j (1 - \lambda e'_j) \neq 0. \quad (1.12)$$

and since $|e'_j| \leq 1$, one can conclude that $|\lambda| < 1$, i.e. $|\sum_{\ell=1}^L \beta_\ell| < 1$ which can be written equivalently as $\sum_{\ell=1}^L |\beta_\ell| < 1$. Thus, in general $\mathbf{I} - \sum_{\ell=1}^L \beta_\ell \mathbf{W}_\ell$ is invertible, if Assumption 1(a), i.e., $\sum_{\ell=1}^L |\beta_\ell| < 1$ holds. \square

Lemma 2. *Let Assumption 1 hold, then*

$$\left(\mathbf{I} - \sum_{\ell=1}^L \beta_\ell \mathbf{W}_\ell \right) \left(\mathbf{I} - \sum_{\ell=1}^L \beta'_\ell \mathbf{W}_\ell \right) = \left(\mathbf{I} - \sum_{\ell=1}^L \beta'_\ell \mathbf{W}_\ell \right) \left(\mathbf{I} - \sum_{\ell=1}^L \beta_\ell \mathbf{W}_\ell \right).$$

Proof of Lemma 2. First, note that by Assumption 1 one has the following cases for all $\ell = 1, 2, \dots, L$: (1) $\beta_\ell \neq 0$, $\boldsymbol{\delta}_\ell, \boldsymbol{\gamma} \neq \vec{0}$, $\forall \ell$, (2) $\beta_1 \neq 0$, at least one $\beta_\ell = 0$, $\forall \ell \neq 1$, and at least one $|\boldsymbol{\gamma} \beta_\ell + \boldsymbol{\delta}_\ell| \neq \vec{0}$, $\forall \ell$, (3) $\beta_1 \neq 0$, at least one $\boldsymbol{\delta}_\ell = \vec{0}$, and at least one $|\boldsymbol{\gamma} \beta_\ell + \boldsymbol{\delta}_\ell| \neq \vec{0}$, $\forall \ell$, (4) $\beta_1 \neq 0$, at least one $\beta_\ell = 0$ and at least one $\boldsymbol{\delta}_\ell = \vec{0}$, $\forall \ell \neq 1$, as well as at least one $|\boldsymbol{\gamma} \beta_\ell + \boldsymbol{\delta}_\ell| \neq \vec{0}$, $\forall \ell$.

In case (1), the equation of interest can be written as follows,

$$\sum_{\ell=1}^L \sum_{\ell'=1, \ell'>\ell}^L (\beta_{\ell}\beta_{\ell}' - \beta_{\ell}'\beta_{\ell}) \mathbf{W}_{\ell}\mathbf{W}_{\ell}' = \sum_{\ell=1}^L \sum_{\ell'=1, \ell'>\ell}^L (\beta_{\ell}\beta_{\ell}' - \beta_{\ell}'\beta_{\ell}) \mathbf{W}_{\ell}'\mathbf{W}_{\ell},$$

where $\mathbf{W}_{\ell}\mathbf{W}_{\ell}' \neq \mathbf{W}_{\ell}'\mathbf{W}_{\ell}$. So, in order for the above equation to hold, one can impose Assumption 1(a) which implies that $\beta_{\ell} = c_{\ell}\beta_1, \forall \ell \in \{2, 3, \dots, L\}$, for any $|c_{\ell}| < +\infty$. Making this assumption along with the fact that both parameter sets $(\alpha, \beta_{\ell}, \gamma, \delta_{\ell})$ and $(\alpha', \beta_{\ell}', \gamma', \delta_{\ell}')$ lead to the same model imply $c_{\ell} = c_{\ell}'$ and $c_{\ell'} = c_{\ell}'$, $\forall \ell \neq \ell'$, where $\ell, \ell' = 2, 3, \dots, L$. That said and given the above assumption, one has that the equation $\beta_{\ell}\beta_{\ell}' = \beta_{\ell}'\beta_{\ell}$ holds, meaning that $(\beta_{\ell}/\beta_1)(\beta_{\ell}'/\beta_1) = (\beta_{\ell}'/\beta_1)(\beta_{\ell}/\beta_1)$ holds, or, equivalently, that $c_{\ell}c_{\ell}' = c_{\ell}'c_{\ell}$ holds, because $c_{\ell} = c_{\ell}'$ and $c_{\ell'} = c_{\ell}'$.

Similarly, arguments apply to cases (2), (3), and (4) concluding the proof. \square

Lemma 3. (Series Expansion) *Let Assumptions 1 and 2 hold, then a series expansion of (1.9) can be written as*

$$\begin{aligned} \mathbf{y} = & \alpha \sum_{r=0}^{\infty} \beta_1^r \mathbf{W}^r \boldsymbol{\iota} + \mathbf{X}\boldsymbol{\gamma} + \sum_{\ell=1}^L \left[\sum_{r=0}^{\infty} \beta_{\ell}^r \mathbf{W}_{\ell}^{r+1} \right] \mathbf{X}(\boldsymbol{\delta}_{\ell} + \boldsymbol{\gamma}\beta_{\ell}) \\ & + \sum_{\ell=1}^L \sum_{\ell'=1, \ell' \neq \ell}^L \left[\sum_{r=0}^{\infty} \sum_{r'=0}^{\infty} \beta_{\ell'}^{r+1} \beta_{\ell}^{r'+1} \mathbf{W}_{\ell'}^{r+1} \mathbf{W}_{\ell}^{r'+1} \right] \mathbf{X}(\boldsymbol{\delta}_{\ell} + \boldsymbol{\gamma}\beta_{\ell}) + \dots + \sum_{r=0}^{\infty} \beta_1^r \mathbf{W}^r \mathbf{e}, \end{aligned}$$

where $\beta_1 \neq 0$, $\mathbf{W} \equiv \mathbf{W}_1 + \sum_{\ell=1}^L (\beta_{\ell}/\beta_1) \mathbf{W}_{\ell}$ for all $\ell = 2, 3, \dots, L$.

Proof of Lemma 3. By equation (1.9) one has

$$\mathbf{y} = \alpha(\mathbf{I} - \sum_{\ell=1}^L \beta_{\ell} \mathbf{W}_{\ell})^{-1} \boldsymbol{\iota} + (\mathbf{I} - \sum_{\ell=1}^L \beta_{\ell} \mathbf{W}_{\ell})^{-1} (\mathbf{X}\boldsymbol{\gamma} + \sum_{\ell=1}^L \mathbf{W}_{\ell} \mathbf{X} \boldsymbol{\delta}_{\ell}) + \\ + (\mathbf{I} - \sum_{\ell=1}^L \beta_{\ell} \mathbf{W}_{\ell})^{-1} \mathbf{e},$$

which, given Assumption 1(a), can be written as

$$\mathbf{y} = \alpha(\mathbf{I} - \beta_1 \mathbf{W})^{-1} \boldsymbol{\iota} + (\mathbf{I} - \beta_1 \mathbf{W})^{-1} (\mathbf{X}\boldsymbol{\gamma} + \sum_{\ell=1}^L \mathbf{W}_{\ell} \mathbf{X} \boldsymbol{\delta}_{\ell}) + (\mathbf{I} - \beta_1 \mathbf{W})^{-1} \mathbf{e},$$

where $\beta_1 \neq 0$, $\mathbf{W} \equiv \mathbf{W}_1 + \sum_{\ell=1}^L \frac{\beta_{\ell}}{\beta_1} \mathbf{W}_{\ell}$ for all $\ell = 2, 3, \dots, L$. Given that $(\mathbf{I} - \beta_1 \mathbf{W})^{-1} = \sum_{r=0}^{\infty} \beta_1^r \mathbf{W}^r$, one has

$$\mathbf{y} = \alpha \sum_{r=0}^{\infty} \beta_1^r \mathbf{W}^r \boldsymbol{\iota} + \sum_{r=0}^{\infty} \beta_1^r \mathbf{W}^r (\mathbf{X}\boldsymbol{\gamma} + \sum_{\ell=1}^L \mathbf{W}_{\ell} \mathbf{X} \boldsymbol{\delta}_{\ell}) + \sum_{r=0}^{\infty} \beta_1^r \mathbf{W}^r \mathbf{e}.$$

By opening the summations of the second term on the right hand side of the equation above and after expanding these terms, then the series expansion of equation (1.9) for $\beta_1, \beta_2, \dots, \beta_L \neq 0$ can be expressed as follows

$$\mathbf{y} = \alpha \sum_{r=0}^{\infty} \beta_1^r \mathbf{W}^r \boldsymbol{\iota} + \boldsymbol{\gamma} \mathbf{X} + \sum_{\ell=1}^L \left[\sum_{r=0}^{\infty} \beta_{\ell}^r \mathbf{W}_{\ell}^{r+1} \right] \mathbf{X} (\boldsymbol{\delta}_{\ell} + \boldsymbol{\gamma} \beta_{\ell}) \\ + \sum_{\ell=1}^L \sum_{\ell'=1, \ell' \neq \ell}^L \left[\sum_{r=0}^{\infty} \sum_{r'=0}^{\infty} \beta_{\ell'}^{r+1} \beta_{\ell}^{r'} \mathbf{W}_{\ell'}^{r+1} \mathbf{W}_{\ell}^{r'+1} \right] \mathbf{X} (\boldsymbol{\delta}_{\ell} + \boldsymbol{\gamma} \beta_{\ell}) + \dots + \sum_{r=0}^{\infty} \beta_1^r \mathbf{W}^r \mathbf{e}. \quad (1.13)$$

This means that except for using Assumptions 1(a) and 1(b), the series expansion implies that there must exist at least one $|\boldsymbol{\delta}_{\ell} + \boldsymbol{\gamma} \beta_{\ell}| \neq \vec{0}$. This is a restriction that can be equivalently

expressed by Assumption 1(c). Thus, the restrictions for the structural parameters can be fully characterized by Assumption 1. \square

Lemma 4. (Consistency of $\widehat{\psi}_{2SLS}$) *Let Assumptions 1–6 hold, then $\widehat{\psi}_{2SLS} \xrightarrow{p} \psi$.*

Proof of Lemma 4. From equation (1.4), the 2SLS estimator can be written as

$$\widehat{\psi}_{2SLS} = \psi + [\mathbf{D}^\top \mathbf{Z} (\mathbf{Z}^\top \mathbf{Z})^{-1} \mathbf{Z}^\top \mathbf{D}]^{-1} \mathbf{D}^\top \mathbf{Z} (\mathbf{Z}^\top \mathbf{Z})^{-1} \mathbf{Z}^\top \mathbf{e}. \quad (1.14)$$

Recall that $\mathbf{D} = [I, \mathbf{X}, \mathbf{W}_1 \mathbf{y}, \mathbf{W}_1 \mathbf{X}, \mathbf{W}_2 \mathbf{y}, \mathbf{W}_2 \mathbf{X}, \dots, \mathbf{W}_L \mathbf{y}, \mathbf{W}_L \mathbf{X}]$, $\psi = (\alpha, \gamma, \boldsymbol{\theta}_1^\top, \boldsymbol{\theta}_2^\top, \dots, \boldsymbol{\theta}_L^\top)^\top$ and

$$\begin{aligned} \mathbf{Z} = & [I, \mathbf{X}, \mathbf{W}_1 \mathbf{X}, \mathbf{W}_2 \mathbf{X}, \dots, \mathbf{W}_L \mathbf{X}, \mathbf{W}_1^2 \mathbf{X}, \mathbf{W}_2^2 \mathbf{X}, \dots, \mathbf{W}_L^2 \mathbf{X}, \mathbf{W}_1 \mathbf{W}_2 \mathbf{X}, \\ & \mathbf{W}_1 \mathbf{W}_3 \mathbf{X}, \dots, \mathbf{W}_1 \mathbf{W}_L \mathbf{X}, \mathbf{W}_2 \mathbf{W}_1 \mathbf{X}, \mathbf{W}_2 \mathbf{W}_3 \mathbf{X}, \dots, \mathbf{W}_2 \mathbf{W}_L \mathbf{X}, \\ & \dots, \mathbf{W}_L \mathbf{W}_1 \mathbf{X}, \mathbf{W}_L \mathbf{W}_2 \mathbf{X}, \dots, \mathbf{W}_L \mathbf{W}_{L-1} \mathbf{X}]. \end{aligned}$$

By Assumption 3 and the continuous mapping theorem as $n \rightarrow \infty$,

$$\begin{aligned} [n^{-1} \mathbf{D}^\top \mathbf{Z} (n^{-1} \mathbf{Z}^\top \mathbf{Z})^{-1} n^{-1} \mathbf{Z}^\top \mathbf{D}]^{-1} n^{-1} \mathbf{D}^\top \mathbf{Z} (n^{-1} \mathbf{Z}^\top \mathbf{Z})^{-1} & \xrightarrow{p} \\ & (\mathbf{Q}_{\mathbf{ZD}}^\top \mathbf{Q}_{\mathbf{ZZ}}^{-1} \mathbf{Q}_{\mathbf{ZD}})^{-1} \mathbf{Q}_{\mathbf{ZD}}^\top \mathbf{Q}_{\mathbf{ZZ}}^{-1}, \end{aligned}$$

which is finite by Assumption 3. Moreover, by Assumption 5 and the law of iterated expectations $E[\mathbf{Z}^\top \mathbf{e}] = \mathbf{0}$, where

$$\begin{aligned}
\mathbf{Z}^\top \mathbf{e} = & \left[\sum_{i=1}^n e_i, \mathbf{X}^\top \mathbf{e}, (\mathbf{W}_1 \mathbf{X})^\top \mathbf{e}, (\mathbf{W}_2 \mathbf{X})^\top \mathbf{e}, \dots, (\mathbf{W}_L \mathbf{X})^\top \mathbf{e}, (\mathbf{W}_1^2 \mathbf{X})^\top \mathbf{e}, \right. \\
& (\mathbf{W}_2^2 \mathbf{X})^\top \mathbf{e}, \dots, (\mathbf{W}_L^2 \mathbf{X})^\top \mathbf{e}, (\mathbf{W}_1 \mathbf{W}_2 \mathbf{X})^\top \mathbf{e}, (\mathbf{W}_1 \mathbf{W}_3 \mathbf{X})^\top \mathbf{e}, \dots, \\
& (\mathbf{W}_1 \mathbf{W}_L \mathbf{X})^\top \mathbf{e}, (\mathbf{W}_2 \mathbf{W}_1 \mathbf{X})^\top \mathbf{e}, (\mathbf{W}_2 \mathbf{W}_3 \mathbf{X})^\top \mathbf{e}, \dots, (\mathbf{W}_2 \mathbf{W}_L \mathbf{X})^\top \mathbf{e}, \\
& \left. (\mathbf{W}_L \mathbf{W}_1 \mathbf{X})^\top \mathbf{e}, (\mathbf{W}_L \mathbf{W}_2 \mathbf{X})^\top \mathbf{e}, \dots, (\mathbf{W}_L \mathbf{W}_{L-1} \mathbf{X})^\top \mathbf{e} \right]^\top.
\end{aligned}$$

In order to show that $n^{-1} \mathbf{Z}^\top \mathbf{e} \xrightarrow{p} E[\mathbf{Z}^\top \mathbf{e}]$, it suffices to show that all components of the vector $n^{-1} \mathbf{Z}^\top \mathbf{e}$ converge in probability to $E[\mathbf{Z}^\top \mathbf{e}]$. For this purpose, one can find the variance of the components of the vector

$$\text{var}_{\mathbf{X}, \mathbf{W}_1, \mathbf{W}_2, \dots, \mathbf{W}_L} \left[n^{-1} \sum_{i=1}^n e_i \right] = n^{-2} E_{\mathbf{X}, \mathbf{W}_1, \mathbf{W}_2, \dots, \mathbf{W}_L} \left(\sum_{i=1}^n e_i \right)^2 = \frac{1}{n^2} \sum_{i=1}^n \sigma_{e_i}^2,$$

where the second equality above follows by Assumption 5.

First, one has that $n^{-1} \sum_{i=1}^n \sigma_{e_i}^2 = O(1)$ by Assumption 5, thus one has $n^{-2} \sum_{i=1}^n \sigma_{e_i}^2 = o(1)$. Next, consider that conditioning on the realizations of $\mathbf{X}, \mathbf{W}_1, \mathbf{W}_2, \dots, \mathbf{W}_L$, one also has

$$\text{var}_{\mathbf{X}, \mathbf{W}_1, \mathbf{W}_2, \dots, \mathbf{W}_L} [n^{-1} \mathbf{X}^\top \mathbf{e}] = \frac{1}{n^2} \sum_{i=1}^n x_{ji}^2 \sigma_{e_i}^2, \tag{1.15}$$

$$\text{var}_{\mathbf{X}, \mathbf{W}_1, \mathbf{W}_2, \dots, \mathbf{W}_L} [n^{-1} (\mathbf{W}_\ell \mathbf{X})^\top \mathbf{e}] = \frac{1}{n^2} \sum_{i=1}^n \bar{x}_{\ell, j(i)}^2 \sigma_{e_i}^2, \tag{1.16}$$

$$\text{var}_{\mathbf{X}, \mathbf{w}_1, \mathbf{w}_2, \dots, \mathbf{w}_L} \left[n^{-1} (\mathbf{W}_\ell^2 \mathbf{X})^\top \mathbf{e} \right] = \frac{1}{n^2} \sum_{i=1}^n \bar{x}_{\ell 2, j(i)}^2 \sigma_{e_i}^2, \quad (1.17)$$

$$\text{var}_{\mathbf{X}, \mathbf{w}_1, \mathbf{w}_2, \dots, \mathbf{w}_L} \left[n^{-1} (\mathbf{W}_\ell \mathbf{W}_{\ell'} \mathbf{X})^\top \mathbf{e} \right] = \frac{1}{n^2} \sum_{i=1}^n \bar{x}_{\ell \ell', j(i)}^2 \sigma_{e_i}^2, \quad (1.18)$$

for all $\ell = 1, 2, \dots, L$ and $\ell \neq \ell' = 1, 2, \dots, L$, where $\bar{x}_{\ell, j(i)} = \mathbf{w}_{i, \ell} \mathbf{x}_j$ represents the average of individual's i connections in the j th characteristic, $\bar{x}_{\ell 2, j(i)} = \mathbf{w}_{i, \ell}^2 \mathbf{x}_j$ is the average of individual's i indirect connections in the j th characteristic and $\bar{x}_{\ell \ell', j(i)} = \mathbf{w}_{i, \ell} \mathbf{w}_{i, \ell'} \mathbf{x}_j$ is the average of individual's i indirect connections involving both layers ℓ, ℓ' in the j th characteristic. The regressors and the adjacency matrices are bounded given Assumptions 2 and 6. Therefore, terms (1.15)–(1.18) are $o(1)$.

Using the Chebychev's inequality $\forall \varepsilon > 0$ along with 1.15–1.18, one has as $n \rightarrow \infty$,

$$\Pr_{\mathbf{X}, \mathbf{w}_1, \mathbf{w}_2, \dots, \mathbf{w}_L} \{ |n^{-1} \mathbf{X}^\top \mathbf{e}| > \varepsilon \} \leq \frac{\text{var}_{\mathbf{X}, \mathbf{w}_1, \mathbf{w}_2, \dots, \mathbf{w}_L} [n^{-1} \mathbf{X}^\top \mathbf{e}]}{\varepsilon^2} \rightarrow 0, \quad (1.19)$$

$$\begin{aligned} \Pr_{\mathbf{X}, \mathbf{w}_1, \mathbf{w}_2, \dots, \mathbf{w}_L} \{ |n^{-1} (\mathbf{W}_\ell \mathbf{X})^\top \mathbf{e}| > \varepsilon \} &\leq \\ &\frac{\text{var}_{\mathbf{X}, \mathbf{w}_1, \mathbf{w}_2, \dots, \mathbf{w}_L} [n^{-1} (\mathbf{W}_\ell \mathbf{X})^\top \mathbf{e}]}{\varepsilon^2} \rightarrow 0, \end{aligned} \quad (1.20)$$

$$\begin{aligned} \Pr_{\mathbf{X}, \mathbf{w}_1, \mathbf{w}_2, \dots, \mathbf{w}_L} \{ |n^{-1} (\mathbf{W}_\ell^2 \mathbf{X})^\top \mathbf{e}| > \varepsilon \} &\leq \\ &\frac{\text{var}_{\mathbf{X}, \mathbf{w}_1, \mathbf{w}_2, \dots, \mathbf{w}_L} [n^{-1} (\mathbf{W}_\ell^2 \mathbf{X})^\top \mathbf{e}]}{\varepsilon^2} \rightarrow 0, \end{aligned} \quad (1.21)$$

$$\Pr_{\mathbf{X}, \mathbf{w}_1, \mathbf{w}_2, \dots, \mathbf{w}_L} \{ |n^{-1} (\mathbf{W}_\ell \mathbf{W}_{\ell'} \mathbf{X})^\top \mathbf{e}| > \varepsilon \} \leq \frac{\text{var}_{\mathbf{X}, \mathbf{w}_1, \mathbf{w}_2, \dots, \mathbf{w}_L} \left[n^{-1} (\mathbf{W}_\ell \mathbf{W}_{\ell'} \mathbf{X})^\top \mathbf{e} \right]}{\varepsilon^2} \rightarrow 0. \quad (1.22)$$

Therefore, 1.19–1.22 imply that $n^{-1} \mathbf{Z}^\top \mathbf{e} \xrightarrow{p} 0$ and $\widehat{\boldsymbol{\psi}}_{\text{SLS}} = \boldsymbol{\psi} + o_p(1)$ proving the result. \square

Lemma 5. (Consistency of $\widehat{\boldsymbol{\theta}}$) *Let Assumptions 1–6 hold, then $\widehat{\boldsymbol{\theta}} \xrightarrow{p} \boldsymbol{\theta}$.*

Proof of Lemma 5. The results follows from Lemma 4 and the continuous mapping theorem. \square

Lemma 6. *Let Assumptions 3–6 hold, then $n^{-1/2} \widehat{\mathbf{Z}}^\top \mathbf{e} = n^{-1/2} \mathbf{Z}^\top \mathbf{e} + o_p(1)$.*

Proof of Lemma 6. Consider the definition of $\widehat{\mathbf{Z}}$ as in equation (1.6). It is sufficient to show that

$$n^{-1/2} (\widehat{\mathbf{Z}} - \mathbf{Z})^\top \mathbf{e} = o_p(1) \quad (1.23)$$

First, in order to show equation (1.23), note that

$$\begin{aligned} \widehat{\mathbf{Z}} - \mathbf{Z} = & [\mathbf{0}, \mathbf{O}, \delta E_{\mathbf{X}, \mathbf{w}_1, \mathbf{w}_2, \dots, \mathbf{w}_L} [\mathbf{W}_1 \mathbf{y}] (\widehat{\boldsymbol{\psi}}), \delta E_{\mathbf{X}, \mathbf{w}_1, \mathbf{w}_2, \dots, \mathbf{w}_L} [\mathbf{W}_2 \mathbf{y}] (\widehat{\boldsymbol{\psi}}), \dots, \\ & \delta E_{\mathbf{X}, \mathbf{w}_1, \mathbf{w}_2, \dots, \mathbf{w}_L} [\mathbf{W}_L \mathbf{y}] (\widehat{\boldsymbol{\psi}}), \mathbf{O}, \mathbf{O}, \dots, \mathbf{O}], \end{aligned}$$

where $\mathbf{0}$ represents a $n \times 1$ vector of zeroes, \mathbf{O} is a $n \times K$ matrix of zeroes, and $\delta E_{\mathbf{X}, \mathbf{w}_1, \mathbf{w}_2, \dots, \mathbf{w}_L} [\mathbf{W}_\ell \mathbf{y}] = E_{\mathbf{X}, \mathbf{w}_1, \mathbf{w}_2, \dots, \mathbf{w}_L} [\mathbf{W}_\ell \mathbf{y}] (\widehat{\boldsymbol{\psi}}) - E_{\mathbf{X}, \mathbf{w}_1, \mathbf{w}_2, \dots, \mathbf{w}_L} [\mathbf{W}_\ell \mathbf{y}] (\boldsymbol{\psi})$, for all $\ell = 1, 2, \dots, L$. From equation (1.2) in the main text, one can write $\mathbf{y} \left(\mathbf{I} - \sum_{\ell=1}^L \beta_\ell \mathbf{W}_\ell \right) = \boldsymbol{\alpha}' + \sum_{\ell=1}^L \mathbf{W}_\ell \mathbf{X} \boldsymbol{\delta}_\ell +$

$\mathbf{X}\boldsymbol{\gamma} + \mathbf{e} \equiv \mathbf{D}\boldsymbol{\phi} + \mathbf{e}$, where $\mathbf{D} = [\boldsymbol{\iota}, \mathbf{X}, \mathbf{W}_1\mathbf{Y}, \mathbf{W}_1\mathbf{X}, \mathbf{W}_2\mathbf{Y}, \mathbf{W}_2\mathbf{X}, \dots, \mathbf{W}_L\mathbf{Y}, \mathbf{W}_L\mathbf{X}]$ and $\boldsymbol{\phi} = (\alpha, \boldsymbol{\delta}_1, \boldsymbol{\delta}_2, \dots, \boldsymbol{\delta}_L, \boldsymbol{\gamma})^\top$. Under Assumptions 1, 5, and using series expansion, for all $\ell = 1, 2, \dots, L$, one can write

$$E_{\mathbf{X}, \mathbf{W}_1, \mathbf{W}_2, \dots, \mathbf{W}_L}[\mathbf{W}_\ell \mathbf{Y}](\boldsymbol{\psi}) = \mathbf{W}_\ell \left(\mathbf{I} - \sum_{\ell=1}^L \beta_\ell \mathbf{W}_\ell \right)^{-1} \mathbf{D}\boldsymbol{\phi} = \mathbf{W}_\ell \sum_{q=0}^{\infty} \lambda^q \mathbf{W}^q \mathbf{D}\boldsymbol{\phi},$$

where $\lambda = \sum_{\ell=1}^L |\beta_\ell|$ and $\mathbf{W} \equiv \sum_{\ell=1}^L \frac{\beta_\ell}{\sum_{\ell=1}^L |\beta_\ell|} \mathbf{W}_\ell$. Thus, this implies

$$\begin{aligned} E_{\mathbf{X}, \mathbf{W}_1, \mathbf{W}_2, \dots, \mathbf{W}_L}[\mathbf{W}_\ell \mathbf{Y}](\boldsymbol{\psi}) &= \mathbf{W}_\ell \mathbf{D}\boldsymbol{\phi} + \mathbf{W}_\ell \mathbf{W} \mathbf{D}\boldsymbol{\phi} \lambda \\ &\quad + \mathbf{W}_\ell \mathbf{W}^2 \mathbf{D}\boldsymbol{\phi} \lambda^2 + \mathbf{W}_\ell \mathbf{W}^3 \mathbf{D}\boldsymbol{\phi} \lambda^3 + \dots \end{aligned}$$

Then, one can write

$$\begin{aligned} \boldsymbol{\delta} E_{\mathbf{X}, \mathbf{W}_1, \mathbf{W}_2, \dots, \mathbf{W}_L}[\mathbf{W}_\ell \mathbf{Y}]^\top &= (\widehat{\boldsymbol{\phi}}_{2\text{SLS}} - \boldsymbol{\phi})^\top (\mathbf{W}_\ell \mathbf{D})^\top \\ &\quad + (\widehat{\boldsymbol{\phi}}_{2\text{SLS}} \widehat{\lambda}_{2\text{SLS}} - \boldsymbol{\phi} \lambda)^\top (\mathbf{W}_\ell \mathbf{W} \mathbf{D})^\top + \dots, \end{aligned}$$

where $\widehat{\boldsymbol{\phi}}_{2\text{SLS}}$ and $\widehat{\lambda}_{2\text{SLS}}$ are elements of $\widehat{\boldsymbol{\psi}}_{2\text{SLS}}$. From the last equation, one has

$$\begin{aligned} \boldsymbol{\delta} E_{\mathbf{X}, \mathbf{W}_1, \mathbf{W}_2, \dots, \mathbf{W}_L}[\mathbf{W}_\ell \mathbf{Y}]^\top \mathbf{e} &= (\widehat{\boldsymbol{\phi}}_{2\text{SLS}} - \boldsymbol{\phi})^\top (\mathbf{W}_\ell \mathbf{D})^\top \mathbf{e} + (\widehat{\boldsymbol{\phi}}_{2\text{SLS}} \widehat{\lambda}_{2\text{SLS}} - \boldsymbol{\phi} \lambda)^\top \\ &\quad (\mathbf{W}_\ell \mathbf{W} \mathbf{D})^\top \mathbf{e} + \dots \end{aligned} \quad (1.24)$$

By Lemma 4 and the continuous mapping theorem, one has $(\widehat{\boldsymbol{\phi}}_{2\text{SLS}} \widehat{\lambda}_{2\text{SLS}} - \boldsymbol{\phi} \lambda) = o_p(1)$,

$\forall q \geq 1$. Now, it is required to bound the elements of the term $(\mathbf{W}_\ell \mathbf{W}^q \mathbf{D})^\top \mathbf{e}$, $\forall q \geq 1$. Moreover, the model's exogeneity assumption guarantees that $E_{\mathbf{X}, \mathbf{w}_1, \mathbf{w}_2, \dots, \mathbf{w}_L}[\mathbf{e}] = \mathbf{0}$. Therefore, $E_{\mathbf{X}, \mathbf{w}_1, \mathbf{w}_2, \dots, \mathbf{w}_L} \left[(\mathbf{W}_\ell \mathbf{W}^q \mathbf{D})^\top \mathbf{e} \right] = 0$, $q \geq 1$, which implies $\delta E_{\mathbf{X}, \mathbf{w}_1, \mathbf{w}_2, \dots, \mathbf{w}_L} [\mathbf{W}_\ell \mathbf{y}]^\top \mathbf{e} = o_p(1)$, for all $\ell = 1, 2, \dots, L$. This result along with the fact that the rest elements of $(\widehat{\mathbf{Z}} - \mathbf{Z})^\top \mathbf{e}$ are equal to zero, for all n , and therefore $o_p(1)$, imply $n^{-1/2} \left(\widehat{\mathbf{Z}} - \mathbf{Z} \right)^\top \mathbf{e} = o_p(1)$, $\forall \ell = 1, 2, \dots, L$, $\forall q \geq 1$.

By Assumption 5, one has that the innovations e_i are independent for each individual i with $E_{\mathbf{X}, \mathbf{w}_1, \mathbf{w}_2, \dots, \mathbf{w}_L} [e_i] = 0$, but they are not identically distributed. Note that for some $\xi > 0$, one can write $E |e_i|^{2+\xi} \leq \sup_{n,i} E |e_i|^{2+\xi} < \infty$, $\forall i = 1, \dots, n$, where the last inequality comes from Assumption 5. Thus, $\sup_{n,i} E |e_i|^{2+\xi} < \infty$. By the same Assumption, $\liminf_{n \rightarrow \infty} n^{-1} \sum_{i=1}^n \sigma_{e_i}^2 > 0$ which implies that

$$\liminf_{n \rightarrow \infty} n^{-1} \sum_{i=1}^n E_{\mathbf{X}, \mathbf{w}_1, \mathbf{w}_2, \dots, \mathbf{w}_L} [e_i^2] > 0$$

holds. Therefore, Lyapunov's condition holds and by the Lindeberg-Feller central limit theorem one has $n^{-1/2} (\mathbf{W}_\ell \mathbf{W}^q \mathbf{D})^\top \mathbf{e} = O_p(1)$ and $n^{-1/2} (\widehat{\mathbf{Z}} - \mathbf{Z})^\top \mathbf{e} = o_p(1)$, $\forall \ell = 1, 2, \dots, L$, $\forall q \geq 1$. □

1.9 Appendix: Monte Carlo Results

In this section one can find further Monte Carlo experiments, beyond what is discussed in the main text, exploring the small sample properties of the proposed G2SLS estimator described in Section ???. In particular, in what follows interest lies on how the estimator

performs as the number of layers, L , increases in (1.1) with $K = 1$, i.e., $\mathbf{W}_\ell = [w_{\ell;i,j}]$ for $\ell = 1, \dots, L$ and $L \in \{2, 3, 4\}$, and the values and signs of the structural parameters, $\boldsymbol{\psi} = (\alpha, \gamma, \beta_1, \beta_2, \dots, \beta_L, \delta_1, \delta_2, \dots, \delta_L)^\top$, can take as permitted by Assumptions 1 and 2. A total of 1,100 data sets, $\{y_i, x_i\}_{i=1}^n$ and $\{\{w_{\ell;i,j}\}_{i=1}^n\}_{j=1}^n, \forall \ell \in \{1, 2, 3, 4\}$, for $n \in \{50, 100, 200\}$ are generated from a combination of 2 different model specifications and network formation models as follows:

Specification 1 (S1): The parameter values of $\boldsymbol{\psi}$ are set to be all positive, i.e., $\alpha = 0.15$, $\gamma = 0.8$, $\beta_\ell = \frac{\phi}{L}$, where $\phi \in \{0.1, 0.9\}$ and $\delta_\ell = \frac{1}{L}, \forall L \in \{2, 3, 4\}$.

Specification 2 (S2): The parameter values of $\boldsymbol{\psi}$ are set to be $\alpha = 0.15$, $\gamma = 0.8$, $\beta_\ell = \sum_{\ell=1}^L (-1)^{\ell+1} \frac{\phi}{L}$, where $\phi \in \{0.1, 0.9\}$ and $\delta_\ell = \sum_{\ell=1}^L (-1)^{\ell+1} \frac{1}{L}, \forall L \in \{2, 3, 4\}$.

Recall that $w_{\ell;i,j} = w_{\ell;i,j}^* / \sum_{j=1}^n w_{\ell;i,j}^*$ with $w_{\ell;i,j}^*$ equals 1 if j is connected with i through a type- ℓ social tie. Below we describe how $\mathbf{W}_\ell^* = [w_{\ell;i,j}^*]$ for $\ell = 1, \dots, L$ and $L \in \{2, 3, 4\}$ are constructed.

Networks Formation Model 1 (M1): The $n \times n$ adjacency matrices $\mathbf{W}_\ell^* = [w_{\ell;i,j}^*]$ are such that \mathbf{W}_1^* is generated as an [Erdős and Rényi's \(1959\)](#) random graph with density 0.01, while the remaining adjacency matrices are defined as $w_{\ell;i,j}^* = w_{\ell-1;i,j}^* c_{1,\ell;i,j} + (1 - w_{\ell-1;i,j}^*) c_{2,\ell;i,j}$, for $i \neq j, \ell \in \{2, 3, 4\}$, where $c_{1,\ell;i,j}$, and $c_{2,\ell;i,j}$ are drawn independently from an independent Bernoulli distribution with parameters 0.5, and 0.99 respectively in each replication.

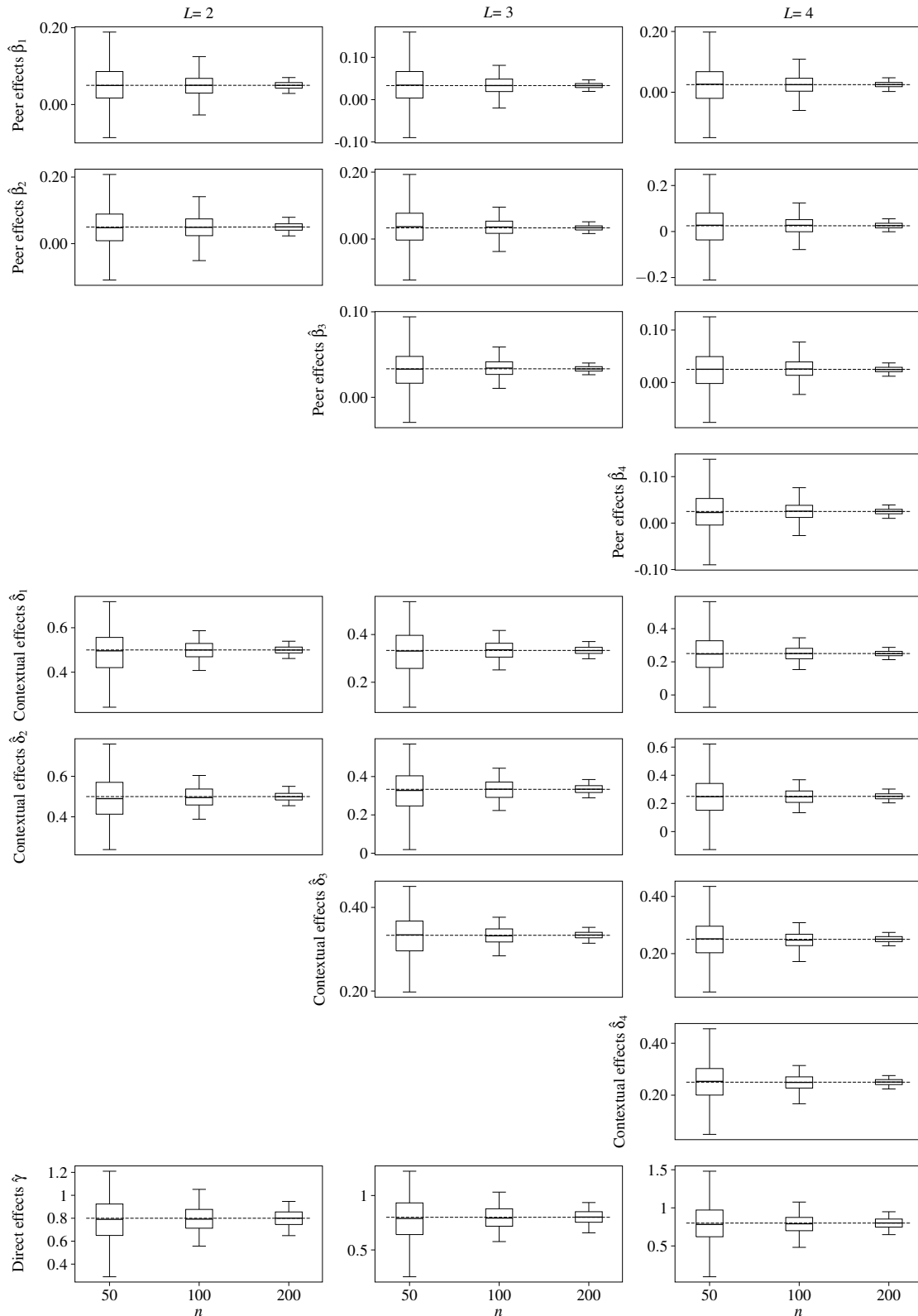
Networks Formation Model 2 (M2): Each adjacency matrix $\mathbf{W}_\ell^* = [w_{\ell;i,j}^*(\sigma)]$ has elements $w_{\ell;i,j}^*(\sigma) = \mathbb{I}[(-1)^{\ell-1} z_i z_j - v_{\ell;i,j} \geq 0], \forall \ell \in \{1, 2, 3, 4\}$, where $\mathbb{I}(\cdot)$ is an indicator function equal to one if its argument is true and zero otherwise. The variable $z \in \{-1, 1\}$ takes each value with probability 0.5, while $v_{\ell;i,j}$ is drawn from a logistic distribution with

mean zero and scale parameter 1.

Finally, the sequences $\{x_i\}_{i=1}^n$ and $\{e_i\}_{i=1}^n$ in (1.1) are generated from independent standard normal distributions.

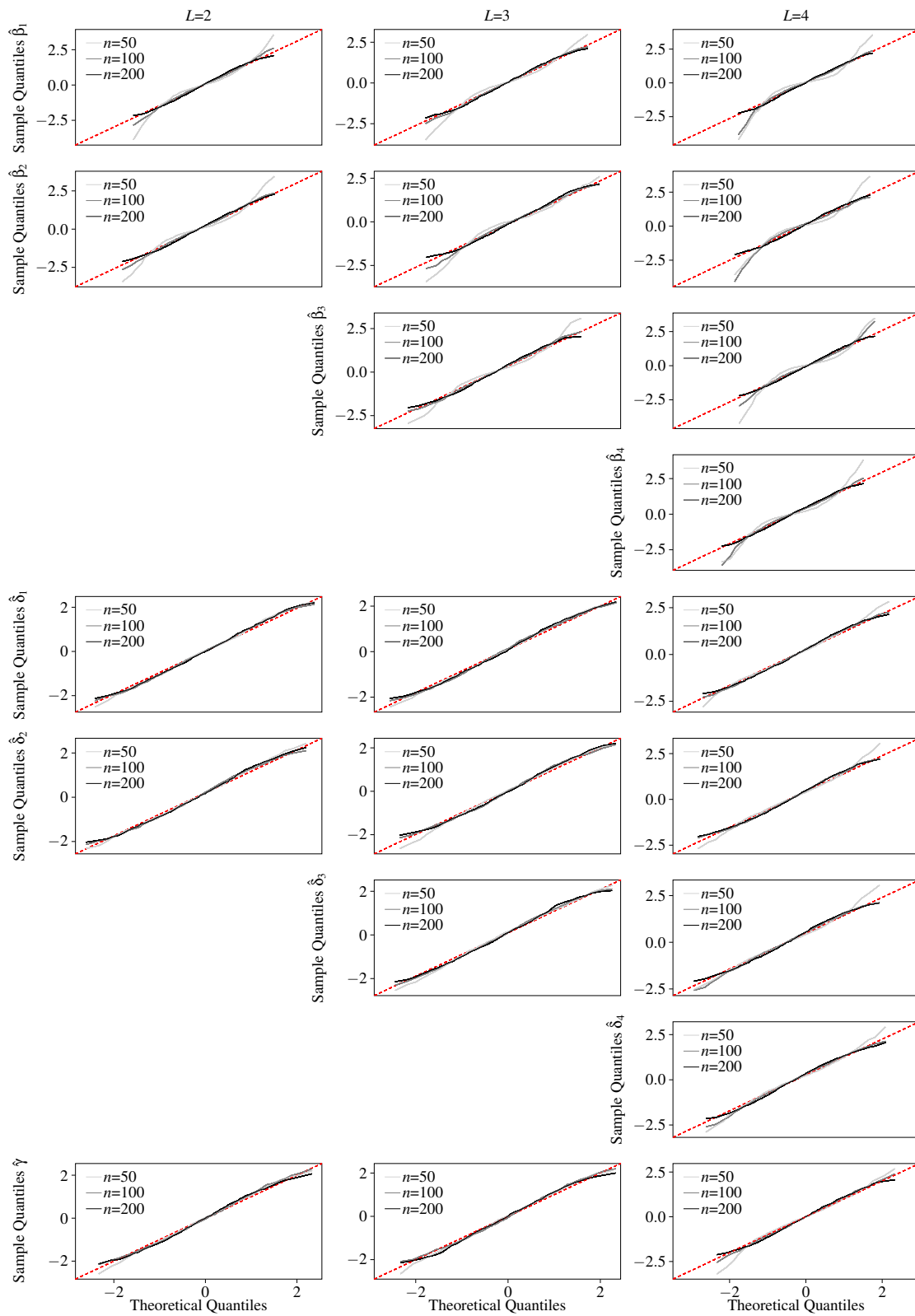
The results for specification S1 with both network formation models, M1 and M2, are shown in Figures 1.2, 1.3, 1.4, and 1.5, while those for model specification S2 with both network formation models, M1 and M2, are shown in Figures 1.6, 1.7, 1.8, and 1.9. Dashed horizontal lines in each box plot represent the true parameter values. Similar results for specification S1 can be found below. Overall, the small sample properties of the proposed G2SLS estimator of all parameters of interest are good, with little to no bias as sample size or the number of layers increases. The asymptotic normal approximation seems adequate even with a sample size of 50 observations and across the number of multilayers.

Figure 1.2: Monte Carlo Box Plots in S1 with M1



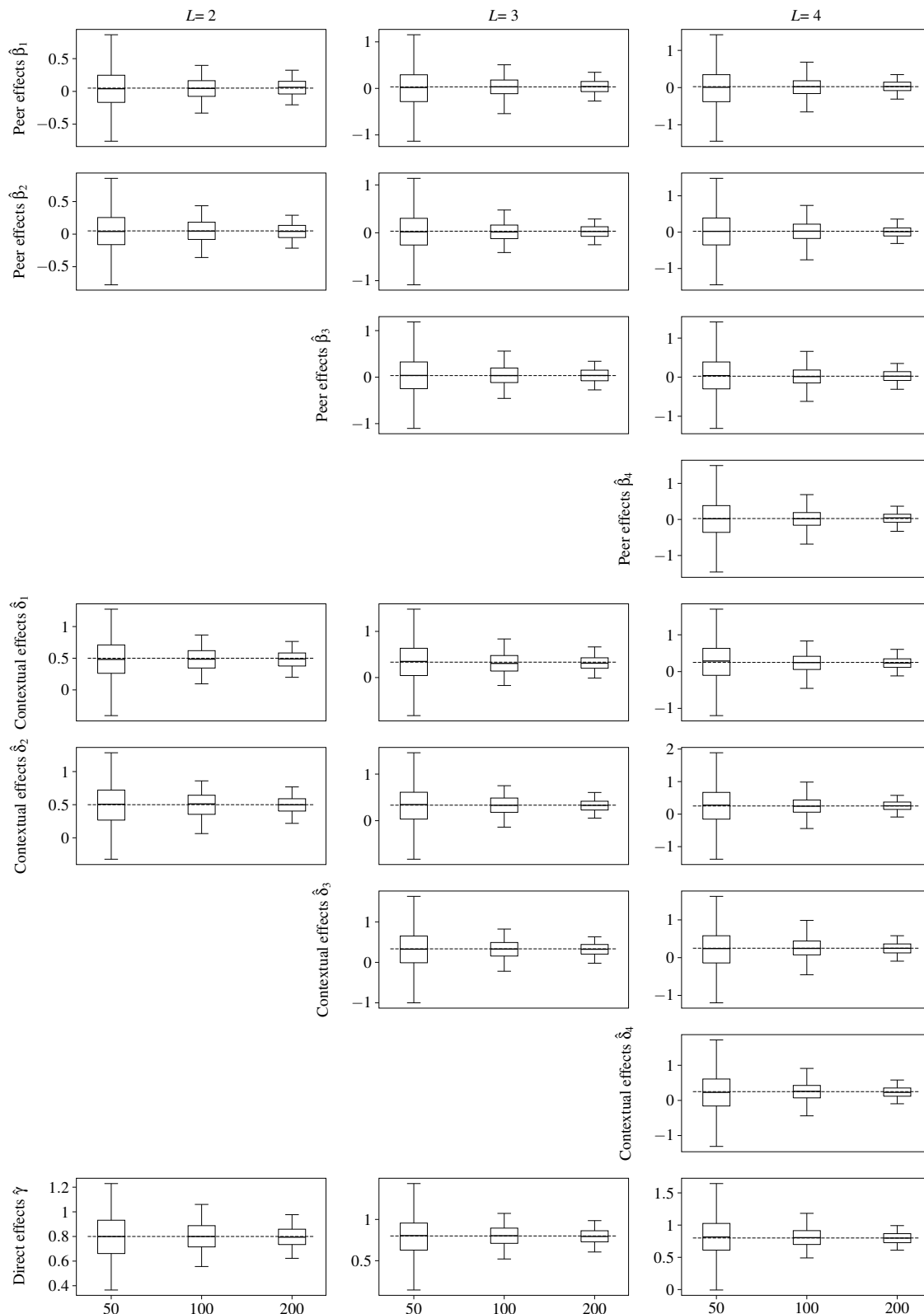
Note: Box plots for each sample size $n \in \{50, 100, 200\}$ for different number of layers $L = \{2, 3, 4\}$ are based on 1, 100 replications using model specification S1 with networks model formation M1.

Figure 1.3: Monte Carlo Q-Q Plots in S1 with M1



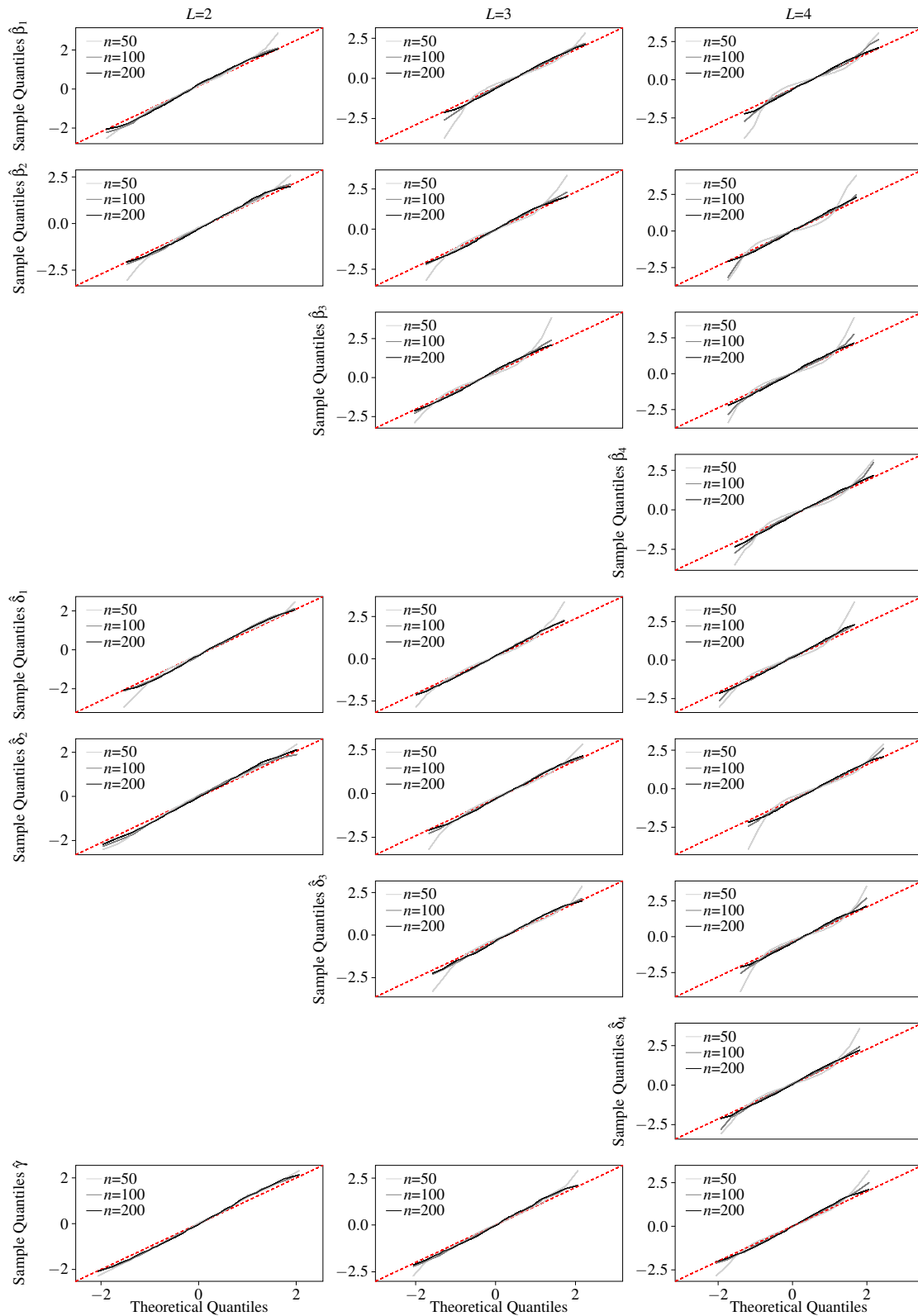
Note: Q-Q plots for each sample size $n = 50$ (light gray), $n = 100$ (gray), and $n = 200$ (black) for different number of layers $L = \{2, 3, 4\}$ are based on 1, 100 replications using model specification S1 with networks model formation M1. Dashed red line in each plot represents the 45-degree line.

Figure 1.4: Monte Carlo Box Plots in S1 with M2



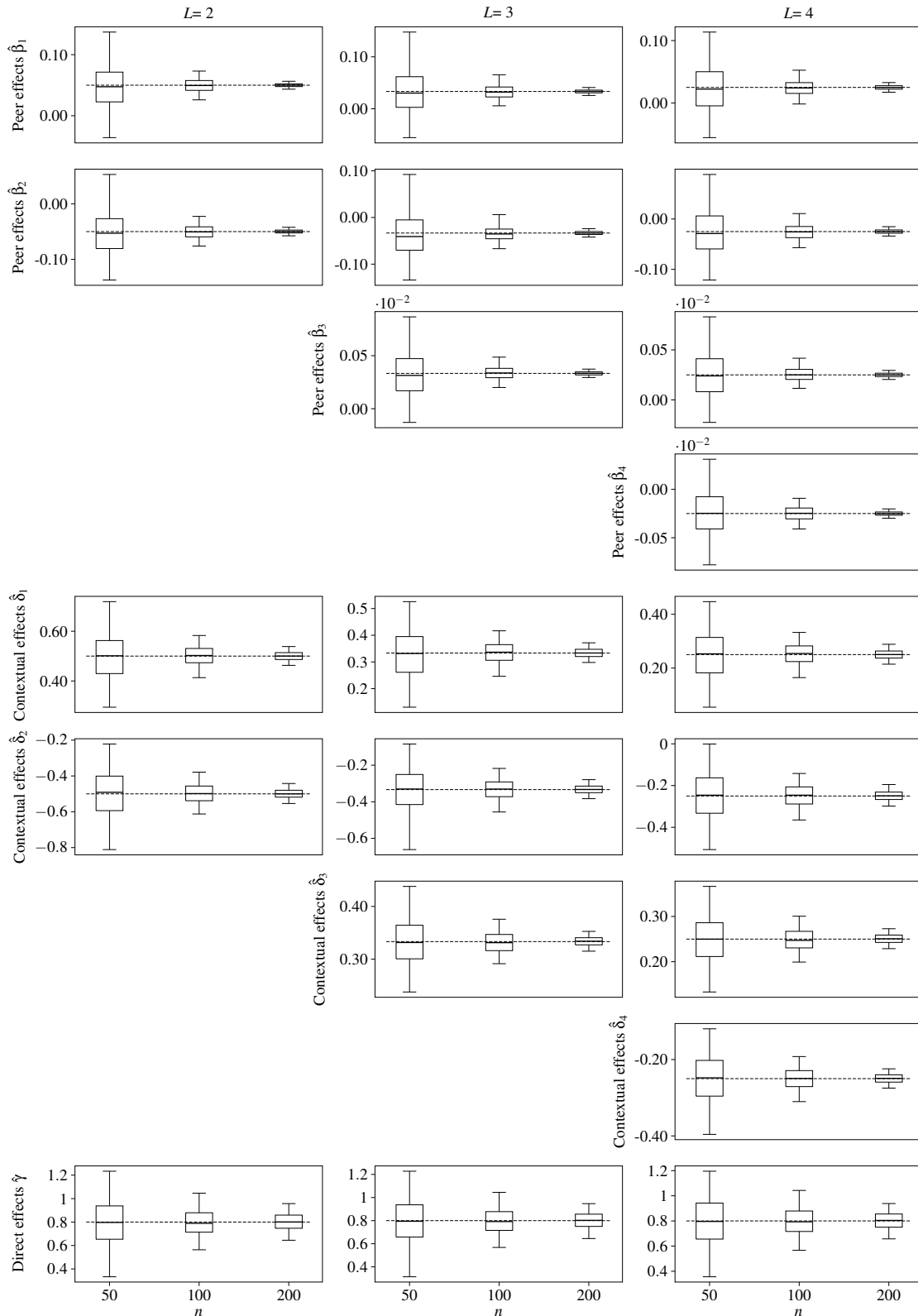
Note: Box plots for each sample size $n \in \{50, 100, 200\}$ for different number of layers $L = \{2, 3, 4\}$ are based on 1, 100 replications using model specification S1 with networks model formation M2.

Figure 1.5: Monte Carlo Q-Q Plots in S1 with M2



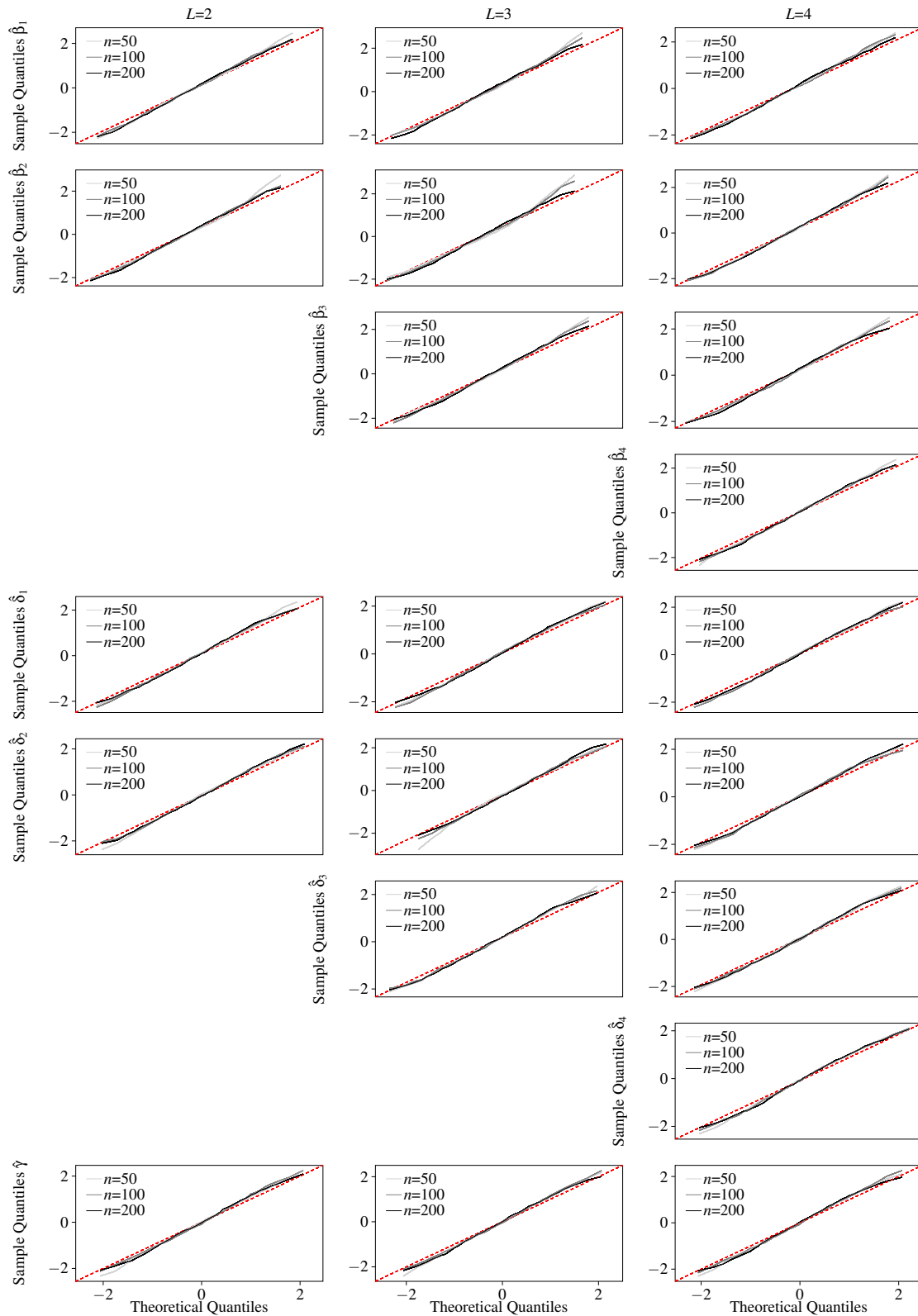
Note: Q-Q plots for each sample size $n = 50$ (light gray), $n = 100$ (gray), and $n = 200$ (black) for different number of layers $L = \{2, 3, 4\}$ are based on 1, 100 replications using model specification S1 with networks model formation M2. Dashed red line in each plot represents the 45-degree line.

Figure 1.6: Monte Carlo Box Plots in S2 with M1



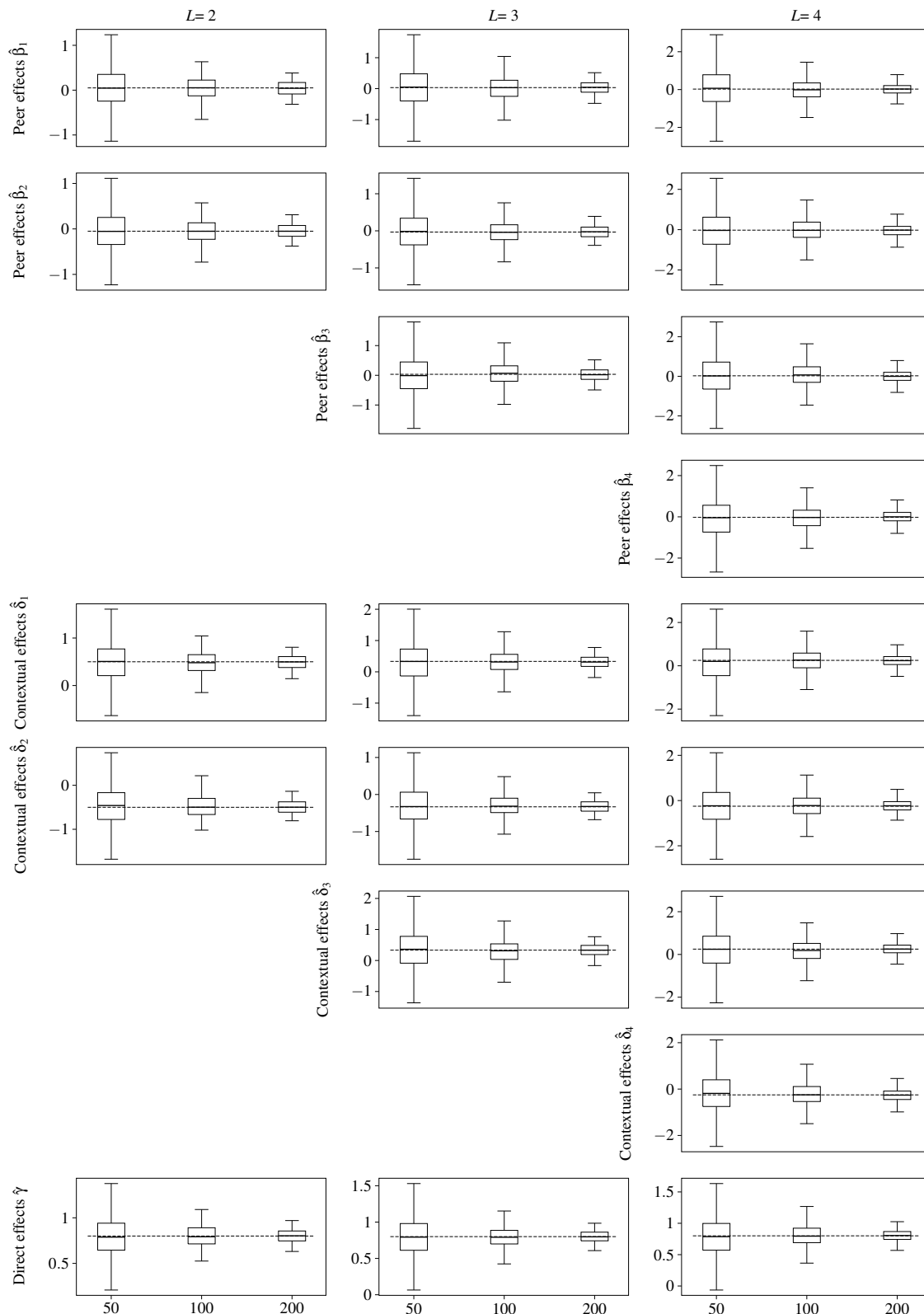
Note: Box plots for each sample size $n \in \{50, 100, 200\}$ for different number of layers $L = \{2, 3, 4\}$ are based on 1, 100 replications using model specification S2 with networks model formation M1.

Figure 1.7: Monte Carlo Q-Q Plots in S2 with M1



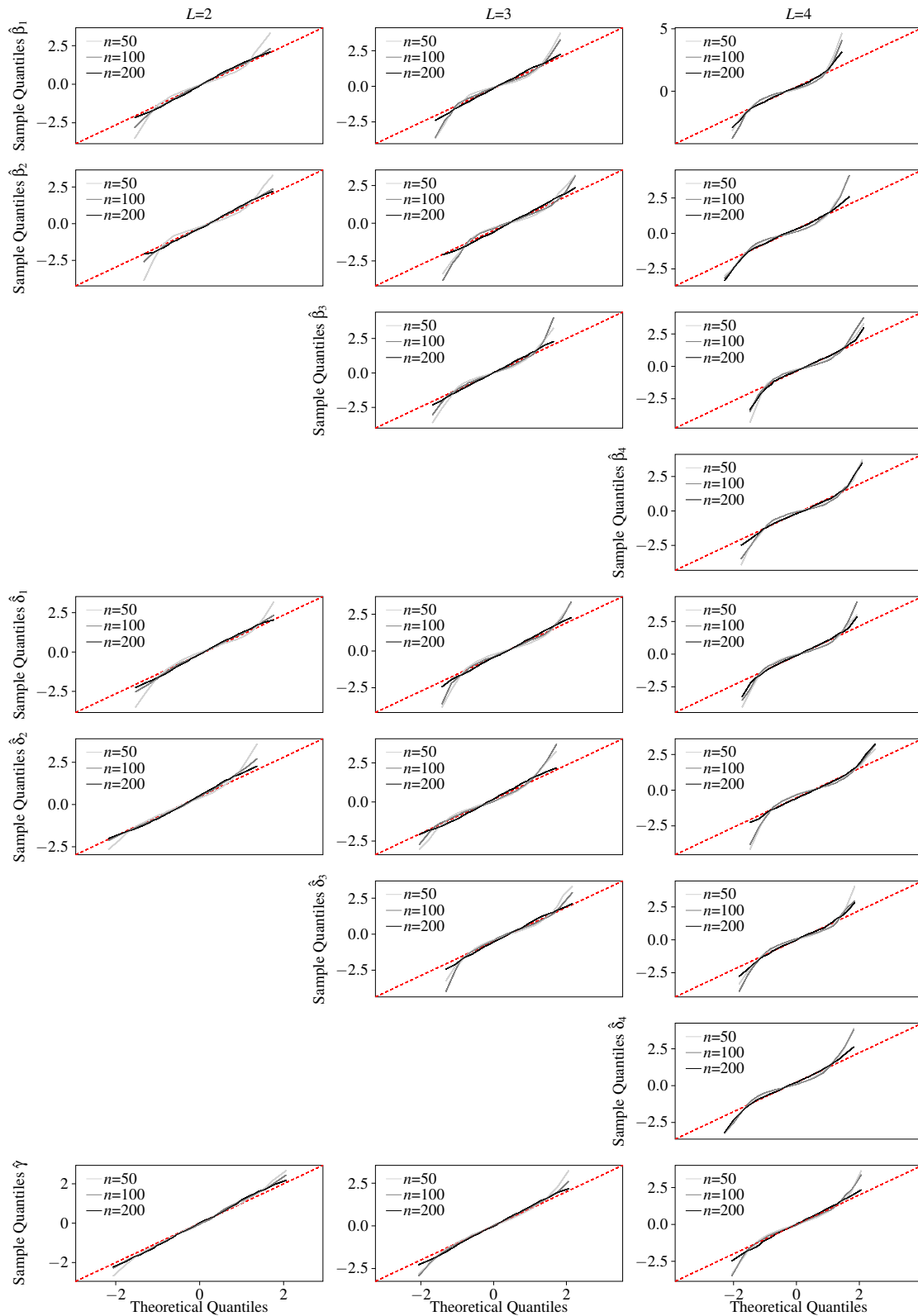
Note: Q-Q plots for each sample size $n = 50$ (light gray), $n = 100$ (gray), and $n = 200$ (black) for different number of layers $L = \{2, 3, 4\}$ are based on 1, 100 replications using model specification S2 with networks model formation M1. Dashed red line in each plot represents the 45-degree line.

Figure 1.8: Monte Carlo Box Plots in S2 with M2



Note: Box plots for each sample size $n \in \{50, 100, 200\}$ for different number of layers $L = \{2, 3, 4\}$ are based on 1, 100 replications using model specification S2 with networks model formation M2.

Figure 1.9: Monte Carlo Q-Q Plots in S2 with M2



Note: Q-Q plots for each sample size $n = 50$ (light gray), $n = 100$ (gray), and $n = 200$ (black) for different number of layers $L = \{2, 3, 4\}$ are based on 1, 100 replications using model specification S2 with networks model formation M2. Dashed red line in each plot represents the 45-degree line.

1.9.1 Supplementary Monte Carlo

In this section we explore the performance of our proposed estimator (version 2 hereafter) that utilizes a larger set of instruments than Lee’s (2003) and Badinger and Egger’s (2011) version of the G2SLS, i.e., version 1 hereafter. A total of 1,100 data sets, $\{y_i, x_i\}_{i=1}^n$ and $\{\{w_{\ell,i,j}\}_{i=1}^n\}_{j=1}^n, \forall \ell \in \{1, 2\}$, for $n \in \{50, 100, 200\}$ are generated from Network Formation Model 1 (M1) and the model Specification 1 (S1), defined above, with $\phi = 0.9, \beta_2 = 0, \delta_2 = 0$ – we call this the Special Design 1 (SD1), and, $\phi = 0.9, \delta_1 = 0, \delta_2 = 0$ – coined the Special Design 2 (SD2) here.

Since SD1 corresponds to the traditional monolayered Linear-in-Means model, Lee’s (2003) version of the G2SLS that uses instruments $[\iota, \mathbf{X}, \mathbf{W}_1^2 \mathbf{X}, \mathbf{W}_1 \mathbf{X}]$ would suffice. Similarly since SD2 corresponds to a bilayered Linear-in-Means model, Badinger and Egger’s (2011) version of the G2SLS uses instruments $[\iota, \mathbf{X}, \mathbf{W}_1^2 \mathbf{X}, \mathbf{W}_2^2 \mathbf{X}, \mathbf{W}_1 \mathbf{W}_2 \mathbf{X}, \mathbf{W}_2 \mathbf{W}_1 \mathbf{X}]$. On the other hand, our proposed estimator uses instruments $[\iota, \mathbf{X}, \mathbf{W}_1^2 \mathbf{X}, \mathbf{W}_2^2 \mathbf{X}, \mathbf{W}_1 \mathbf{X}, \mathbf{W}_2 \mathbf{X}, \mathbf{W}_1 \mathbf{W}_2 \times \mathbf{X}, \mathbf{W}_2 \mathbf{W}_1 \mathbf{X}]$ instead.

The results are summarized in Tables 1.2 and 1.3 in terms of Monte Carlo bias (Bias), standard deviation (Std. Dev.), and root mean squared error (RMSE). Overall our proposed version displays uniformly better bias in SD1 and comparable RMSE for a sample size of 200 observations. On the other hand, our estimator is outperformed in all metrics for SD2.

1.10 Appendix: Empirical Application

1.10.1 Data Description

Our data set comes from TransUnion[®], a major credit bureau in Canada. It contains anonymized account-level information on loan types, outstanding balances, consumer credit scores, as well as their age and the encrypted postal code of their primary residence. For privacy protection, postal codes are encrypted in a way that we only observe the first 3 digits, known as the **Forward Sortation Area (FSA)**. The last 3 digits, known as the local delivery unit, is encrypted and replaced by a unique identifier. We are able to use this information to construct the neighborhoods in our geographical network, by matching individuals living in the same encrypted postal code without knowing their actual residential locations.

The data set covers major loan types including mortgages, credit cards, auto loans, lines of credit, and installment loans. While home ownership is not reported in the data set, we constructed a homeowner indicator following the method in [Bhutta and Keys \(2016\)](#). Total non-residential debt includes all loan types in the data set, except mortgages and home-equity lines of credit. Consumers are divided into age groups in 5-year increments except the youngest and the oldest ones, there are: 18-25, 25-30, 30-35, 35-40, 40-45, 45-50, 50-55, 55-60, 60-65, and 65 or above.

For constructing our sample, accounts that have not been updated for 90 days (1 quarter) or with missing information concerning outstanding balance are dropped. Outstanding account balances are then aggregated to individual-level. We only include individuals aged 18 or above, who possess 1 or more credit cards and have resided in the urban service area

for 6 or more months prior to the time of our analysis. Individuals with missing credit scores, age, or neighborhood information are also excluded.

Descriptive statistics for the data set is reported in Table 1.4. It contains 47,593 individuals, residing in 1,190 neighborhoods that are geographically divided into 36 dissemination areas (DA). Each DA contains about 35 neighborhoods. On average, there are about 40 individuals living in a neighborhood and about 1322 people in a DA. When individuals are divided into DA-specific age groups, there are on average about 132 people per age group.

Consumer characteristics and their outstanding loans contains substantial variation and heavily skewed to the right, as exhibited in the top panel. When aggregated to consumer groups, the distribution of neighborhoods and age-groups are similar in the mean and the variation of outstanding credit card and auto loan balances, as reported in the middle and the bottom panel. They also have similar distributions in terms of average credit scores and its standard deviation within a group.

1.10.2 Supplementary Estimation Results

The estimated interactive terms for the linear-in-mean model on credit-card balances are reported in Figure 1.10. The top panel shows the age group \times homeowner fixed effects, where we find older age groups have lower credit-card balances than those in age 18–25. This finding is consistent with individuals' credit card use reported in [Henry et al. \(2018\)](#) that younger card holders have higher revolving balances. The bottom panel reports the DA \times homeowner fixed effects. We find that the average credit-card balance for renters have smaller variations across neighborhoods, when compared to that for homeowners.

Similarly, the estimated interactive terms for auto loans are shown in Figure 1.11. Interestingly, the top panel shows that homeowners below age 55 have higher values of auto loans, mainly because homeowners are more likely to own cars. The average auto-loan balance for homeowners also have bigger variations across neighborhoods than that for renters, as indicated in the bottom panel.

Table 1.2: Monte Carlo Results of SD1

Parameters	n	G2SLS Version 1			G2SLS Version 2		
		Bias	Std. Dev.	RMSE	Bias	Std. Dev.	RMSE
β_1	50	-0.403	0.136	0.425	-0.401	0.235	0.464
	100	-0.406	0.086	0.415	-0.404	0.112	0.420
	200	-0.401	0.043	0.403	-0.401	0.052	0.404
β_2	50				0.001	0.257	0.256
	100				0.004	0.111	0.111
	200				0.001	0.047	0.047
δ_1	50	-0.012	0.151	0.152	-0.009	0.215	0.215
	100	-0.000	0.098	0.098	0.001	0.113	0.112
	200	-0.002	0.053	0.053	-0.001	0.058	0.058
δ_2	50				-0.000	0.267	0.267
	100				-0.005	0.117	0.117
	200				0.001	0.055	0.055
γ	50	-0.008	0.167	0.167	-0.002	0.268	0.268
	100	0.003	0.111	0.111	0.002	0.139	0.139
	200	0.000	0.078	0.078	0.002	0.089	0.089

Note: Monte Carlo bias (Bias), standard deviation (Std. Dev.), and root mean squared error (RMSE). Version 1 implements [Lee's \(2003\)](#) G2SLS, while Version 2 implements our proposed G2SLS.

Table 1.3: Monte Carlo Results of SD2

Parameters	n	G2SLS Version 1			G2SLS Version 2		
		Bias	Std. Dev.	RMSE	Bias	Std. Dev.	RMSE
β_1	50	-0.442	0.286	0.526	-0.551	0.839	1.003
	100	-0.422	0.164	0.453	-0.494	0.943	1.064
	200	-0.407	0.082	0.415	-0.447	0.827	0.940
β_2	50	-0.455	0.328	0.328	-0.758	0.830	0.885
	100	-0.443	0.173	0.173	-0.682	0.738	0.773
	200	-0.410	0.075	0.085	-0.515	0.640	0.643
δ_1	50				0.089	0.603	0.729
	100				0.047	0.710	0.842
	200				0.031	0.629	0.784
δ_2	50				0.250	0.610	0.658
	100				0.196	0.551	0.584
	200				0.083	0.470	0.477
γ	50	-0.072	0.278	0.287	-0.027	0.320	0.321
	100	-0.045	0.161	0.167	-0.028	0.208	0.210
	200	-0.014	0.091	0.092	0.002	0.137	0.137

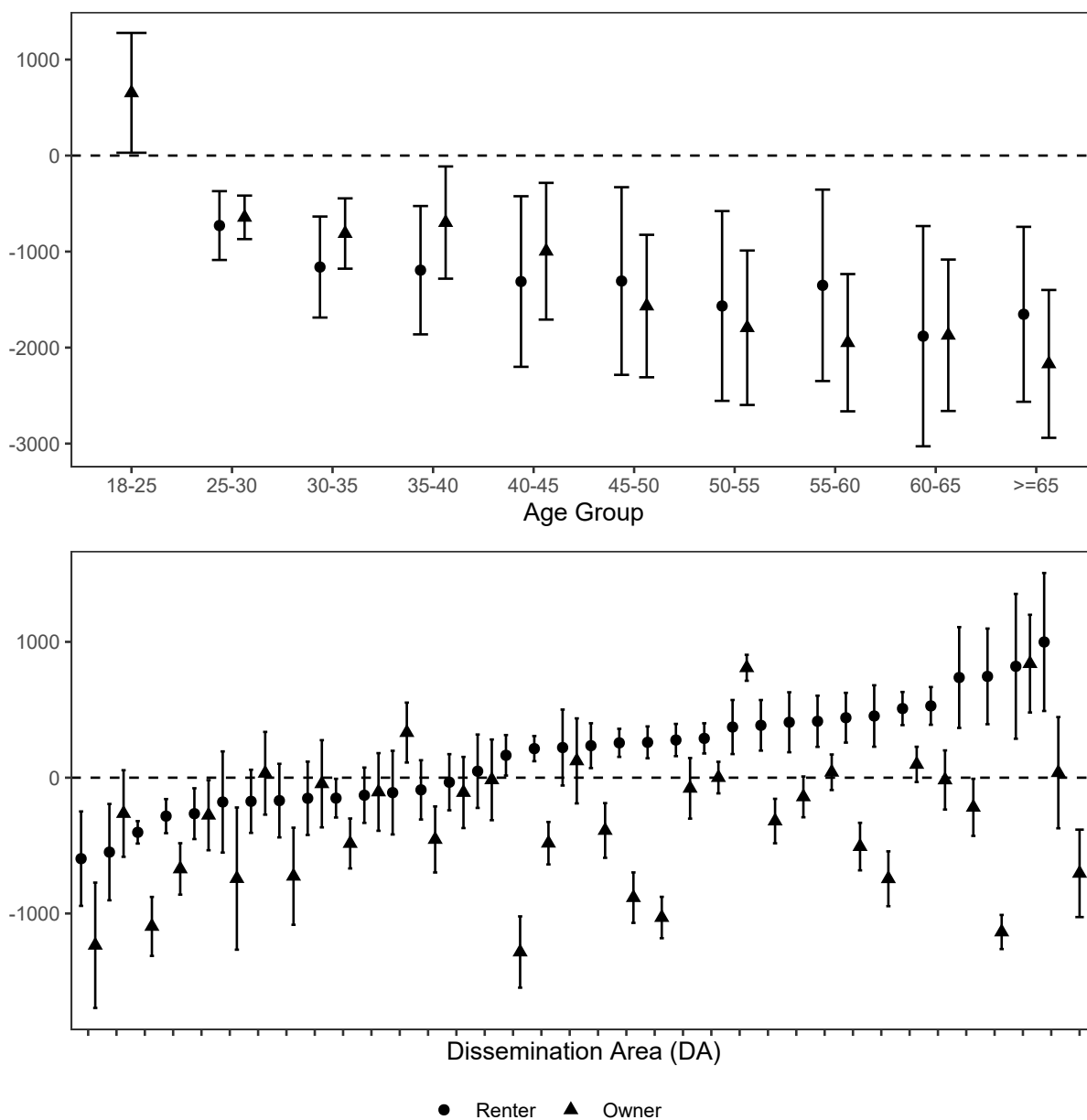
Note: Monte Carlo bias (Bias), standard deviation (Std. Dev.), and root mean squared error (RMSE). Version 1 implements [Badinger and Egger's \(2011\)](#) G2SLS, while Version 2 implements our proposed G2SLS.

Table 1.4: Descriptive Statistics

	P25	P50	P75	Mean	SD	N
<i>By individuals</i>						
Credit card	234	2057	7349	5979.41	10010.41	47593
Auto loan	0	0	25198	15091.79	24861.22	47593
Consumer debt	2016	17407	49418	34216.94	47761.20	47593
Credit scores	666	771	839	737.78	117.27	47593
Age	32.5	41.6	53.8	43.34	13.41	47593
<i>By neighborhoods</i>						
N_i	12	30	59	39.95	40.48	1190
Credit card	4417.16	5706.22	7187.28	6158.01	3542.70	1190
Auto loan	9648.00	14167.10	19157.54	14669.76	7822.58	1190
Avg. credit scores	717.07	740.65	762.46	738.88	40.58	1190
Sd. credit scores	97.80	112.77	125.55	109.86	28.86	1190
<i>By age groups</i>						
N_i	69.5	111	174	132.20	87.71	360
Credit card	4382.21	6081.21	7448.44	5865.26	2209.72	360
Auto loan	10229.82	14131.09	18405.66	14344.51	5620.80	360
Avg. credit scores	713.82	734.37	762.25	737.18	33.04	360
Sd. credit scores	106.31	114.52	121.20	113.62	13.10	360
N_i per DA	747.5	1313.5	1796.5	1322.03	693.31	36
N_a per DA	23	32.5	44	34.58	18.47	36

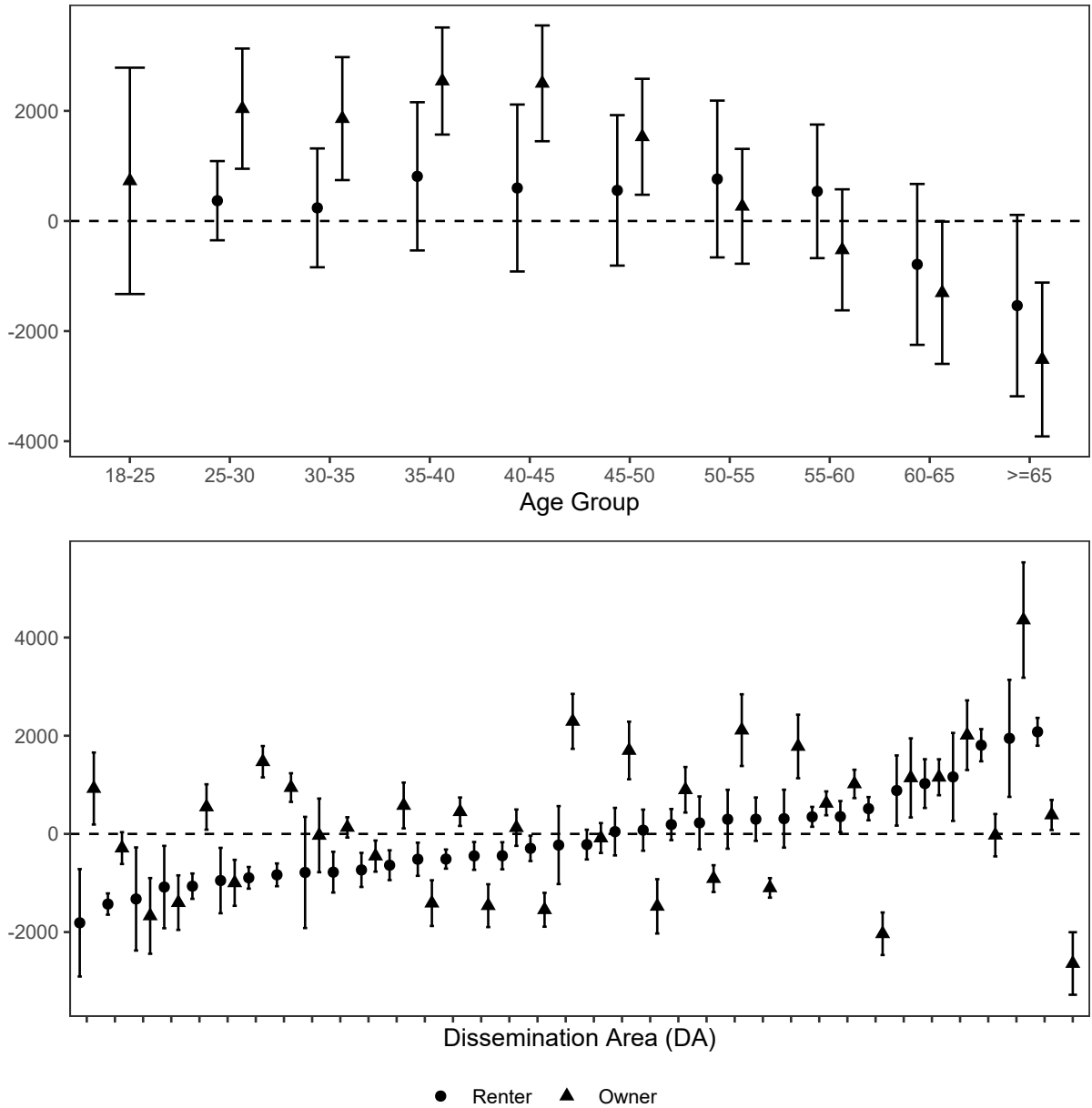
Note: Credit card and auto loans refer to the outstanding balance in the respective categories. Consumer debt and credit scores refers to the levels at the end of last quarter. N_i denotes the number of individuals, and N_a denotes the number of neighborhoods. Avg. and sd. credit scores refer to the average and the standard deviation of credit scores within a specific group. P25, P50, and P75 denotes the 25th, 50th, and 75th percentiles, respectively. SD is standard deviation and N refers to the number of observations.

Figure 1.10: Estimated Interactive Terms for Credit Card



Note: The top panel reports the estimated interaction terms of age group \times homeowner, benchmarked to renters in age group 18–25. The bottom panel reports the estimated interaction terms of Dissemination Area (DA) \times homeowner, benchmarked to renters in DA displayed in the last column. The dot points are the estimates for renters and the triangular points are the estimates for homeowners. The vertical line shows the range of ± 1.96 standard errors.

Figure 1.11: Estimated Interactive Terms for Auto Loan



Note: The top panel reports the estimated interaction terms of age group \times homeowner, benchmarked to renters in age group 18–25. The bottom panel reports the estimated interaction terms of Dissemination Area (DA) \times homeowner, benchmarked to renters in DA displayed in the last column. The dot points are the estimates for renters and the triangular points are the estimates for homeowners. The vertical line shows the range of ± 1.96 standard errors.

Chapter 2

Risk Transmission across European entities using Networks: A Wide

Replication of [Gross and Siklos \(2020\)](#)

This paper replicates [Gross and Siklos \(2020\)](#) estimation results, figures and tables in a wide sense, having extended their daily dataset from July 28, 2017 to May 19, 2022. Their approach monitors credit risk transmission among European sovereigns, financial and non-financial entities over time, from 2006 to 2017. This paper is completed using Python software instead of using the original code, written in Matlab. Additionally, the extension of the dataset provides new insights on the credit risk transmission behavior for the static and the dynamic full-sample approaches. In particular, one of the findings suggests that during the pandemic the main senders of risk belong to non-financial industries.

2.1 Introduction

[Gross and Siklos \(2020\)](#) is an empirical application paper that evaluates credit risk transmission among European institutions using daily data on a panel of Credit Default Swaps (CDS) spreads. Their analysis' results uncover how a network of European sovereigns, non-financial and financial sector institutions, depicting risk exchanges, evolves over time. The directed network connections shared by couples of institutions represent the estimated spillover effects. In other words, their work estimates spillover effects among the aforementioned types of institutions and depicts those estimated spillover effects using networks. Their analysis is conducted for the full-sample, as well as for sub-sample periods where important events took place, such as the Lehman Brother's bankruptcy, and they approach risk interactions both statically, and dynamically using rolling window estimation.

This paper replicates the authors' code using Python. Additionally, in this work all results come from an extended version of the original dataset, obtained using Datastream. The data in this work range from October 23, 2006 up to May 19, 2022. The sections of the paper are organized as follows. In section 2.2, the resulting tables and figures for the static full-sample analysis are provided and discussed. In section 2.3, I provide all the dynamic results in tables and figures by estimating the Vector Autoregressive (VAR) model using rolling window estimation with increment size 1 day and window sizes 150, 200, and 250 days. Finally, the last section offers some concluding remarks.

2.2 Replication Static results

In this section, I am going to provide a discussion on the extended dataset used, the methodology and the replicated figures and tables comparing to those of the [Gross and Siklos \(2020\)](#) paper.

[Gross and Siklos \(2020\)](#), henceforth GS, have a dataset of 152 entities on CDS spreads. These entities are European sovereigns and institutions from the Automotive, Consumer, Energy and Telecommunication industries as well as from the financial sector. Table 2.1 is a representative table of all the dataset's entities including information regarding *Entity Names*, *Sector* classification, *Sub-Sector* classification, *Country* of headquarters and the respective three digit *Name Code*. The dataset used for the GS paper can be found at the [Journal of Applied Econometrics Data Archive](#). In this replication section, the exact same entities are used in order to provide the replicated estimation results, figures and tables.

It is important to note that the replicated results of the GS paper presented below are produced using solely Python software. The Python code is written in jupyter notebook, an open-source web application which allows for code and output being coexistent in one script. Specific Python modules such as `statsmodels` and `sklearn`, were of particular importance for this replication as they are part of the Python code script and helped in providing the key results of this work in an efficient way. Overall, the replicated results provided match closely to the GS paper results. In what follows, I will comment on the outputs while describing the empirical replication's methodology using Python.

GS are interested in the pure contagion effect, so they first apply the Generalized dynamic factor model by [Barigozzi and Hallin \(2017\)](#), in order to remove the common com-

ponent and focus on studying the idiosyncratic component of the logarithmic CDS spreads. The number of factors is determined by the [Hallin and Liška \(2007\)](#) IC_2 criterion and Figure 2.1 indicates one common factor for the full-sample. More specifically, the resulting Figure 2.1 provides a similar result as Figure A.1 of the original paper where one common factor was also suggested.

The estimated common factor is represented in Figure 2.2 for the full-sample period 2006-2022. The corresponding figure in the original paper is Figure A.2 which looks very similar to the replicated Figure 2.2. Around 2020, after the pandemic started the estimated common factor is characterized by higher volatility. Next, properties of the common factor can be found in Table 2.2, where results are in close match. More specifically, panel A shows the explanatory power of the estimated common factor by sub-sector and overall. In panel B of Table 2.2, the VIX dataset used matches the start and end dates of the CDS dataset, i.e. it spans from October 23, 2006, up to May 19, 2022. However, the dates on the CDS dataset and the VIX dataset are not exactly the same. In order to handle this, the intersection of the two datasets dates is used and, therefore, only the matching data is used for Panel B.

The raw and the estimated idiosyncratic returns are illustrated in the summary statistics at Table 2.3, equivalent to Table A.3 in the GS paper. The idiosyncratic returns presented in this table are used to estimate the coefficient matrix and the variance covariance matrix of the residuals in the context of a Vector Autoregressive (VAR) model.

However, the issue of high dimensionality makes it meaningful to use a penalized regression method for estimation. Elastic Net shrinkage is found to be the most suitable penalization method compared to others and it is the one chosen for estimation. Table 2.4

provides illustrative results on why the Elastic Net penalization method is used relative to others. The results slightly differ from GS's Table 3 because of the higher tolerance chosen for code efficiency and the randomness incorporated in the 10-fold cross validation.

The estimated coefficient matrix gives insights on Granger causality. Figure 2.3, the analogous of the original Figure A.6, pictures Granger causality from sovereigns to non-financial sub-sectors.

Post-estimation, GS compute the generalized variance decompositions (GVDs). According to [Diebold and Yilmaz \(2014\)](#) when represented in matrix form, the variance decomposition matrix can be also considered to be a network's adjacency matrix and thus, estimated variance decompositions can be visually depicted in a network plot. In this case, the variance decomposition's network plot, consists of the 152 institutions as the network's nodes. The directed links, which represent the amount of risk being transmitted from one node to another, the node location that represents how much risk a node holds - the more central the bigger the risk, the more peripheral the lower the risk-, and the link thickness which prints how strong the risk exchanges are between two nodes.

Figures 2.4, 2.5, 2.6, and 2.7 replicate versions¹ of Figures 1, A.8, A.9, and A.10, respectively. They are the network representation plots of the full sample period for forecast horizon $h = 10$, $h = 5$, $h = 15$ and $h = 20$, respectively. The replicated figures match closely to the original ones, however there are some differences such as the clustering in financial institutions in two instead of one groups which makes the group of banks that is closer to the center of the network holding more risk relatively to the other.

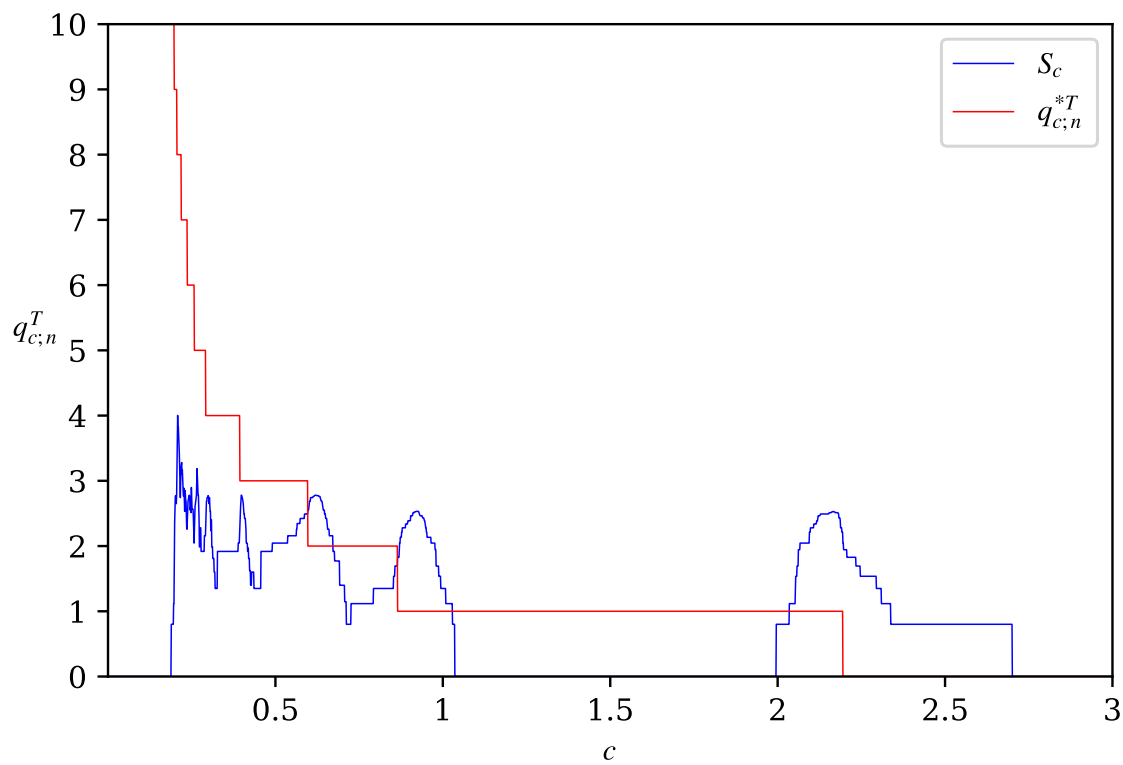
¹In networks, the positioning of nodes, the so-called "layout", can be user-specified or algorithm-based. Here, the layout is based on the strength of the connections, creating appealing and repulsive forces. More specifically, it is specified by the [Fruchterman and Reingold \(1991\)](#) force-directed algorithm.

In addition, the case where two common factors are included in the model, under forecast horizon $h = 10$, is considered and the resulting network representation can be visualized in Figure 2.8 which corresponds to the original Figure A.11. To evaluate in which extent the different model specifications are correlated with the basic model with one factor for $h = 10$, GS provide Table A.4. Its replicated version is Table 2.5 which calculates the respective rank correlation coefficients of the other specifications compared to the basic model. The replication results are similar, although somewhat differ when the two factor model is compared to the basic model. This may most likely happen due to the larger dataset used in this work.

From the estimated variance decomposition matrix, the authors get connectedness among the entities and produce Table 1 and Figures 2, 3. Using the full-sample data, the corresponding tables can be viewed in Table 2.6 and Figures 2.9, 2.10. The findings are in close match overall with the original ones, having only some differences. For instance, in figure 2.10, where cross-sectoral connectedness in the Energy sub-sector is higher from the financial sector than from the sovereigns. Geographical connectedness is depicted in Figure 2.11 which corresponds to original Figure 4 with different connectedness magnitudes and color schemes. The resulting geographical connectedness gives insights on the magnitude of nodes and on country colors depicting the full-sample (2006-2022) country and sector level risk exchanges. The findings show that the non-financial sector in the UK, Portugal, Spain, France, Netherlands, Germany, Switzerland is ranked in the top financial risk receiver for the full-sample 2006-2022. On the other hand, Italy, Spain and Portugal's non-financial sector is the top receiver of sovereign risk.

Geographical connectedness is evaluated using data from the consolidated banking statistical database of the Bank for International Settlements (BIS) for Table 2.7, the replicated version of Table 2. Note that the results differ probably due to alternative data selection, cleaning and merging. The BIS data used in this replication includes all available countries in the countries in the database that are present in Table 2.1's 'Country' column and for the dates that the CDS dataset extends. The estimated values with three asterisks are the ones with p-value less or equal to 0.01. The estimated regression coefficient that is significant shows that the higher the directional connectedness from sovereign j to the non-financial sector of country i , the higher the risk exposure of country i to all the sectors of j .

All the replicated figures and tables are presented below. The methodology followed is identical to the one employed in the GS paper. Also, the connectedness measures used in this wide replication are discussed in the GS paper. More intuition on the connection between variance decompositions and networks can be found in [Diebold and Yilmaz \(2014\)](#).

Figure 2.1: Hallin and Liska (2007) IC_2 criterion

Note: The Hallin and Liska (2007) IC_2 criterion suggests the number of common factors to be used in a dynamic factor model. This figure presents the $q_{c;n}^T$ and S_c as functions of c , where $q_{c;n}^T$ comes from the penalty function $p(n, T) = (M_T^{-2} + M_T^{0.5}T^{-0.5} + n^{-1}) \log(\min[n, M_T^2, M_T^{-0.5}T^{0.5}])$. S_c equals zero in three intervals called “stability intervals”, for $c \in \{[0, 0.22], [1.04, 1.99], [2.72, 2.99]\}$. Hallin and Liska (2007) suggest to use the indicated number of factors from the second stability interval, which in this case yields $q_{c;n}^T = 1$, i.e. one common factor.

Table 2.1: List of CDS entities in the panel dataset

Entity Name	Sector	Sub-Sector	Country	Name Code
Adecco	Non-financial	Autos & Industrials	Switzerland	ADE
Volvo	Non-financial	Autos & Industrials	Sweden	VOL
Akzo Nobel	Non-financial	Autos & Industrials	Netherlands	AKN
Alstom	Non-financial	Autos & Industrials	France	ALS
Anglo American	Non-financial	Autos & Industrials	UK	ANA
Astrazeneca	Non-financial	Autos & Industrials	UK	ASZ
Atlantia	Non-financial	Autos & Industrials	Italy	ATL
Bae Systems	Non-financial	Autos & Industrials	UK	BAE
BASF	Non-financial	Autos & Industrials	Germany	BAS
Bayer	Non-financial	Autos & Industrials	Germany	BAY
BMW	Non-financial	Autos & Industrials	Germany	BMW
Bouygues	Non-financial	Autos & Industrials	France	BOU
Clariant	Non-financial	Autos & Industrials	Switzerland	CLA
Saint-Gobain	Non-financial	Autos & Industrials	France	SAG
Michelin	Non-financial	Autos & Industrials	Switzerland	MIC
Continental	Non-financial	Autos & Industrials	Germany	CON
Daimler	Non-financial	Autos & Industrials	Germany	DAI
Deutsche Post	Non-financial	Autos & Industrials	Germany	DPO
Evonik	Non-financial	Autos & Industrials	Germany	EVO
Finmeccanica	Non-financial	Autos & Industrials	Italy	FME
GKN Holding	Non-financial	Autos & Industrials	UK	GKN
Glencore	Non-financial	Autos & Industrials	Switzerland	GLC
Koninklijke DSM	Non-financial	Autos & Industrials	Netherlands	DSM
Air Liquide	Non-financial	Autos & Industrials	France	AIR
Lanxess	Non-financial	Autos & Industrials	Germany	LAX
Linde	Non-financial	Autos & Industrials	Germany	LIN
Peugeot	Non-financial	Autos & Industrials	France	PEU
Renault	Non-financial	Autos & Industrials	France	REN
Rentokil Initial	Non-financial	Autos & Industrials	UK	REI
Rolls-Royce	Non-financial	Autos & Industrials	UK	ROR
Sanofi-Aventis	Non-financial	Autos & Industrials	France	SAA
Siemens	Non-financial	Autos & Industrials	Germany	SIE
Stora Enso Oyj	Non-financial	Autos & Industrials	Finland	SEO
Solvay	Non-financial	Autos & Industrials	Belgium	SOL
ThyssenKrupp	Non-financial	Autos & Industrials	Germany	THK
UPM-Kymmene Oyj	Non-financial	Autos & Industrials	Finland	UPM
Valeo	Non-financial	Autos & Industrials	France	VAL
Vinci	Non-financial	Autos & Industrials	France	VIN
Volkswagen	Non-financial	Autos & Industrials	Germany	VOL
Wendel	Non-financial	Autos & Industrials	France	WEN
Accor	Non-financial	Consumers	France	ACC
Electrolux	Non-financial	Consumers	Sweden	ELE
Auchan	Non-financial	Consumers	France	AUC
Alliance Boots	Non-financial	Consumers	UK	ALL
Carrefour	Non-financial	Consumers	France	CAR
Casino Guichard	Non-financial	Consumers	France	CAG
Compass	Non-financial	Consumers	UK	COM
Danone	Non-financial	Consumers	France	DAN
Lufthansa	Non-financial	Consumers	Germany	LUF
Diageo	Non-financial	Consumers	UK	DIA
Experian Finance	Non-financial	Consumers	UK	EXF

(Table 2.1 continued)

Entity Name	Sector	Sub-Sector	Country	Name Code
Henkel	Non-financial	Consumers	Germany	HEN
Ladbrokes	Non-financial	Consumers	UK	LAD
Imperial Brands	Non-financial	Consumers	UK	IMB
ISS Global	Non-financial	Consumers	Denmark	ISS
J Sainsbury	Non-financial	Consumers	UK	JSA
Kering	Non-financial	Consumers	France	KER
Kingfisher	Non-financial	Consumers	UK	KIN
Koninklijke Ahold Delhaize	Non-financial	Consumers	Netherlands	AHO
Koninklijke Philips	Non-financial	Consumers	Netherlands	PHI
LVMH	Non-financial	Consumers	France	LVM
Marks & Spencer	Non-financial	Consumers	UK	M&S
Metro	Non-financial	Consumers	Germany	MET
Nestlé	Non-financial	Consumers	Switzerland	NES
Next	Non-financial	Consumers	UK	NEX
PernodRicard	Non-financial	Consumers	France	PER
Safeway	Non-financial	Consumers	UK	SAF
Svenska Cellulosa	Non-financial	Consumers	Sweden	SCE
Swedish Match	Non-financial	Consumers	Sweden	SWM
Tate & Lyle	Non-financial	Consumers	UK	T&L
Tesco	Non-financial	Consumers	UK	TES
Unilever	Non-financial	Consumers	UK	UNI
BP	Non-financial	Energy	UK	BP
Centrica	Non-financial	Energy	UK	CEN
EON	Non-financial	Energy	Germany	EON
Edison	Non-financial	Energy	Italy	EDI
Energias de Portugal	Non-financial	Energy	Portugal	EDP
Electricité de France	Non-financial	Energy	France	EDF
ENBW	Non-financial	Energy	Germany	ENB
ENEL	Non-financial	Energy	Italy	ENE
ENGIE	Non-financial	Energy	France	ENG
Fortum OYJ	Non-financial	Energy	Finland	FOY
Gas Natural SDG	Non-financial	Energy	Spain	SDG
Iberdrola	Non-financial	Energy	Spain	IBE
National Grid	Non-financial	Energy	UK	NGR
Royal Dutch Shell	Non-financial	Energy	Netherlands	RDS
RWE	Non-financial	Energy	Germany	RWE
Statoil	Non-financial	Energy	Norway	STA
Total	Non-financial	Energy	France	TOT
United Utilities	Non-financial	Energy	UK	UNU
British Telecom	Non-financial	TMT	UK	BTE
Deutsche Telekom	Non-financial	TMT	Germany	DTE
Hellenic Telecom	Non-financial	TMT	Greece	HTE
ITV	Non-financial	TMT	UK	ITV
Nokia	Non-financial	TMT	Finland	NOK
Orange	Non-financial	TMT	France	ORA
Pearson	Non-financial	TMT	UK	PEA
Publicis	Non-financial	TMT	France	PUB
Relx	Non-financial	TMT	UK	REL
St Microelectronics	Non-financial	TMT	Switzerland	STM
Ericsson	Non-financial	TMT	Sweden	ERI
Telefonica	Non-financial	TMT	Spain	TEF
Telekom Austria	Non-financial	TMT	Austria	TEA

(Table 2.1 continued)

Entity Name	Sector	Sub-Sector	Country	Name Code
Telenor	Non-financial	TMT	Norway	TEL
Telia	Non-financial	TMT	Sweden	TEI
Vivendi	Non-financial	TMT	France	VIV
Vodafone	Non-financial	TMT	UK	VOD
Wolters	Non-financial	TMT	Netherlands	WOL
WPP	Non-financial	TMT	UK	WPP
Aegon	Financial		Netherlands	AEG
Generali	Financial		Germany	ALL
Aviva	Financial		Italy	GEN
AXA	Financial		UK	AVI
Hannover Rueck	Financial		France	AXA
Munich RE	Financial		Germany	HRE
Swiss RE	Financial		Germany	MRE
Zurich Insurance	Financial		Switzerland	SRE
Dexia	Financial		Switzerland	ZIN
BNP Paribas	Financial		Belgium	DEX
Crédit Agricole	Financial		France	BNP
Société Générale	Financial		France	CAG
Deutsche Bank	Financial		France	SOG
Commerzbank	Financial		Germany	DBA
Bank of Ireland	Financial		Germany	COB
Intesa Sanpaolo	Financial		Ireland	BOI
Banca Monte Di Paschi	Financial		Italy	BMP
Banca Popolare	Financial		Italy	BPO
Unicredit	Financial		Italy	UNI
Mediobanca	Financial		Italy	MED
ING	Financial		Netherlands	ING
Rabobank	Financial		Netherlands	RAB
Banco Comercial Port.	Financial		Portugal	BCP
Santander	Financial		Spain	SAN
BBVA	Financial		Spain	BBV
Royal Bank of Scot.	Financial		UK	RBS
HSBC Bank	Financial		UK	HSB
Barclays Bank	Financial		UK	BAB
Lloyds Bank	Financial		UK	LLB
Standard Chartered	Financial		UK	SCH
UBS	Financial		Switzerland	UBS
Credit Suisse	Financial		Switzerland	CSU
Austria	Sovereign		Austria	AUT
Belgium	Sovereign		Belgium	BEL
France	Sovereign		France	FRA
Germany	Sovereign		Germany	GER
Ireland	Sovereign		Ireland	IRE
Italy	Sovereign		Italy	ITA
Netherlands	Sovereign		Netherlands	NED
Portugal	Sovereign		Portugal	POR
Spain	Sovereign		Spain	ESP
UK	Sovereign		UK	UK

Figure 2.2: Evolution of the common factor over the full-sample period ranging from October 23, 2006 up to May 19, 2022. The common factor is estimated using the Generalized dynamic factor model of [Barigozzi and Hallin \(2016\)](#).

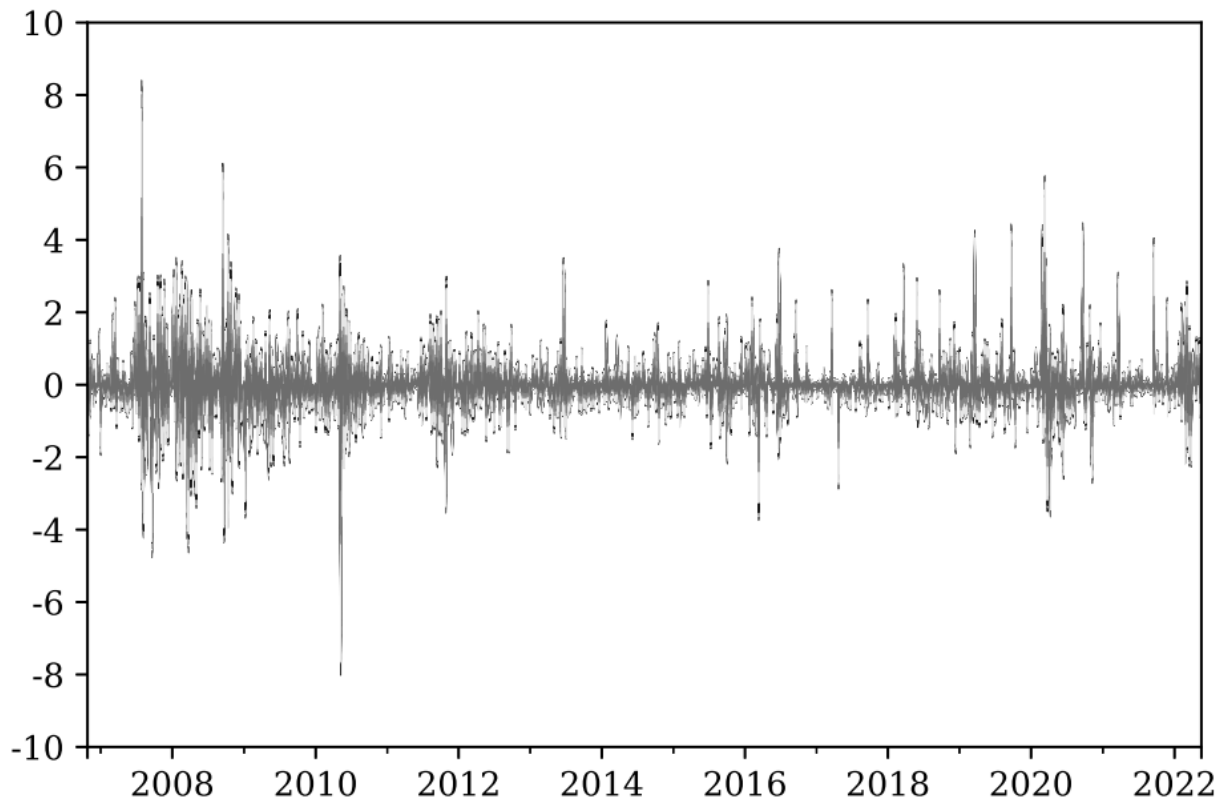


Table 2.2: Properties of the estimated common factor

Panel A: CDS non-financial corporations							
Sector	Autos & In- dustrials	Consumers	Energy	TMT	Financial	Sovereign	All CDS
R^2	0.465	0.431	0.439	0.473	0.433	0.110	0.332
Panel B: Correlation with global uncertainty (VIX)							
$\rho(F_t, \Delta VIX)$	ΔVIX_t		ΔVIX_{t-1}		R^2		
0.526	0.347***		0.029		0.279		

Note: Panel A presents the coefficient of determination R^2 of the common factor for the CDS spreads averaged by sub-sector. Panel B shows how the common factor is related to global uncertainty as captured by VIX for the full-sample data ranging from October 23, 2006 up to May 19, 2022. $\rho(F_t, \Delta VIX_t)$ is the Pearson's correlation coefficient. ΔVIX_t , ΔVIX_{t-1} and R^2 provided come from regressing the common factor F_t on the contemporaneous and first lag VIX returns as follows: $F_t = c + \Delta VIX_t + \Delta VIX_{t-1} + \varepsilon_t$. *** denotes 1% significance level based on Newey-West standard errors.

Table 2.3: Summary statistics of CDS data by country and by sector

Panel A: CDS non-financial corporations									
Countries	Entities	Raw returns				Idiosyncratic returns			
		Mean	Std. dev.	Min	Max	Mean	Std. dev.	Min	Max
Austria	1	-0.0	3.09	-24.78	25.16	-0.00	1.99	-15.56	18.79
Belgium	1	0.0	3.16	-25.04	27.41	0.00	2.03	-12.32	27.80
Denmark	1	0.0	3.10	-83.37	38.12	0.00	2.83	-83.19	33.99
Finland	4	-0.0	3.29	-83.88	37.76	-0.00	2.46	-83.99	36.76
France	24	-0.0	3.19	-58.92	60.03	-0.00	2.19	-59.64	57.33
Germany	19	-0.0	3.23	-33.53	103.18	0.00	2.25	-32.31	101.87
Greece	1	0.0	4.34	-33.16	54.41	-0.00	3.40	-26.46	44.23
Italy	4	-0.0	3.49	-53.71	71.65	-0.00	2.63	-52.52	71.37
Netherlands	6	-0.0	3.29	-77.99	80.75	-0.00	2.35	-80.01	77.87
Norway	2	-0.0	2.88	-25.64	32.04	0.00	2.21	-16.26	31.52
Portugal	1	-0.0	3.63	-39.06	29.29	0.00	2.47	-30.87	20.58
Spain	3	-0.0	3.64	-40.02	30.49	0.00	2.36	-22.07	30.92
Sweden	6	-0.0	2.75	-28.89	51.85	0.00	1.96	-23.44	52.26
Switzerland	6	0.0	3.27	-44.13	44.09	0.00	2.37	-36.28	38.14
UK	30	-0.0	3.14	-127.06	140.42	0.00	2.31	-130.71	139.93
Panel B: CDS financial institutions									
Countries	Entities	Raw returns				Idiosyncratic returns			
		Mean	Std. dev.	Min	Max	Mean	Std. dev.	Min	Max
Belgium	1	0.0	4.21	-104.95	86.57	-0.00	4.08	-104.65	86.85
France	4	-0.0	4.52	-44.02	62.63	0.00	3.07	-22.93	42.46
Germany	5	0.0	4.64	-47.70	61.30	0.00	3.21	-38.62	40.51
Ireland	1	-0.0	4.89	-86.97	60.40	0.00	4.75	-86.62	59.11
Italy	6	0.0	4.40	-59.37	75.31	0.00	3.27	-57.52	54.90
Netherlands	3	-0.0	4.24	-39.06	67.60	-0.00	3.29	-38.14	62.27
Portugal	1	0.0	3.80	-35.50	40.60	-0.00	3.19	-32.76	47.94
Spain	2	0.0	4.74	-45.77	33.94	-0.00	3.44	-30.52	36.16
Switzerland	4	-0.0	4.25	-41.10	56.21	0.00	2.93	-32.86	31.83
UK	6	0.0	4.50	-70.75	65.74	-0.00	3.32	-61.30	57.12
Panel C: CDS sovereigns									
Countries	Entities	Raw returns				Idiosyncratic returns			
		Mean	Std. dev.	Min	Max	Mean	Std. dev.	Min	Max
Austria	1	0.0	8.83	-200.19	153.10	0.01	8.61	-197.26	153.06
Belgium	1	-0.0	4.27	-28.81	69.79	-0.00	3.80	-27.29	59.69
France	1	0.0	8.69	-200.19	153.11	0.00	8.46	-197.44	153.06
Germany	1	0.0	8.13	-133.54	154.00	0.01	7.95	-133.29	153.97
Ireland	1	-0.0	13.62	-208.68	207.15	0.00	13.55	-207.35	207.51
Italy	1	0.0	4.00	-37.76	33.75	0.00	3.44	-37.21	34.77
Netherlands	1	-0.0	5.55	-65.97	65.88	0.00	5.43	-65.20	69.18
Portugal	1	0.0	4.28	-51.32	32.08	0.00	3.76	-34.03	25.61
Spain	1	0.0	5.10	-57.12	56.99	0.00	4.71	-58.54	56.68
UK	1	0.0	4.11	-62.82	93.58	0.00	3.87	-59.52	92.87

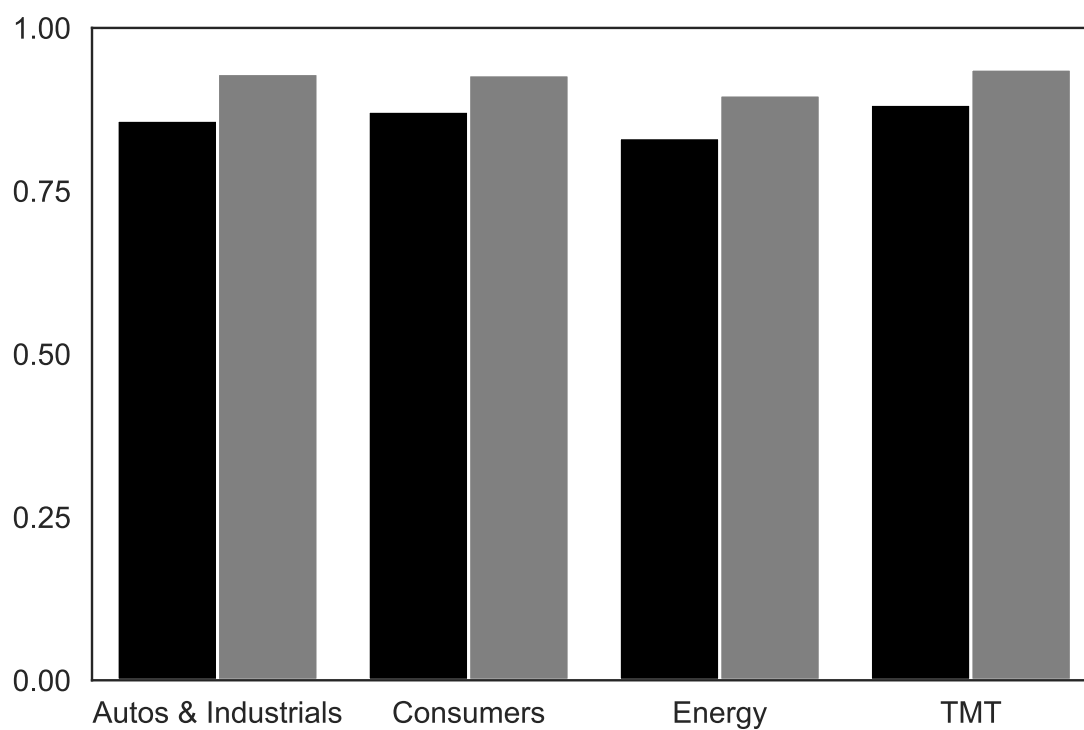
Note: The table shows the descriptive statistics of the demeaned raw panel of 152 CDS spreads and the estimated idiosyncratic returns arranged by country and by sector.

Table 2.4: Out-of-sample forecast results

	Autos & Industri- als	Consumers	Energy	TMT	Financial	Sovereign	Total
Optimal Elastic Net	5.1431	5.7205	4.9571	5.0559	5.1358	7.9649	5.4158
Constant mean	5.1804	5.5311	5.6314	5.0265	5.3575	9.4660	5.6088
AR(1)	4.7800	6.5543	5.4467	5.1840	5.4776	8.7328	5.6945
Ridge	5.9409	6.0039	6.3823	5.7661	6.1038	8.9663	6.2190
Constant Elastic Net	4.9729	5.0968	5.3705	5.6586	5.5573	9.5917	5.5625

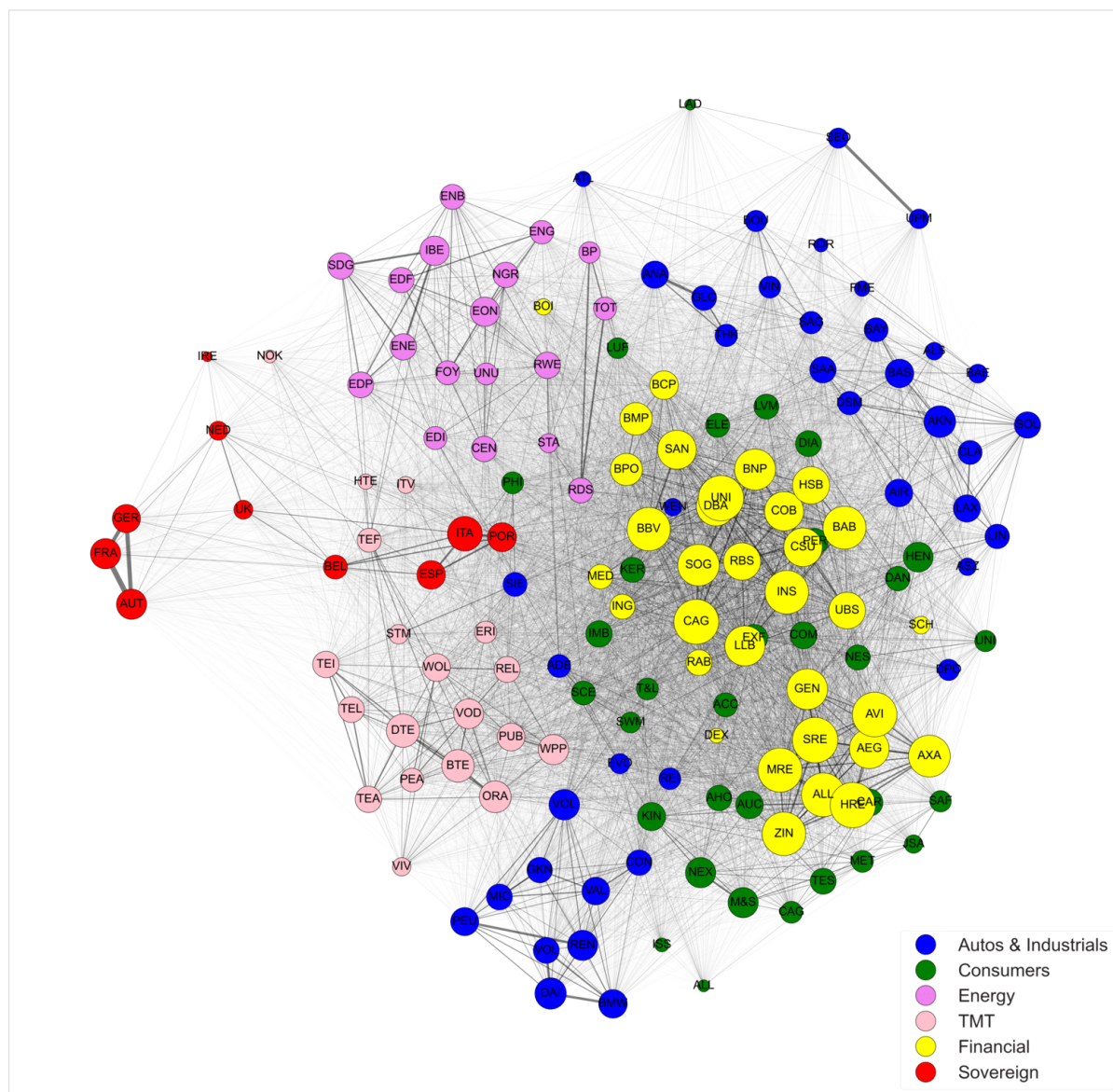
Note: The in-sample period is 10/23/2006 - 12/31/2019, the out-of-sample period corresponds to 01/01/2020-05/19/2022. The table shows the mean squared error (MSE) of the chosen estimation penalization method of optimal elastic net by sector and compares it to constant mean, AR(1), Ridge regression and Constant elastic net models. The optimal elastic net model chooses the optimal mixing parameter $\alpha \in \{[0.1, 0.2, 0.3, 0.4, 0.5, 0.6, 0.7, 0.8, 0.9, 1]\}$ and the penalty tuning parameter λ jointly in the shrinkage and selection process. The constant mean model uses the in-sample mean of each variable as forecasts. The AR(1) model conducts forecasts based on the fitted values from a persistent process. Ridge regression applies shrinkage in the VAR with $\alpha = 1$ and constant elastic net uses $\alpha = 0.5$ and chooses only the optimal λ in the penalty function.

Figure 2.3: Static Granger-causality cross-sectoral network connectedness



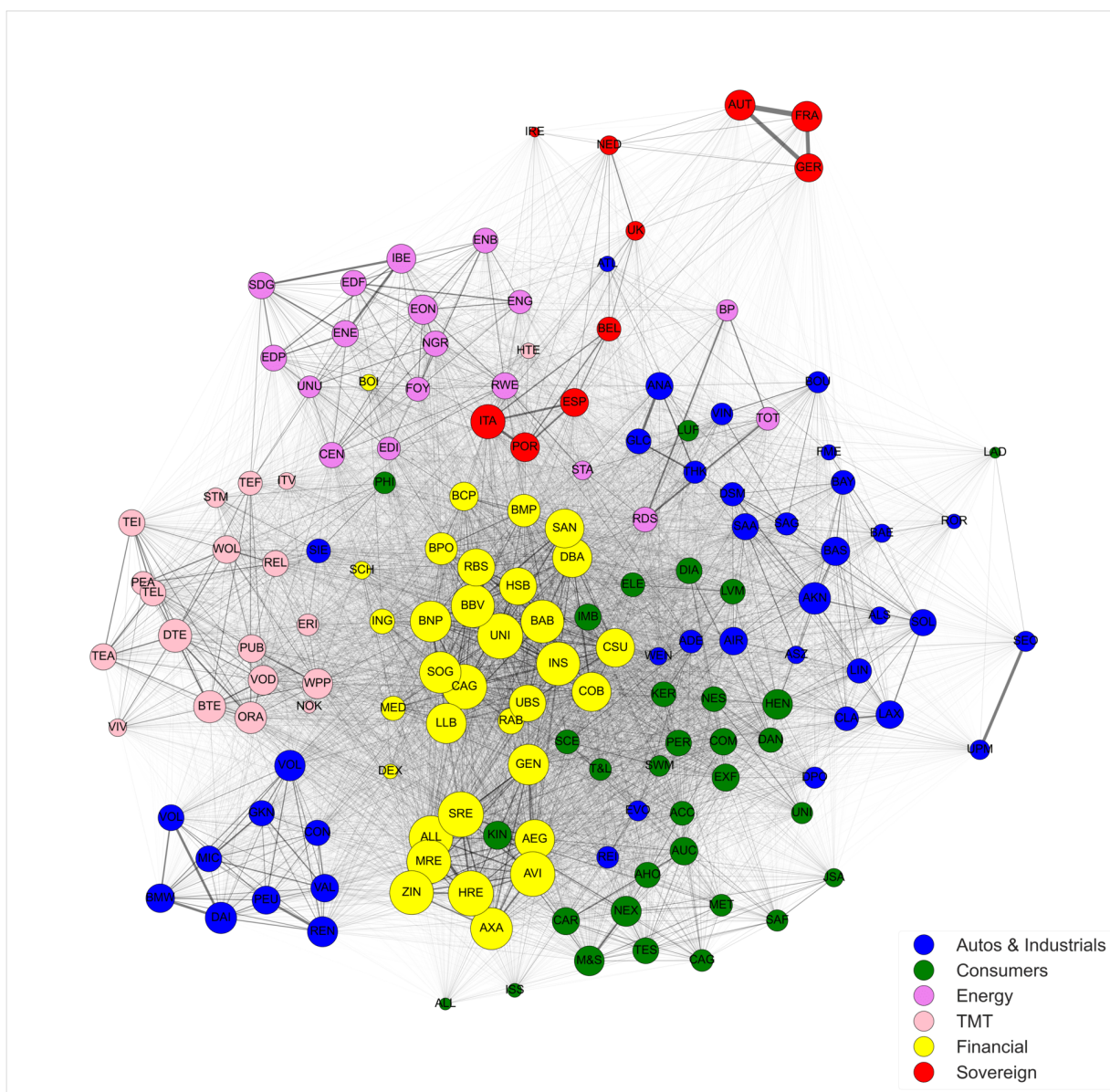
Note: This figure shows the cross-sectoral share of Granger-causality connections using the ratio of non-zero connections over the total number of possible connections originating from Non-financial subsectors to Financial institutions (black bars) and to Sovereigns (grey bars).

Figure 2.4: CDS network plot for the full-sample period (2006-2022) under forecast horizon $h = 10$



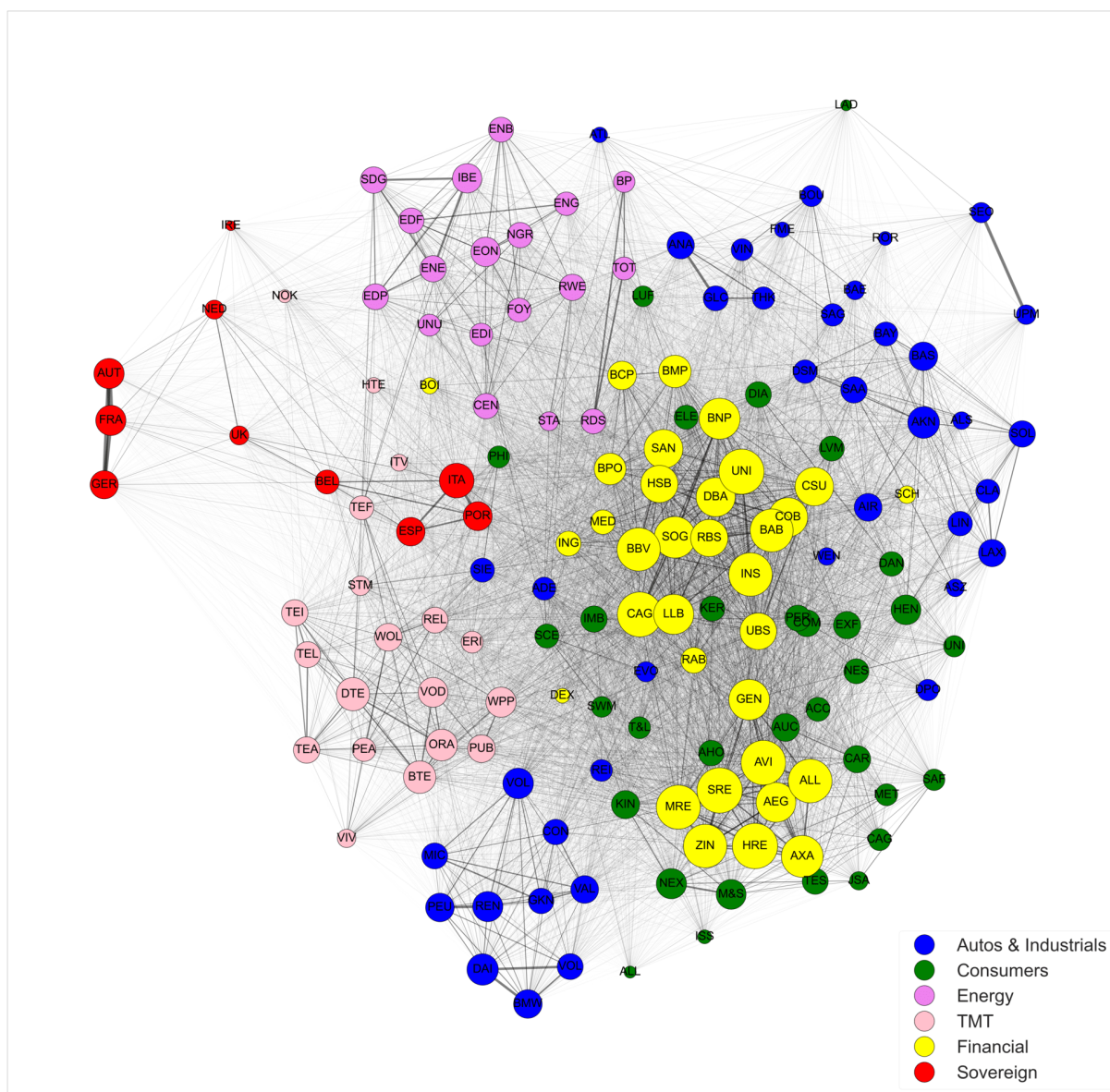
Note: The network's nodes are the CDS individual institutions colored by sub-sector and named according to the institutions' corresponding *Name Code* in Table 2.1. Their size represents the number and strength of outgoing connections they have, the bigger the size the more the risk they transmit to others. They are positioned based on the force-directed algorithm of Fruchterman and Reingold (1991), which places nodes close to each other according to how strongly they are connected. The connections are estimated using h -step forecast error variance decompositions. The number of common factors used is equal to two here but when applying the Hallin and Liška (2007) IC_2 criterion, the suggested number of factors is equal to one.

Figure 2.5: CDS network plot for the full-sample period (2006-2022) under forecast horizon $h = 5$



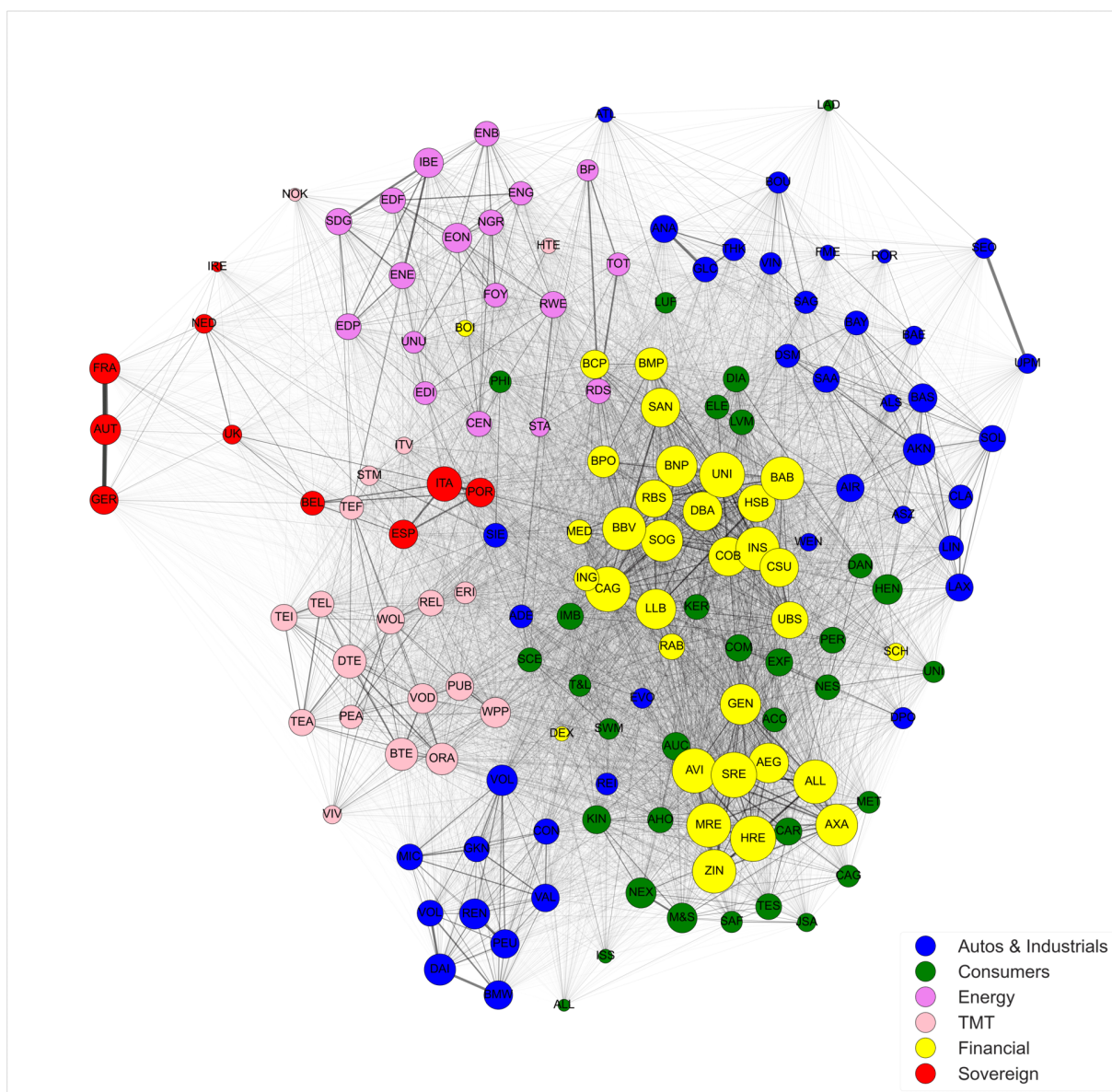
Note: The network's nodes are the CDS individual institutions colored by sub-sector and named according to the institutions' corresponding *Name Code* in Table 2.1. Their size represents the number and strength of outgoing connections they have, the bigger the size the more the risk they transmit to others. They are positioned based on the force-directed algorithm of [Fruchterman and Reingold \(1991\)](#), which places nodes close to each other according to how strongly they are connected. The connections are estimated using h -step forecast error variance decompositions. The number of common factors used is equal to two here but when applying the [Hallin and Liška \(2007\)](#) IC_2 criterion, the suggested number of factors is equal to one.

Figure 2.6: CDS network plot for the full-sample period (2006-2022) under forecast horizon $h = 15$



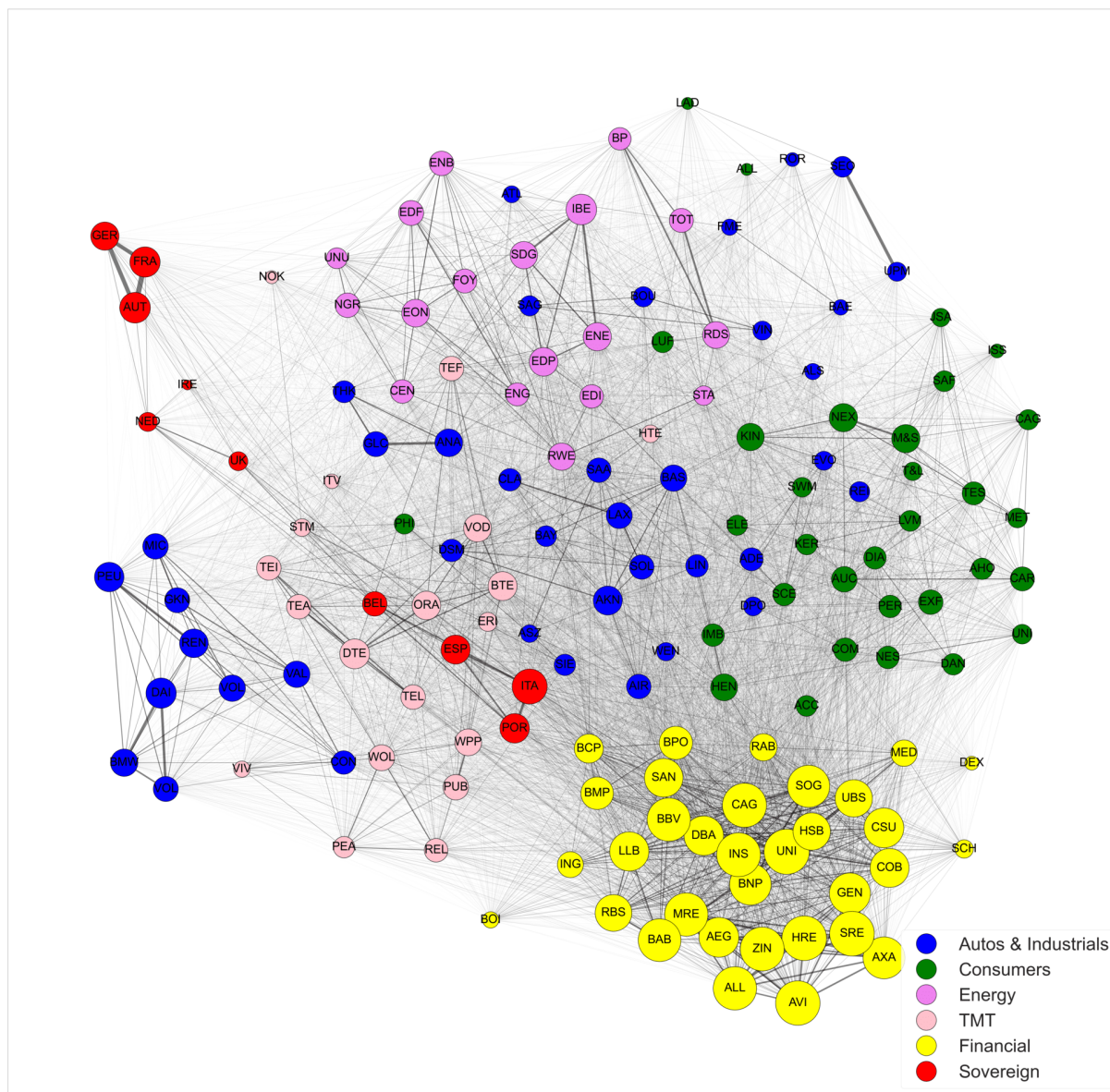
Note: The network's nodes are the CDS individual institutions colored by sub-sector and named according to the institutions' corresponding *Name Code* in Table 2.1. Their size represents the number and strength of outgoing connections they have, the bigger the size the more the risk they transmit to others. They are positioned based on the force-directed algorithm of [Fruchterman and Reingold \(1991\)](#), which places nodes close to each other according to how strongly they are connected. The connections are estimated using h -step forecast error variance decompositions. The number of common factors used is equal to two here but when applying the [Hallin and Liška \(2007\)](#) IC_2 criterion, the suggested number of factors is equal to one.

Figure 2.7: CDS network plot for the full-sample period (2006-2022) under forecast horizon $h = 20$



Note: The network's nodes are the CDS individual institutions colored by sub-sector and named according to the institutions' corresponding *Name Code* in Table 2.1. Their size represents the number and strength of outgoing connections they have, the bigger the size the more the risk they transmit to others. They are positioned based on the force-directed algorithm of [Fruchterman and Reingold \(1991\)](#), which places nodes close to each other according to how strongly they are connected. The connections are estimated using h -step forecast error variance decompositions. The number of common factors used is equal to two here but when applying the [Hallin and Liška \(2007\)](#) IC_2 criterion, the suggested number of factors is equal to one.

Figure 2.8: CDS network plot for the full-sample period (2006-2022) under forecast horizon $h = 10$ when imposing two common factors



Note: The network's nodes are the CDS individual institutions colored by sub-sector and named according to the institutions' corresponding *Name Code* in Table 2.1. Their size represents the number and strength of outgoing connections they have, the bigger the size the more the risk they transmit to others. They are positioned based on the force-directed algorithm of [Fruchterman and Reingold \(1991\)](#), which places nodes close to each other according to how strongly they are connected. The connections are estimated using h -step forecast error variance decompositions. The number of common factors used is equal to two here but when applying the [Hallin and Liška \(2007\)](#) IC_2 criterion, the suggested number of factors is equal to one.

Table 2.5: Rank correlation coefficients between the baseline model (1 factor, 10 days forecast horizon) and alternative specifications

	Ranking of Senders	Ranking of Receivers
<u>Financial to Non-Financial</u>		
<u>Forecast Horizon</u>		
5 days	0.9991***	0.9982***
15 days	0.9999***	0.9997***
20 days	0.9999***	0.9997***
<u>2 common factors</u>	0.8595***	0.8871***
<u>Sovereign to Non-Financial</u>		
5 days	0.9985***	0.9934***
15 days	0.9999***	0.9994***
20 days	0.9998***	0.9994***
<u>2 common factors</u>	0.9173***	0.8915***

Note: The table reports the Spearman rank correlation coefficient for rankings of senders and receivers between the baseline VAR model with one common factor and $h = 10$ days forecast horizon and alternative model specifications. Rank correlation coefficient equal to one means that ranking is exactly equal in the models under comparison, while a positive rank correlation implies that rankings move to the same direction (e.g. both increase) for both models under comparison. *** indicates that the associated p-value is equal to or less than 1%.

Table 2.6: Ranking of largest senders and receivers of credit risk

(a) Financial \rightarrow Non-Financial

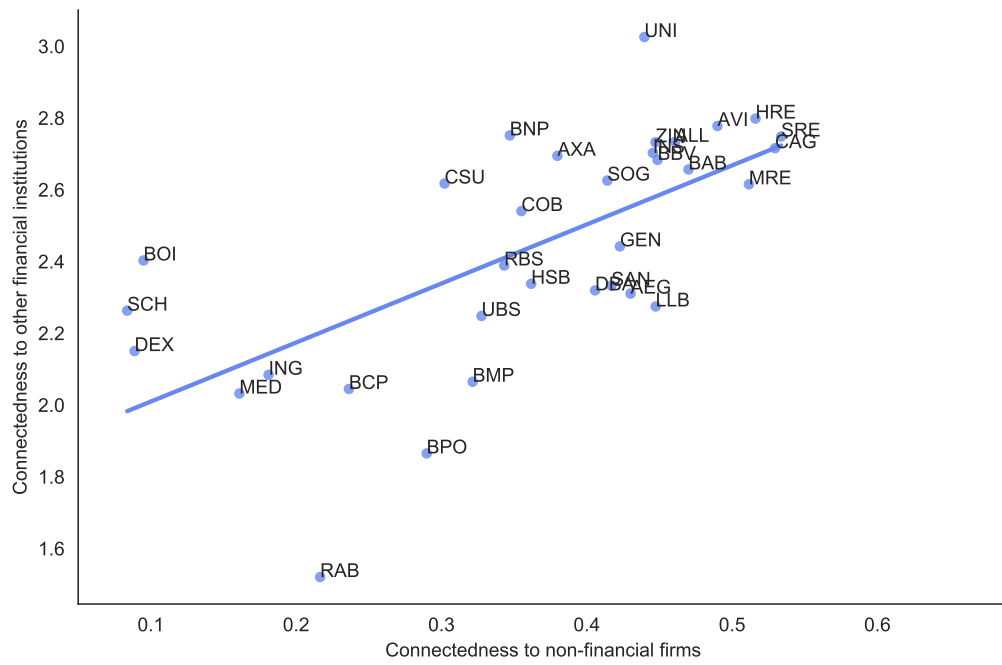
Sender			Receiver		
Rank	Name	Connectedness "To"	Rank	Name	Connectedness "From"
1	Swiss RE	0.53	1	Air Liquide	0.85
2	Credit Agricole	0.53	2	Accor	0.72
3	Hannover Rueck	0.52	3	Henkel	0.72
4	Munich RE	0.51	4	WPP	0.63
5	Aviva	0.49	5	Kering	0.62
6	Barclays Bank	0.47	6	Imperial Brands	0.62
7	Allianz	0.46	7	Compass	0.62
8	BBVA	0.45	8	Continental	0.60
9	Lloyds Bank	0.45	9	Experian Finance	0.60
10	Zurich Insurance	0.45	10	LVMH	0.58
⋮	⋮	⋮	⋮	⋮	⋮
29	ING	0.18	105	Atlantia	0.09
30	Mediobanca	0.16	106	Stora Enso Oyj	0.08
31	Bank of Ireland	0.09	107	Nokia	0.07
32	Dexia	0.09	108	Iberdrola	0.07
33	Standard Chartered	0.08	109	Ladbrokes	0.06

(b) Sovereign \rightarrow Non-Financial

Sender			Receiver		
Rank	Name	Connectedness "To"	Rank	Name	Connectedness "From"
1	Italy	0.25	1	Electricité de France	0.28
2	Spain	0.17	2	Energias de Portugal	0.28
3	Portugal	0.16	3	ENEL	0.26
4	Belgium	0.12	4	Hellenic Telecom	0.26
5	UK	0.08	5	EON	0.25
6	Netherlands	0.06	6	Compass	0.25
7	France	0.06	7	United Utilities	0.23
8	Germany	0.05	8	ENGIE	0.22
9	Austria	0.05	9	National Grid	0.21
10	Ireland	0.03	10	ENBW	0.20
⋮	⋮	⋮	⋮	⋮	⋮
⋮	⋮	⋮	⋮	⋮	⋮
⋮	⋮	⋮	105	Michelin	0.03
⋮	⋮	⋮	106	ThyssenKrupp	0.02
⋮	⋮	⋮	107	Volvo	0.02
⋮	⋮	⋮	108	Telekom Austria	0.02
⋮	⋮	⋮	109	Metro	0.02

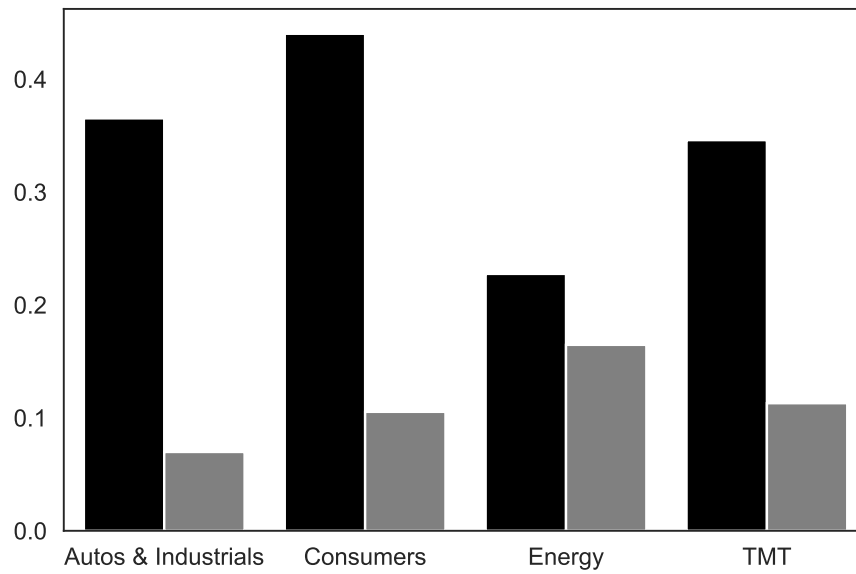
Note: The tables ranks senders and receivers according to the strength of their incoming or outgoing connections relatively to others. The table represents connectedness by taking into account the total number of entities, therefore the displayed connectedness is the average value per entity.

Figure 2.9: Individual senders of financial risk for the full-sample period (2006-2022)



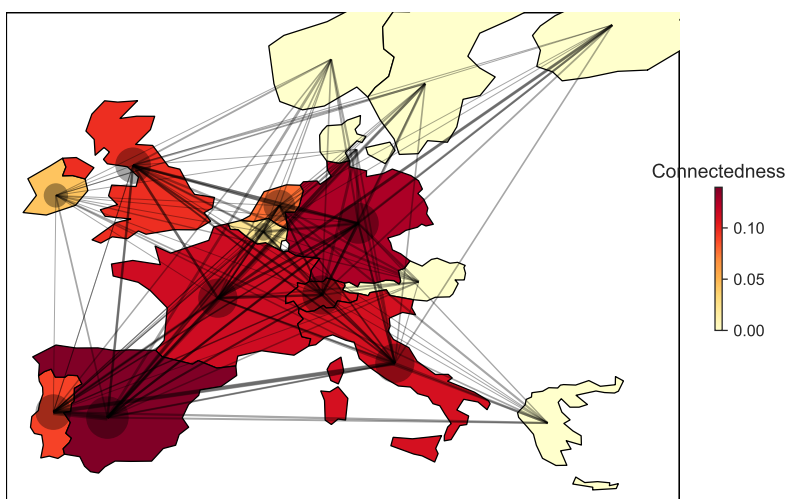
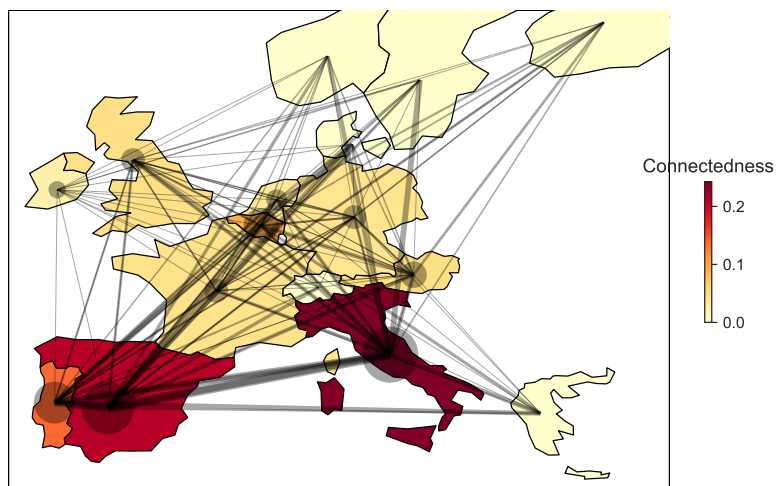
Note: The figure shows the financial entities' total connectedness to other financial institutions versus other non-financial firms.

Figure 2.10: Aggregate cross-sectoral connectedness



Note: The figure shows the directional connectedness from financial entities (black bars) and sovereigns (grey bars) respectively to non-financial firms by sub-sector and normalizing based on the number of entities.

Figure 2.11: Geographical connectedness

(a) Financial \rightarrow Non-financial(b) Sovereign \rightarrow Non-financial

Note: The figures show directional connectedness by country for the full-sample period (2006-2022). Each entity has its headquarters in a specific country listed in Table 2.1. The color of countries indicates the magnitude of incoming connectedness in non-financial institutions from (a) financial entities, and (b) sovereigns (connectedness “from”). The black circles size shows the magnitude of outgoing connectedness from (a) financial entities, and (b) sovereigns of the corresponding countries (connectedness “to”). The connections’ thickness shows the connections strength.

Table 2.7: Geographical connectedness and financial linkages

	(1)	(2)
	Financial → Non-financial	Sovereign → Non-financial
Bilateral bank claims		
(i) All sectors	0.044 (0.032)	0.075*** (0.033)
(ii) Non-bank private sector	0.013 (0.012)	0.086 (0.044)

Note: The table shows the results of regressing pairwise cross-country connectedness measures on bilateral bank claims. The data for bilateral bank claims are available at the consolidated banking statistics database of the Bank for International Settlements (BIS) and they measure a country's risk exposure by capturing the banks ultimate risk basis. Here, there is a distinction of bilateral bank claims of country i (a) to all sectors, and (b) to non-bank private sector, of country j . The bilateral bank claims are divided by the country's GDP. The OLS regressions include a constant and country dummy variables. In parentheses the standard errors can be found and *** show significance at 1% level.

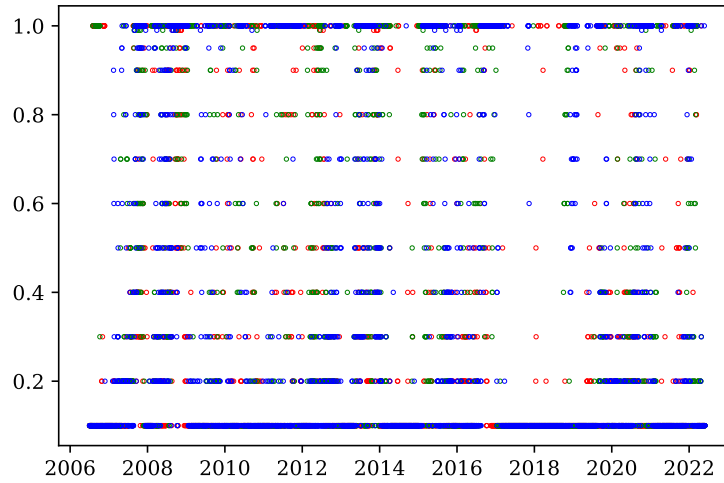
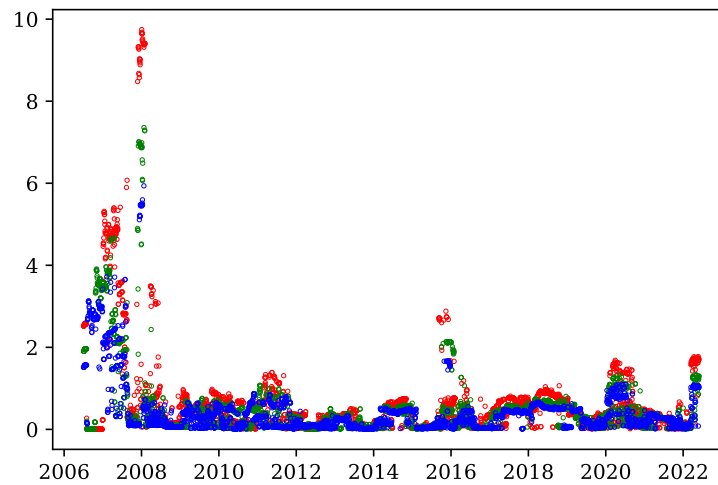
2.3 Replication Dynamic results

In addition, I provide dynamic connectedness results as GS do, using rolling window estimation with window sizes 150, 200 and 250 days for the extended dataset. The baseline dynamic model has a window size of 200 days. The dynamic rolling window estimation uses increment size 1 and `sklearn`'s `ElasticNetCV` python class which sets the mixing parameter α to get one value from $[0.1, 0.2, 0.3, 0.4, 0.5, 0.6, 0.7, 0.8, 0.9, 1]$ while performing 10-fold cross validation. This estimation method which has similarities on the authors' method is not the most time efficient way to conduct the rolling window estimation because of very low increment size and the selection of both the mixing parameter α and the penalty tuning parameter λ . The fact that α in this work is not allowed to take possible values that extend to the second decimal makes these results and the GS results to have some differences, see the replicated Figure 2.12 and the corresponding GS Figure A.5.

Figure 2.13 and the original Figure 5 depict the global financial crisis prior to and after the Lehman Brothers bankruptcy. Also, Figure 2.14 replicates the original Figure 6 and shows credit risk concentration to European sovereigns. The figures look similar to the original ones, given that this work's findings use the extended version of the data. Figures 2.15 and 2.16 on the system-wide connectedness, Figures 2.17, 2.18 and 2.19 on the cross-sectoral connectedness, and 2.20 on country groups connectedness replicate closely but with some magnitude differences the respective Figures 7 and A.12, 8, A.3 and A.4, and 9 of the GS paper. The findings seem to reveal that during the pandemic of 2020, (a) the main senders of risk were from the non-financial sector, and, (b) the connectedness percentage ratio of the estimated connections over all possible connections was higher rather than any

other period. Also, Figure 2.21 on the Dynamic Granger-causality connectedness on window size 200 well corresponds to the original Figure A.7.

Figure 2.12: Distribution of elastic net parameters for different window sizes

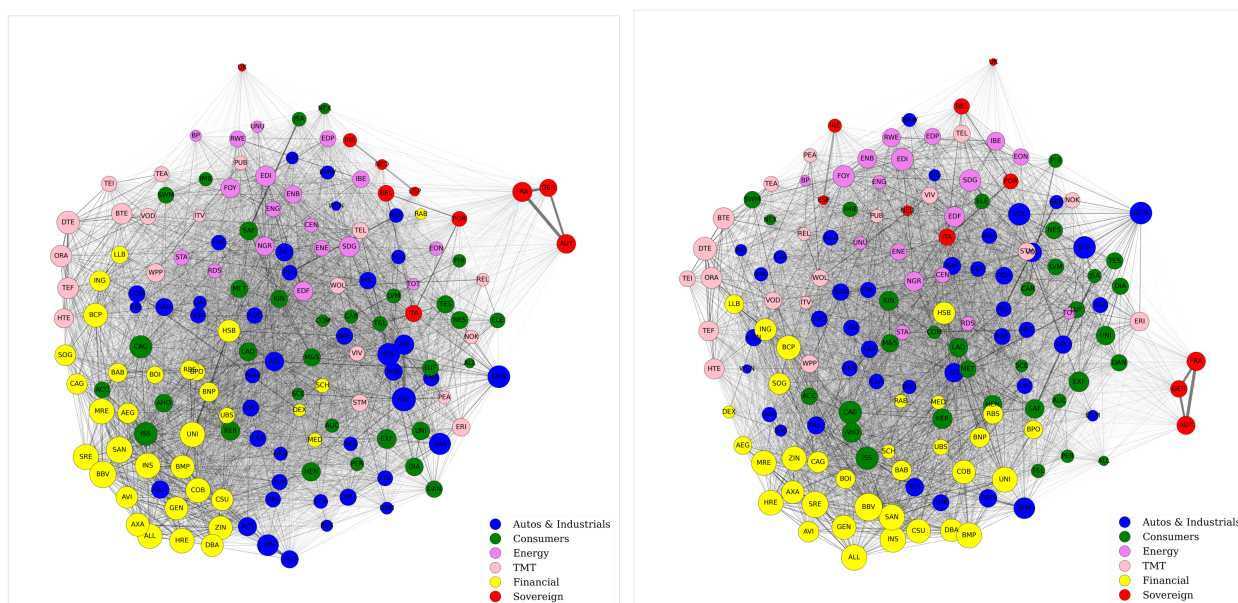
(a) Mixing parameter α (b) Penalty tuning parameter λ 

Note: The figure shows how the mixing parameter α in (a) and the penalty tuning parameter λ evolve over time for the full-sample period (2006-2022) using dynamic rolling window estimation. Both parameters presented are averaged for the panel of 152 VAR equations for each window. The window sizes are 150, 200, and 250 days and their corresponding parameters are in red, green, and blue color, respectively.

Figure 2.13: CDS network before and after Lehman Brother's bankruptcy

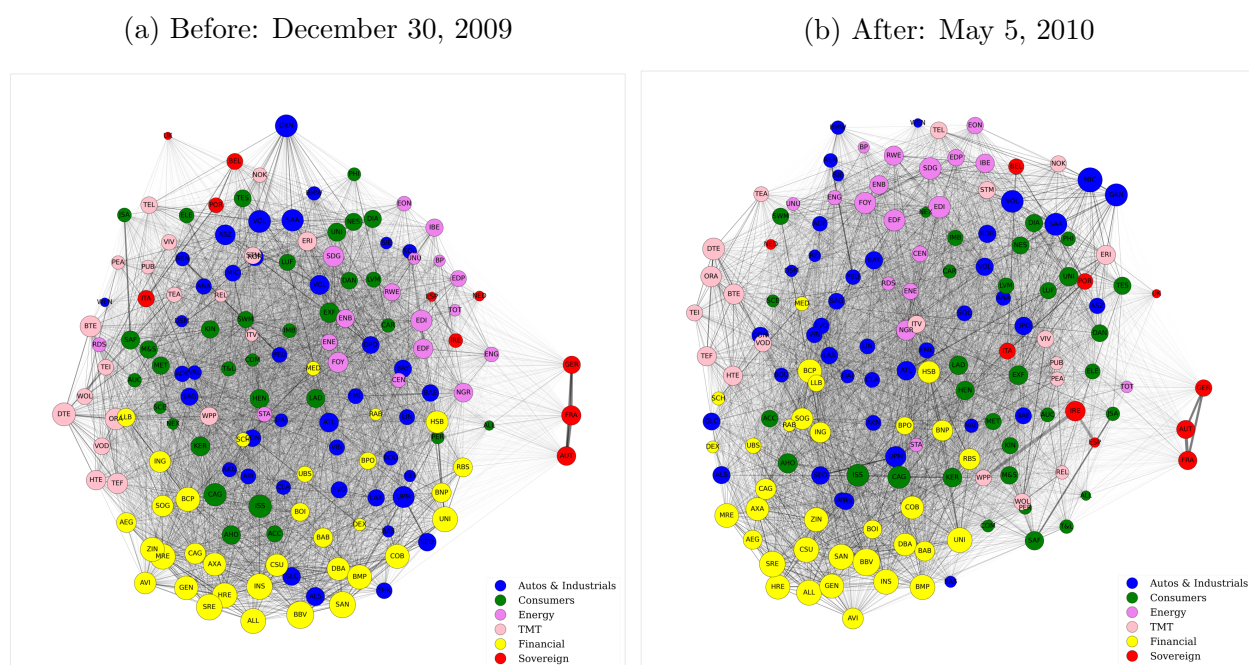
(a) Before: September 1, 2008

(b) After: November 6, 2008



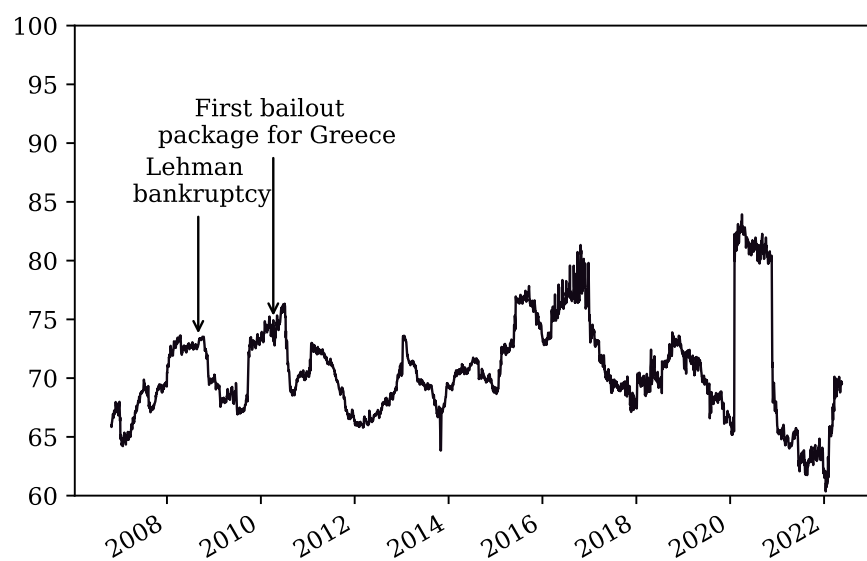
Note: The networks are produced using rolling window dynamic estimation of 200 days. Note: The network's nodes are the CDS individual institutions colored by sub-sector and named according to the institutions' corresponding *Name Code* in Table 2.1. Their size represents the number and strength of outgoing connections they have, the bigger the size the more the risk they transmit to others. They are positioned based on the force-directed algorithm of Fruchterman and Reingold (1991), which places nodes close to each other according to how strongly they are connected. The connections are estimated using h -step forecast error variance decompositions. The number of common factors used is equal to two here but when applying the Hallin and Liška (2007) IC_2 criterion, the suggested number of factors is equal to one.

Figure 2.14: CDS network before and after the onset of the sovereign debt crisis



Note: The networks are produced using rolling window dynamic estimation of 200 days. Note: The network's nodes are the CDS individual institutions colored by sub-sector and named according to the institutions' corresponding *Name Code* in Table 2.1. Their size represents the number and strength of outgoing connections they have, the bigger the size the more the risk they transmit to others. They are positioned based on the force-directed algorithm of [Fruchterman and Reingold \(1991\)](#), which places nodes close to each other according to how strongly they are connected. The connections are estimated using h -step forecast error variance decompositions. The number of common factors used is equal to two here but when applying the [Hallin and Liška \(2007\)](#) IC_2 criterion, the suggested number of factors is equal to one.

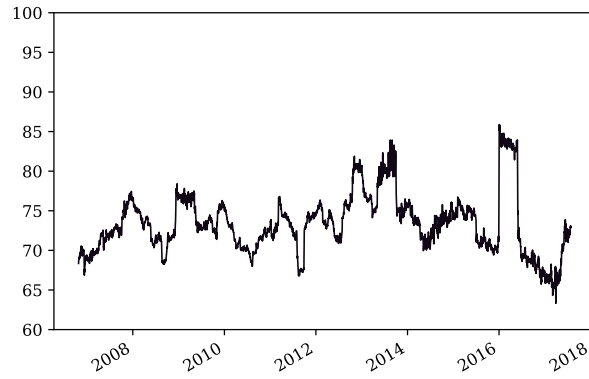
Figure 2.15: Dynamic system-wide connectedness



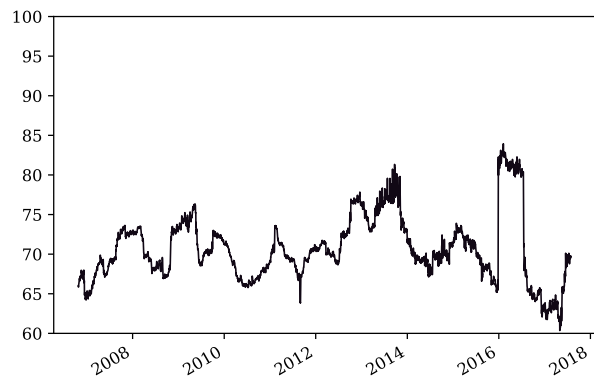
Note: This figure shows dynamic system wide connectedness which is calculated from $h = 10$ -step forecast error variance decompositions using a rolling window of 200 days.

Figure 2.16: Dynamic system-wide connectedness for different window sizes

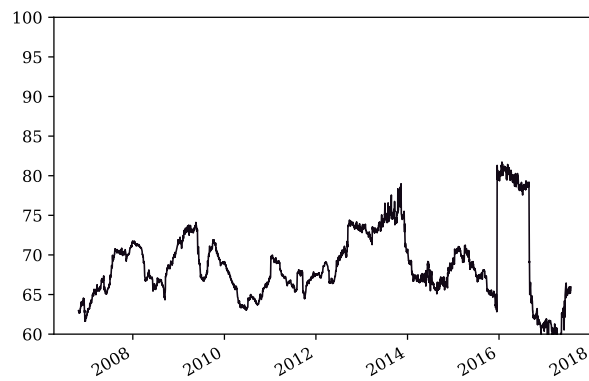
(a) 150 days



(b) 200 days

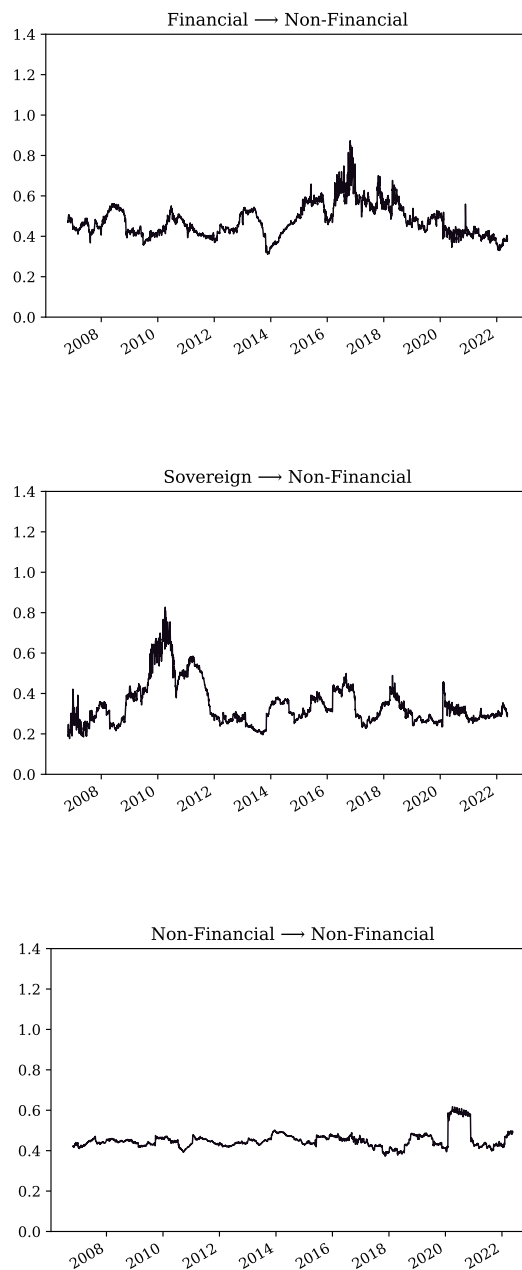


(c) 250 days



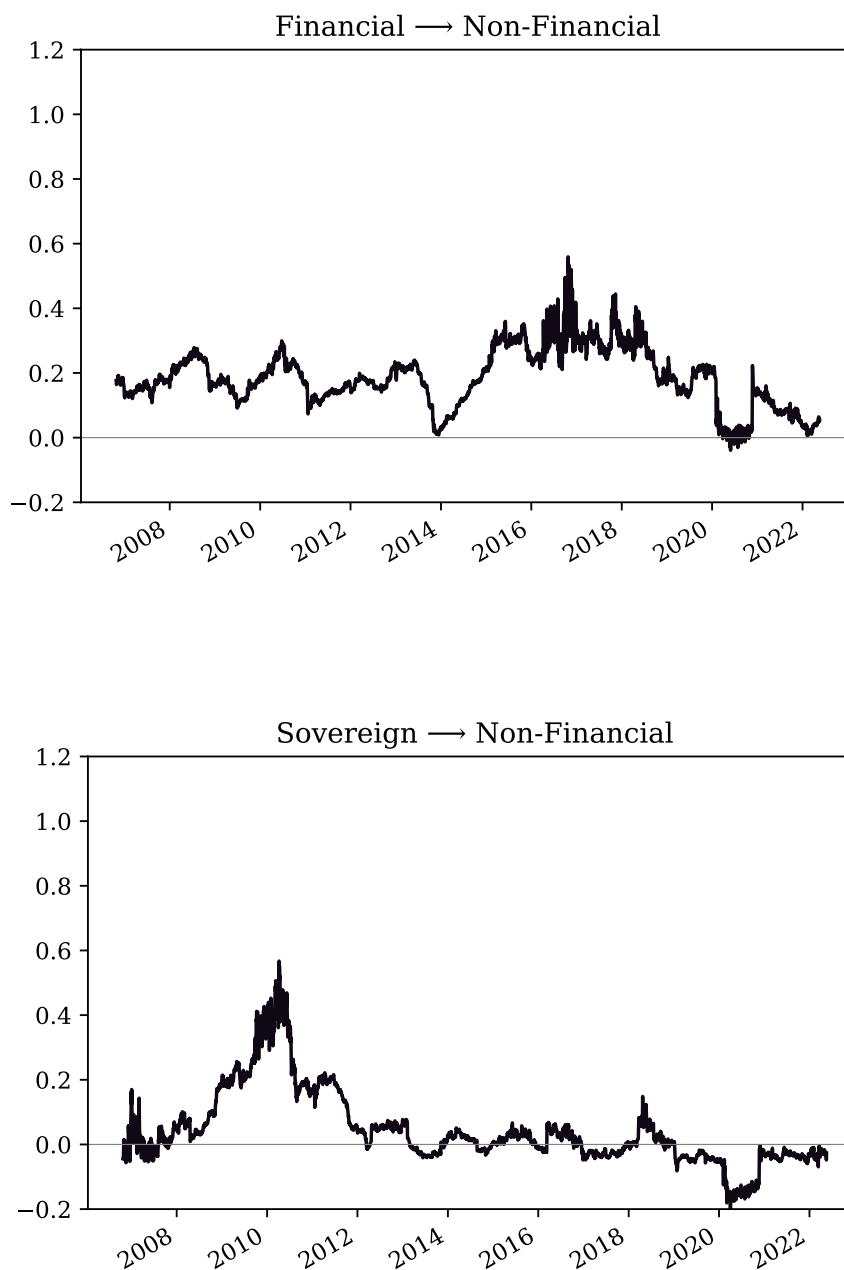
Note: These figures show dynamic system wide connectedness which is calculated from $h = 10$ -step forecast error variance decompositions using rolling windows of 150, 200, and 250 days.

Figure 2.17: Dynamic cross-sectoral connectedness



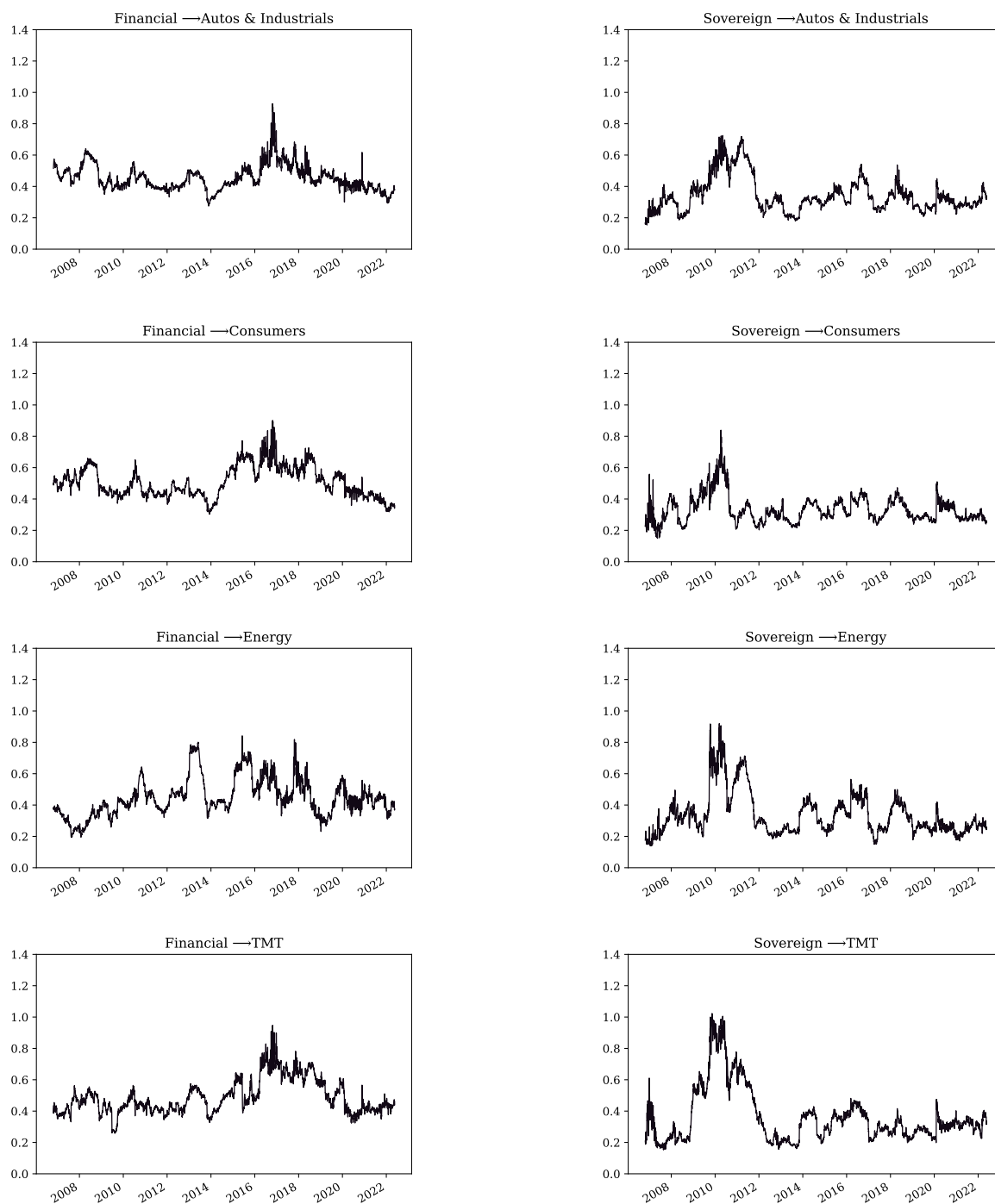
Note: The figure shows dynamic cross-sectoral connectedness from Financial institutions (a) and from Sovereigns (b) and Non-financial firms (c) to Non-financial firms. The estimated connectedness comes from $h = 10$ -step forecast error variance decompositions calculated from a dynamic rolling window estimation of 200 days. Each measure is averaged by the number of entities in each sector.

Figure 2.18: Dynamic cross-sectoral connectedness, net distribution



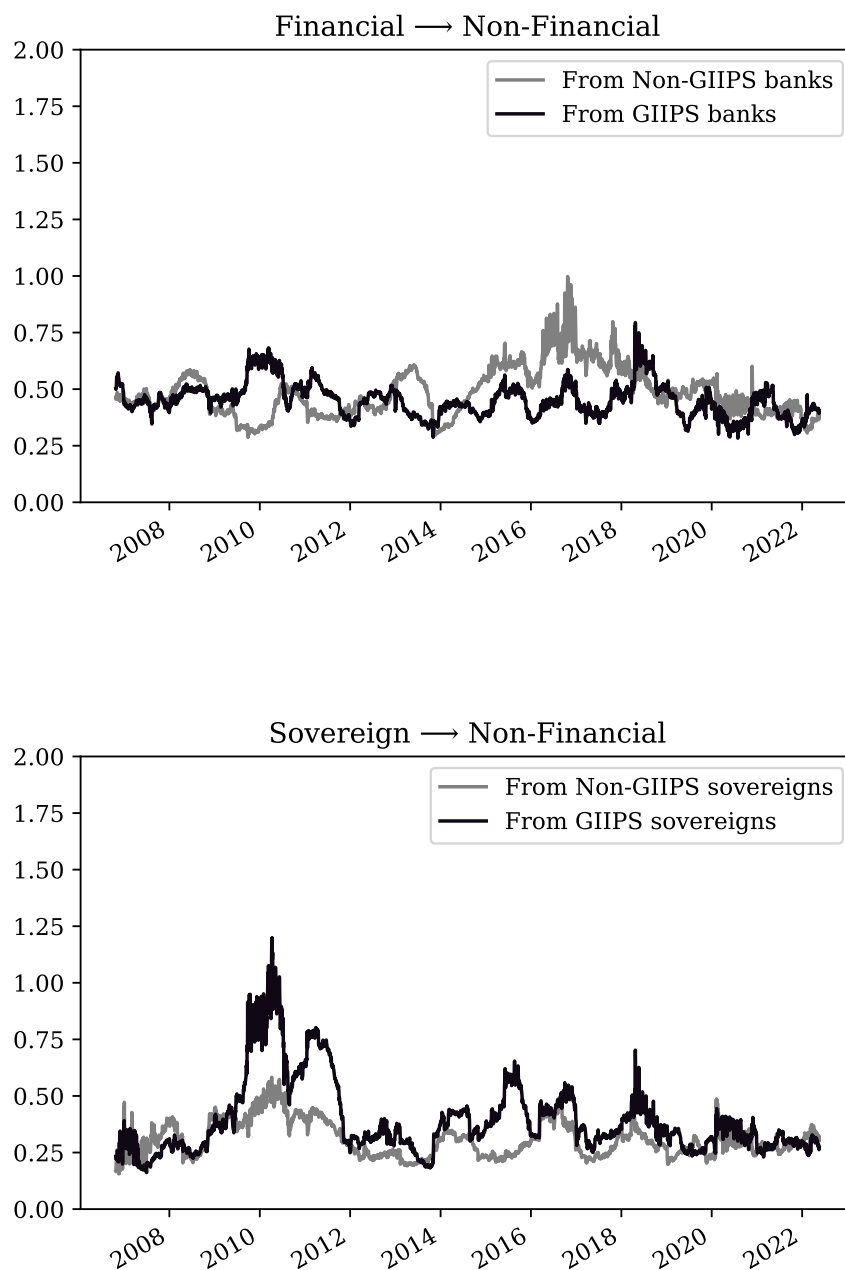
Note: The figure shows dynamic net contribution of cross-sectoral connectedness from Financial institutions (a) and from Sovereigns (b) to Non-financial firms. The estimated connectedness comes from $h = 10$ -step forecast error variance decompositions calculated from a dynamic rolling window estimation of 200 days. The net contribution is the estimated connectedness from X entities to Y entities minus connectedness from Y entities to X entities. Each measure is averaged by the number of entities in each sector.

Figure 2.19: Dynamic cross-sectoral connectedness, sub-sectors



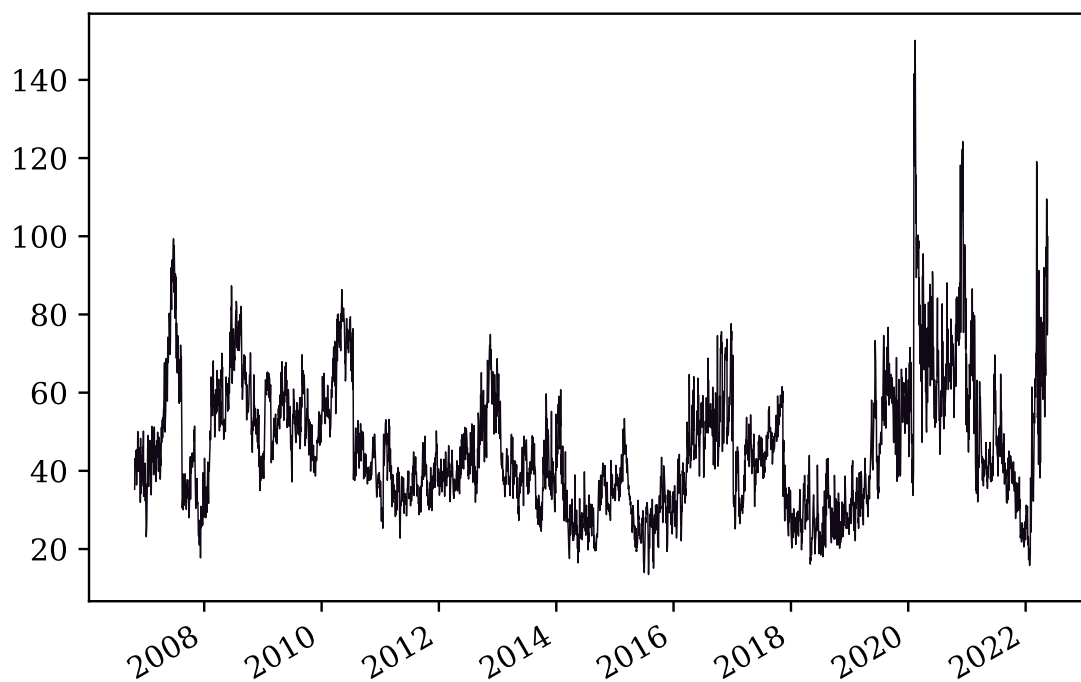
Note: The figure shows dynamic cross-sectoral connectedness from financial institutions (a) and from sovereigns (b) to non-financial sub-sectors. The estimated connectedness comes from $h = 10$ -step forecast error variance decompositions calculated from a dynamic rolling window estimation of 200 days. Each measure is averaged by the number of entities in each sector and sub-sector.

Figure 2.20: Dynamic network connectedness across country groups



Note: These figures show dynamic network connectedness which is calculated from $h = 10$ -step forecast error variance decompositions using a rolling window of 200 days across two country groups: GIIPS and non-GIIPS. GIIPS countries refers to Greece, Italy, Ireland, Portugal and Spain, but Greece is not included in this analysis due to data unavailability. The non-GIIPS countries included in this analysis can be found in Table 2.1. The measures are normalized by the number of entities in each group.

Figure 2.21: Dynamic Granger-causality connectedness



Note: This figure shows dynamic Granger causality connections among CDS entities by presenting the share of non-zero links over the total number of possible links. The connections originate from the estimated coefficient matrix of the estimated VAR with a rolling window estimation of 200 days.

2.4 Conclusion

This paper provides a replication of the [Gross and Siklos \(2020\)](#) paper using data up to 2022 and Python instead of Matlab. It offers new python classes that can be directly used for estimating the generalized dynamic factor model and for the calculation of the generalized variance decomposition matrix. The results shed light onto the credit risk transmission scheme when the pandemic crisis period that started in 2020 is included in the full sample period. The findings are matching closely to the original ones and uncover risk interactions among European entities when the full-sample spans from 2006 to 2022. The findings show that risk transmission followed different schemes during the pandemic crisis affecting Europe in an alternative way than the financial and the sovereign crisis of the late '00s and early '10s. In particular, risk exchanges are found to be more intense during the pandemic of 2020 versus 2008-2010, and risk senders do not seem to belong in the financial or the sovereign sectors, but rather originating from the non-financial industries.

Chapter 3

Estimated spillover effects of block factors

This paper estimates spillover effects among sub-sector specific European economic entities of the following types: a) institution-to-institution, see e.g. [Gross and Siklos \(2020\)](#), b) institution-to-block, c) block-to-institution, d) block-to-block. The economic entities studied belong to six sub-sectors: the Automobile, Consumer, Energy, Telecommunication industries, Financial firms, and, Sovereigns and this analysis' main contribution is that it evaluates the spillover estimates from blocks of entities to others and vice versa. This sheds light onto how credit risk is transmitted within a network of non-financial firms, sovereigns, banks and their estimated block-specific common factors over time, taking into account the dependencies within and between the factors. The sub-sample findings of the analysis show high spillover effects (i) towards the block-specific common factors during and at the beginning of a financial crisis period, (ii) among the block-specific common factors for the following periods.

3.1 Introduction

Financial crisis periods can cause a series of shocks, and they have been associated with public debt increases and economic activity declines. Notably, the most recent global financial crisis of 2007-2008 emerged as a European sovereign debt crisis in 2010 which constitutes one of the biggest post-millennium critical points. For financial stability purposes, and since there has been evidence that systemic risk may have negative impact to other sectors of the economy, see [De Bandt et al. \(2009\)](#), central banks have developed systemic risk monitoring procedures. One aspect of systemic risk comes from disruption in financial services. Another aspect of systemic risk is the so-called *contagion* ([De Bandt and Hartmann \(2000\)](#) and [Constancio et al. \(2012\)](#)). Contagion can be referred as negative effects starting from an institution or a group of institutions in distress and affecting others ([Dornbusch et al. \(2000\)](#), [Forbes and Rigobon \(2002\)](#)). Estimating spillover effects across different types of economic entities and across time can uncover network connections' existence, transmission, and amplification mechanisms, and, therefore, the existence or not of contagion. How will a shock starting from the financial sector and having no short-run effects to others, emerge overtime and will this vivify the contagion?

This project makes two main contributions: The first contribution is the two-step methodology which proposes the inclusion of estimated block-specific common factors in a Vector Autoregressive (VAR) model in order to estimate spillover effects among blocks of industries and the rest of the variables in the VAR model. This analysis evaluates both components of systemic risk, the common and the idiosyncratic. Financial institutions hold government debt, so they are exposed to sovereign risk, and banking crises can have negative

implications to economic activity, see, e.g., [Dell’Ariccia, Ferreira, Jenkinson, Laeven, Martin, Minoiu and Popov \(2018\)](#). Therefore, the proposed methodology provides full-sample and sub-sample evidence of the existence of contagion and its evolution over time. Secondly, the proposed methodology followed by a network analysis and its measures offer useful tools for the evaluation of the primary senders and receivers of risk, the strength of links, the distance among agents as well as the systemic importance of each agent in the network. The implementation of networks allows for further exploration of systemic risk behavior across large numbers of entities and their blocks providing visuals which are holding multiple types of useful information.

Following [Diebold and Yilmaz \(2014\)](#), [Gross and Siklos \(2020\)](#), [Demirer et al. \(2018\)](#), I estimate and graphically represent the monolayer network of European corporations, sovereigns and banks both for the full-sample period (2006-2022) but also for three sub-samples defined inside 2006-2022 panel dataset’s time period, each one covering: the financial crisis of 2007-2008, the sovereign crisis of 2010 and the Covid-19 pandemic of 2020. In both analyses, connectedness comes from the estimated variance decomposition of a VAR of the idiosyncratic component and the block-specific factors initially extracted from the Dynamic Hierarchical Factor model by [Moench, Ng and Potter \(2013\)](#) and modelled together in the same VAR.

The findings show that the inclusion in the full and sub-sample analysis of the block factors reveals the contagion effect and its implications during the onset of the global financial crisis of 2008. More specifically, the findings of these three periods’ sub-sample analysis suggest to further examine the periods of global financial crisis in 2008 and the European

sovereign crisis in 2010. Thus, I further examine four narrower periods during around the end of October, 2006 up to early August, 2010, where each period is covering before an event of special importance took place such as a) the BNP Paribas freezing \$2.2 billion of funds due to the subprime mortgage sector, b) the Lehman Brothers' bankruptcy, c) the G20 decision to finance the financial sector, d) Eurozone's decision provide bailout packages to certain of its country members.

From a policy standpoint, the methodology proposed is of particular importance for the monitoring and potential prevention of future risk oriented financial and sovereign crises. More specifically, a policy maker is able to see signals of an upcoming economic crisis by studying the behavior of the idiosyncratic and the block factors. When the block factors are positioned close to the rest of the network, and if this is due to idiosyncratic entities transmitting risk to the block factors, this would mean the contagion has been activated.

3.2 Motivation

Recent literature has studied network connectedness using *variance decompositions* estimated from Vector Autoregressive (VAR) models. While some authors adopt *generalized* variance decompositions (Diebold and Yilmaz (2014), Gross and Siklos (2020), Demirer et al. (2018), Nițoi and Pochea (2021), Wang et al. (2021)), others, following full identification, use the *orthogonalized* variance decompositions (Diebold and Yilmaz (2009), Barigozzi and Hallin (2017), Yang et al. (2021), Galariotis et al. (2016)), the definitions of which are in Pesaran and Shin (1998). On the one hand, the generalized VAR framework is not able to provide economic interpretation of the VAR innovations, on the other hand, identification

of structural shocks requires making assumptions that are hard to justify in high dimensional VARs. Nevertheless, policy-relevant literature has employed *variance decompositions* to evaluate interactions among individuals in the EU sovereign credit market (Claeys and Vašíček (2014)), interactions among the latter and EU financial institutions (Alter and Beyer (2014)), spillovers among sovereigns and international banks in the US, Europe and Japan (Gross and Kok (2013)), and, spillovers between US and Europe's fixed income markets (Nyholm (2016)).

The methodology to be followed is constructed for credit risk monitoring and can stand as a valuable tool for policy-making institutions. For this purpose, and following Diebold and Yilmaz (2014), Gross and Siklos (2020), Demirer et al. (2018), the goal is to estimate and graphically represent the 2-D and monolayer network of European corporations, sovereigns and banks both for the full-sample period (2006-2022) but also in sub-samples having three successive periods covering the financial crisis of 2007-2008, the sovereign crisis of 2010 and the Covid-19 pandemic of 2020. In addition, results are provided for four more periods, successive to each other, where all together cover from the end of 2006 up to around mid-2010. The dynamic analysis is of particular importance for policy-related conclusions and remarks. In all analyses, connectedness is based on the *generalized* variance decomposition definition, as proposed by Pesaran and Shin (1998).

The following section describes the methodology which starts by applying a Hierarchical Dynamic Factor Model (HDFM) in order to estimate the idiosyncratic component and the block-specific common factors. Following this step, a high-dimensional VAR is constructed which incorporates the block-specific common factors as well as the estimated idiosyncratic

component of the previous step. The issue of dimensionality can be tackled by choosing the data-appropriate penalized regression method, see [Melkumova and Shatskikh \(2017\)](#), [Zou and Hastie \(2005\)](#), [Zou \(2006\)](#), [Yuan and Lin \(2006\)](#): Ridge, Lasso, Elastic net shrinkage, Adaptive lasso, Group lasso. After comparing a handful of methods, the chosen penalization method is the Elastic Net. Under this framework, the researcher can estimate network connectedness as proposed by [Diebold and Yilmaz \(2014\)](#) and adapted by [Barigozzi and Hallin \(2017\)](#), by estimating the variance decompositions (VDs) defined by [Pesaran and Shin \(1998\)](#). Each entry ij of the VDs measures the proportion of how a shock in a block-specific common factor or in variable j affects the h -step ahead forecast error variance (FEV) of variable i , over the effect on the FEV of i because of shocks to all other variables and the factors.

3.3 Methodology

The methodology I am following employs first the Dynamic Hierarchical Factor Model (DHF) proposed by [Moench, Ng and Potter \(2013\)](#) assuming data can be organized in B blocks and each block can have a total of N_{F_b} *block-specific factors*. First, the Dynamic Hierarchical Factor Model is applied. This way the dependence of the block-specific factors to the global common factor as well as dependencies of variables within and across block factors are taken into account. Secondly, a suitable penalized regression method can be applied, especially on a high-dimensional Vector Autoregressive (VAR) model composed of the idiosyncratic component and block factors estimated in the previous step. Finally, one can calculate the generalized variance decompositions which can be represented as a square

h -step forecast error variance decomposition (VD) matrix, which can also be viewed as a network adjacency matrix, thus, it can be depicted as a network plot according to the networks literature. This two-step methodology enables the estimation of the spillover effects among institutions and blocks of institutions and can provide more insights on the existence of contagion and the process of its vivification.

3.3.1 The Dynamic Hierarchical Factor Model (DHFm)

Let N be the total number of variables in the panel dataset with a total of T observations across time, for $n = 1, \dots, N$ variables and time $t = 1, \dots, T$. Considering a stationary, mean zero and unit variance panel dataset Y which can be organized into blocks, define b to be the block-specific index, η to be the variable-specific index in a given block b and N_b to be the total number of variables in block b , for $b = 1, \dots, B$, such that $\eta = 1, \dots, N_b$, and $N = N_1 + \dots + N_B$. One can assume in this model there exists a total number of N_X global common factors $X_t = (X_{1t}, \dots, X_{N_X t})$ and a total of N_{F_b} block-specific factors $F_{bt} = (F_{b1t}, \dots, F_{bN_{F_b}t})$ for block b , where $\rho = 1, \dots, N_X$ and $r = 1, \dots, N_{F_b}$.

By [Moench, Ng and Potter \(2013\)](#), one can write a Dynamic Hierarchical Factor Model (DHFm) with common, idiosyncratic and block-specific components for all b, η, ρ and r , as follows,

$$Y_{b\eta t} = \lambda_{F_b}^\eta(L)F_{bt} + e_{Y_{b\eta t}}, \quad (3.1)$$

$$F_{brt} = \lambda_{X_b}^r(L)X_t + e_{F_{brt}}, \quad (3.2)$$

$$\psi_{X_\rho}(L)X_{\rho t} = \varepsilon_{X_{\rho t}}, \quad \varepsilon_{X_{\rho t}} \sim N(0, \sigma_{X_\rho}^2), \quad (3.3)$$

$$\psi_{Y_{b\eta}}(L)e_{Y_{b\eta t}} = \varepsilon_{Y_{b\eta t}}, \quad \varepsilon_{Y_{b\eta t}} \sim N(0, \sigma_{Y_{b\eta}}^2), \quad (3.4)$$

$$\psi_{F_{br}}(L)e_{F_{brt}} = \varepsilon_{F_{brt}}, \quad \varepsilon_{F_{brt}} \sim N(0, \sigma_{F_{br}}^2), \quad (3.5)$$

where $\lambda_{F_b}^\eta(L)$ and $\lambda_{X_b}^r(L)$ are distributed lag of loadings on the $N_{F_b} \times 1$ vector of the block-specific factors $F_{bt} = (F_{b1t}, \dots, F_{bN_{F_b}t})$ and on the $N_X \times 1$ vector of the global common factors $X_t = (X_{1t}, \dots, X_{N_X t})$, respectively.

All the factors and the idiosyncratic components are assumed to be stationary autoregressive processes of order q_{X_ρ} , $q_{F_{br}}$, $q_{Y_{b\eta}}$, respectively.

In this setting, there exists correlation among the variables in the same block through the global common factors X_t , or through $e_{F_{brt}}$. Correlation also exists across different blocks but only through the global common factor X_t . [Moench, Ng and Potter \(2013\)](#) also provide a more extended version introducing subblocks into their model.

For identification, it is assumed that the loadings λ are constant and lower triangular matrices of order zero with diagonal elements of fixed sign and that the innovations to the factors have fixed variances.¹

¹[Moench, Ng and Potter \(2013\)](#) make these identification assumptions too.

Estimation of DHFM using Markov Chain Monte Carlo

One could choose to estimate the DHFM in a sequential fashion, which means one could first estimate for the global common factors X_t and then for the block-specific factors F_{bt} , using in both cases principal components. However, in this way any dependencies or correlations of variables within or across blocks would not be taken into account.

I choose to estimate this model using MCMC and more specifically Gibbs Sampling, a method that has also been employed by [Kose, Otrok and Whiteman \(2003\)](#), [Moench, Ng and Potter \(2013\)](#), [Goldstein and Browne \(2014\)](#) and others. The algorithm's steps can be found below for $\Lambda = (\Lambda_X, \Lambda_F)$, $\Psi = (\Psi_X, \Psi_F, \Psi_Y)$ and $\Sigma = (\Sigma_X, \Sigma_F, \Sigma_Y)$.

1. Get the initial values for the factors by estimating sequentially and using principal components. Based on these initial values estimate the initial values for Λ, Ψ, Σ .
2. Conditional on Λ, Ψ, Σ , the global common factor X_t and the data Y_t , draw $F_{bt}, \forall b$.
3. Conditional on Λ, Ψ, Σ , the block-specific factors F_t , draw X_t .
4. Conditional on X_t and F_t , draw Λ, Ψ, Σ .
5. Return to step 2.

The Gibbs sampling one can run can have a total of $n_{\text{Gibbs}} = 100,000$ draws, out of which 50,000 draws are set to belong to the burn-in samples and the draws after the first 50 thousand are kept.

3.3.2 A Vector Autoregressive (VAR) model with block factors

In this section, a high-dimensional Vector Autoregressive (VAR) model will be constructed using the estimated idiosyncratic component and the block factors of the previous section.

More specifically, the dependent variable will be composed of the $N \times 1$ idiosyncratic components \widehat{E}_t along with the block-specific factors $\widehat{F}_t = \left(\widehat{F}_{brt} \right)_{r=1, \dots, N_{F_b}}^{b=1, \dots, B}$. The idiosyncratic components \widehat{E}_t are obtained from fitting Y_t on the DHFM estimated global common factors \widehat{X}_t , i.e. \widehat{E}_t is equal to the residual of this regression. Rewriting equations (3.1) and (3.2) for $N_{F_b} = 1 \forall b$,

$$Y_{b\eta t} = \lambda_{F_b}^\eta(L) \left(\lambda_{X_b}^r(L) \widehat{X}_t + \widehat{e}_{F_{brt}} \right) + \widehat{e}_{Y_{b\eta t}},$$

which implies that the idiosyncratic component \widehat{E}_t is a linear combination of $\widehat{e}_{F_{brt}}$ and $\widehat{e}_{Y_{b\eta t}}$, $\forall b$. Then, the VAR representation can be written as follows,

$$\widehat{\mathbf{G}}_t = A \widehat{\mathbf{G}}_{t-1} + \mathbf{v}_t, \quad (3.6)$$

where $\widehat{\mathbf{G}}_t = \left(\widehat{E}_t, \widehat{F}_{11t}, \dots, \widehat{F}_{1N_{F_1}t}, \dots, \widehat{F}_{B1t}, \dots, \widehat{F}_{BN_{F_B}t} \right)$ is an $(N + \sum_{b=1}^B N_{F_b}) \times 1$ vector and \widehat{E}_t is $N \times 1$. The vector moving average representation, see [Lütkepohl \(2005\)](#), can be written as follows,

$$\mathbf{G}_t = \sum_{h=0}^{\infty} \Theta_h \mathbf{v}_{t-h}. \quad (3.7)$$

Estimation

For high-dimensional VAR models, one can use a penalized regression method. Assuming that A the VAR coefficient matrix is sparse, one can calculate the generalized impulse

response function and the generalized variance decomposition based on [Pesaran and Shin \(1998\)](#). The basic idea here is to use a penalized regression method that has a good fit, and get the estimated coefficient matrix Θ and the estimated variance-covariance matrix Σ of the residuals. Then, having the estimated Θ and Σ , one can calculate the generalized variance decomposition matrix which uncovers the estimated spillover effects among the VAR variables and can be also thought as an adjacency matrix in the network literature.

Generalized Variance Decomposition of the VAR process

As [Diebold and Yilmaz \(2014\)](#) explain, they use the infinite MA representation of the non-orthogonalized (generalized) VAR. More specifically, he defines the H -step generalized variance decomposition matrix $D^{gH} = [d_{ij}^{gH}]$ to have entries

$$d_{ij}^{gH} = \frac{\sigma_{jj}^{-1} \sum_{h=0}^{H-1} (e_i' \Theta_h \Sigma e_j)^2}{\sum_{h=0}^{H-1} (e_i' \Theta_h \Sigma \Theta_h' e_i)}$$

where e_j is a selection vector with the j^{th} element being unity and zeros elsewhere, Θ_h is the coefficient matrix multiplying the h -lagged shock vector in the infinite moving-average representation of the generalized VAR, Σ is the covariance matrix of the shock vector in the generalized VAR, and σ_{jj} is the j th diagonal element of Σ . Because shocks are not necessarily orthogonal in the GVD environment, sums of forecast error variance contributions are not necessarily unity (that is, row sums of D^g are not necessarily unity). Hence, the generalized connectedness measure will not be D^g , but rather $\tilde{D}^g = [\tilde{d}_{ij}^g]$, where $\tilde{d}_{ij}^g = \frac{d_{ij}^g}{\sum_{j=1}^N d_{ij}^g}$. By construction, $\sum_{j=1}^N \tilde{d}_{ij}^g = 1$ and $\sum_{i,j=1}^N \tilde{d}_{ij}^g = N$. Using \tilde{D}^g we can immediately calculate the generalized connectedness measures.

By definition, the resulting generalized variance decomposition (GVD) matrix \tilde{D}^g of the model is square, thus, it can also represent the so called *adjacency matrix* in the network literature. Each \tilde{d}_{ij}^{gH} measures the proportion of the h -step forecast error variance (FEV) of variable i accounted for by exogenous shocks to variable j .

3.4 Empirical Results

In this section, the aforementioned two-step methodology will be utilized in the context of an empirical application. The purpose of this empirical application exercise is to apply the proposed two-step methodology and at the same time get more intuition on the contagion effect, how it is created and the stages of its evolution.

The panel dataset used is from October 23, 2006 up to May 19, 2022 on the 5-year daily Credit Default Swaps (CDS) spreads² of financial institutions, sovereigns and non-financial institutions from the Automobile, Consumer, Energy, and Telecommunication industries. The total number of institutions in the panel dataset is 152. More specifically, it consists of 33 financial institutions, 10 sovereigns and 109 non-financial institutions: 40 Automobile, 32 Consumer, 18 Energy, 19 TMT (Technology, Media & Telecommunications) industry companies, see Table 3.1. Essentially, the dataset used in this work is a Datastream-updated version with respect to time of the dataset that [Gross and Siklos \(2020\)](#) have in their paper (which was covering the period 2006-2017 in daily frequency). Note that the panel dataset employed in this section includes the global financial crisis of 2008, the European sovereign crisis of 2010 as well as the recent Covid-19 pandemic period of 2020.

²CDS spreads measure credit risk and can be seen by the policy maker as numerical evaluations of financial vulnerability, investor fear and economic health.

The methodology I am following applies first the Dynamic Hierarchical Factor Model (DHF) proposed by [Moench, Ng and Potter \(2013\)](#) assuming data can be organized in B blocks and each block can have a total of N_{F_b} *block-specific factors*. Under this context, I assume that there are $B = 6$ block-specific factors to be estimated, as many as the sub-sector blocks of institutions in my dataset³. Specifically, I am using 6 blocks based on the sub-sector classification types of institutions I have available: Automobile, Consumer, Energy, Telecommunication, Financial institutions, and Sovereigns. Also, I assume no subblocks exist in this setting⁴.

Secondly, I combine the estimated idiosyncratic component and the block factors to be the dependent variable of a Vector Autoregressive (VAR) model. Then, I choose a suitable penalized regression method to be applied, especially on a high-dimensional Vector Autoregressive (VAR) model that we have in this case, since it is composed of the idiosyncratic component of 152 time series and the block factors estimated in the previous step. Finally, one can calculate the generalized variance decompositions, see section 3.3.1, which can be represented as a square 158×158 (152 series of institutions and 6 estimated block factors) h -step forecast error variance decomposition (VD) matrix, which can also be viewed as a network adjacency matrix, see [Diebold and Yilmaz \(2014\)](#), [Demirer et al. \(2018\)](#) and [Diebold and Yilmaz \(2009\)](#), thus, it can be depicted as a network plot according to the network literature.

This two-step methodology enables the estimation of the spillover effects among insti-

³See Table 3.1.

⁴One could assume there are a total of 3 blocks based on the sector classification: non-financial, financial and sovereign. Another assumption would be that there are 3 blocks and 6 subblocks, based on the sector and sub-sector classifications, respectively. These cases are not studied in this work in order to see the evolution of each of the 6 block factors without assuming further hierarchical patterns other than the assumption that all depend on the global common factor (along with other identification assumptions of the DHFM).

tutions and blocks of institutions. It provides more insights on the existence of contagion and the process of its vivification, which is of particular importance to policy makers.

3.4.1 Full-sample Results

First, to estimate the global common factor and the six block-specific common factors I apply the Dynamic Hierarchical Factor Model (DHFV). In the DHFV, the dependent variable is the panel of the CDS spreads of the 152 institutions which are assumed to be classified in $B = 6$ blocks where each block has a total of one factors in order for the model to return 6 series of estimated block-specific common factors, one for each block. Another input that has to be set in the model is the number of global common factors.

The number of global common factors has been determined using the [Hallin and Liška \(2007\)](#) criterion to be equal to one. Applying this criterion, I get Figure 3.1, which shows that for c in the intervals $[0, 0.217]$, $[0.996, 2.046]$, and $[2.509, 2.999]$, S_c equals zero and these intervals are called “stability intervals” as the authors define them. For the stability interval that is for values of c close to zero the number of common factors indicated is $q_{c,n}^T = q_{\max}$. Also, for the stability interval where $c = [2.509, 2.999]$ the indicated number of factors is zero. The authors propose to choose the number of common factors that is indicated by the second stability interval. The second interval in which $c = [0.996, 2.046]$, the criterion proposes one common factor to be used, $q_{c,n}^T = 1$.

The estimation of the DHFV is completed using Markov Chain Monte Carlo (MCMC), see section 3.3.1. The Gibbs sampling runs for a total of $n_{\text{Gibbs}} = 100,000$ draws, out of which 50,000 draws are set to belong to the burn-in samples and the draws after the first

50 thousand are kept, while saving results per 50 draws. The advantage of this estimation method is that the dependencies of the block-specific factors to the global common factor as well as dependencies of variables within and across block factors are taken into account. More details in the assumed correlations can be found in section 3.6.

The model's outputs to be used for the next step are the *global* common factor and the 6 *block-specific* common factors. The estimated factors evolution over time can be found in figures 3.2 and 3.3. In the global common factor plot, it is easy to see higher and persistent volatility starting around mid-2007 up to 2009, next around mid-2010 and 2016 and finally in 2020. It is not random at all that in these volatile periods important economic events took place: the global financial crisis of 2008, the European sovereign crisis of 2010, in 2016 the Chinese stock market fall, the cut of production in the Organization of Petroleum Exporting Countries (OPEC) along with the Great Britain's exit from the European Union (EU), and lastly the pandemic crisis of 2020. The sovereign-specific factor appears to have the smallest variance relatively to the rest factors over time. On the other hand, the Consumer, Energy, TMT industry companies and the financial sector seem to be volatile enough depicting events that characterize historically the European economy, some of which are mentioned above.

In addition, the explanatory power of the estimated factors is evaluated using OLS regression. In Table 3.2, one can view the resulting table representing the explanatory power of the global common factor and the block-specific factors. The coefficient of determination R^2 is higher for each block-specific common factor on their corresponding own block versus other factors. Also, the global common factor's R^2 is equal to 0.339 for all 152 CDS series, when at the same time it is greater than 0.429 in all series belonging to the first five blocks,

while for the last one, the sovereign block it is equal to 0.115. The fact that the explanatory power of the estimated block factors is relatively high makes it possible that the block factors uncover post-estimation results that are valuable for evaluating risk exchanges able to create the contagion.

After estimating the global common factor by the DHFM, one can get the estimated idiosyncratic component too. Table 3.3 presents the summary statistics of the standardized raw CDS spreads and the idiosyncratic ones organized based on country and sector.

The second step is to construct a Vector Autoregressive (VAR) model consisting of the $N = 152$ time series of the estimated idiosyncratic components and the time series of $\sum_{b=1}^B N_{F_b} = B = 6$ block-specific common factors see section 3.3.2. The constructed VAR is a high-dimensional VAR, thus it seems necessary to employ a penalized regression method to tackle high dimensionality. A handful of methods are being compared to each other based on out-of-sample forecast results and the output is represented in Table 3.4 based on Mean Squared Error (MSE).

Therefore, the Elastic Net penalization method is chosen to be applied for the estimation of the VAR model. The Elastic Net chooses the mixing parameter α and the penalty tuning parameter λ jointly using 10-fold cross validation. The code implementation of this methodology uses python package `sklearn` and its `ElasticNetCV` python class which sets the mixing parameter α to get one value from $[0.1, 0.2, 0.3, 0.4, 0.5, 0.6, 0.7, 0.8, 0.9, 1]$ when performing the 10-fold cross validation⁵.

From the estimated VAR model, one can calculate the variance decompositions and

⁵This can be changed by setting the step for alpha's values less than 0.1. but it would be computationally very time inefficient using the same package.

represent them in matrix form which in this case will be a 158×158 matrix where 158 is the sum of the 152 series plus the block-specific factors which are six (one for each of the $B = 6$ blocks). After calculating the variance decompositions based on section 3.3.2, it is clear that this can be thought as a connectedness measure, also called *directional connectedness*, see [Gross and Siklos \(2020\)](#) and [Diebold and Yilmaz \(2014\)](#).

For the full-sample analysis of 2006-2022 referred also as the static analysis of this work, connectedness reveals interesting risk exchanges among the entities of the analysis. Table 3.5 shows the top and bottom senders and receivers of risk based on the connectedness measure defined in section 3.3.2. The table studies the financial sector's and the sovereign entities as senders and the non-financial sector as the receiver. In addition, figure 3.4 represents the risk transmission magnitude in terms of connectedness from financial sector's entities towards other financial institutions and non-financial firms. The line depicts the trend which shows a monotonic relationship, i.e. the more a bank is connected to another bank the more it affects the non-financial sector entities and vice versa.

The estimated connectedness is represented as a network graph in figure 3.5. The depicted network presents the full-sample period in one figure which is very informative. First, in the center of this network, lie the entities that hold the more risk, and, in the periphery of it, the ones that hold the less risk. For example, Hellenic Telecom (HTE) which is a pink colored node in the figure lies in the center of the network graph meaning that it holds more risk relatively to other nodes for the full-sample period. Notice that this node appears in Table 3.5 as being the first best out of 109 non-financial receiver of sovereign risk. Secondly, the presence of the block-specific factors in the full-sample network reveals

that the factors are strongly connected not only with each other but also with the entities of the block they represent as well as they are positioned close to the entire idiosyncratic CDS network. This means that as idiosyncratic disruptions had the ability to set in distress the whole network during 2006-2022. More details on this conclusion will be discussed in the sub-sample analysis that follows.

In order to visualize how different the network structure would be without the block factors in the graph, figure 3.6 is provided. It represents the estimated network of the VAR which dependent variable consists of just the 152 idiosyncratic CDS entities, see the details of these entities at Table 3.1. In these two network plots, the only visible difference to figure 3.5 is the weaker connections certain sovereigns have to others (see Germany, France and Austria), and their positioning to be closer to the periphery of the network.

The connectedness matrix used in the network plot of figure 3.5 is represented in the form of a heatmap in figure 3.7. The connectedness matrix is among the 152 idiosyncratic CDS entities and the 6 block factors. The order of the entities and the sub-sector specific factors is the same as in Table 3.1. The bolder the color in the heatmap, the stronger the connection between two entities. From this heatmap, one can make two main observations. The first is that the connections of idiosyncratic CDS entities are stronger when they belong in the same block (same sub-sector), similarly the block-specific factors representing 6 blocks are also strongly connected. Secondly, a given block-specific common factor, let block β is strongly connected to the idiosyncratic entities belonging in the same block β . This last observation can be easily verified by looking at the bottom two lines of 3.7(b) and 3.7(c) which seem to be bold enough to be visible.

The heatmap represents a 158×158 connectedness matrix, therefore each entry represents a connection, with the diagonal entries being normalized to equal zero. Focusing on the estimated connectedness at the bottom right part of the heatmap, at 3.7(c), one can see that this column represents the sovereign block factor and its connections towards others. Specifically, in 3.7(c), because of the zooming in, the estimated connections are represented numerically indicating the strength of the connection. To interpret the resulting connectedness in figure 3.7, one can refer first to its definition at section 3.3.2. For instance, in the last column at 3.7(c), the entries are $\{2, 7, 3, 2, 1, 8, 4, 9, 8, 4, 6, 6, 6, 6, 5, 0\}$. This means that an exogenous shock to the sovereign block factor F_{sov} affects the 10-step forecast error variance (FEV) of Austria by 2 when all exogenous shocks to all variables indexed by j affect Austria by 100 in total. In other words, 2% of Austria's 10-step forecast error variance (FEV) comes from an exogenous shock to the sovereign block factor. Similarly, from 3.7(c), an exogenous shock to the sovereign block factor in the full-sample period 2006-2022, affects the $p\%$ 10-step forecast error variance of c , where $p \in \{2, 7, 3, 2, 1, 8, 4, 9, 8, 4, 6, 6, 6, 6, 5, 0\}$, $c \in \{\text{Austria, Belgium, France, Germany, Ireland, Italy, Netherlands, Portugal, Spain, UK, Fauto, Fcons, Fenrg, Ftmt, Ffin, Fsov}\}$, respectively. Note that all diagonal elements of the connectedness measure have been set to zero prior its normalization.

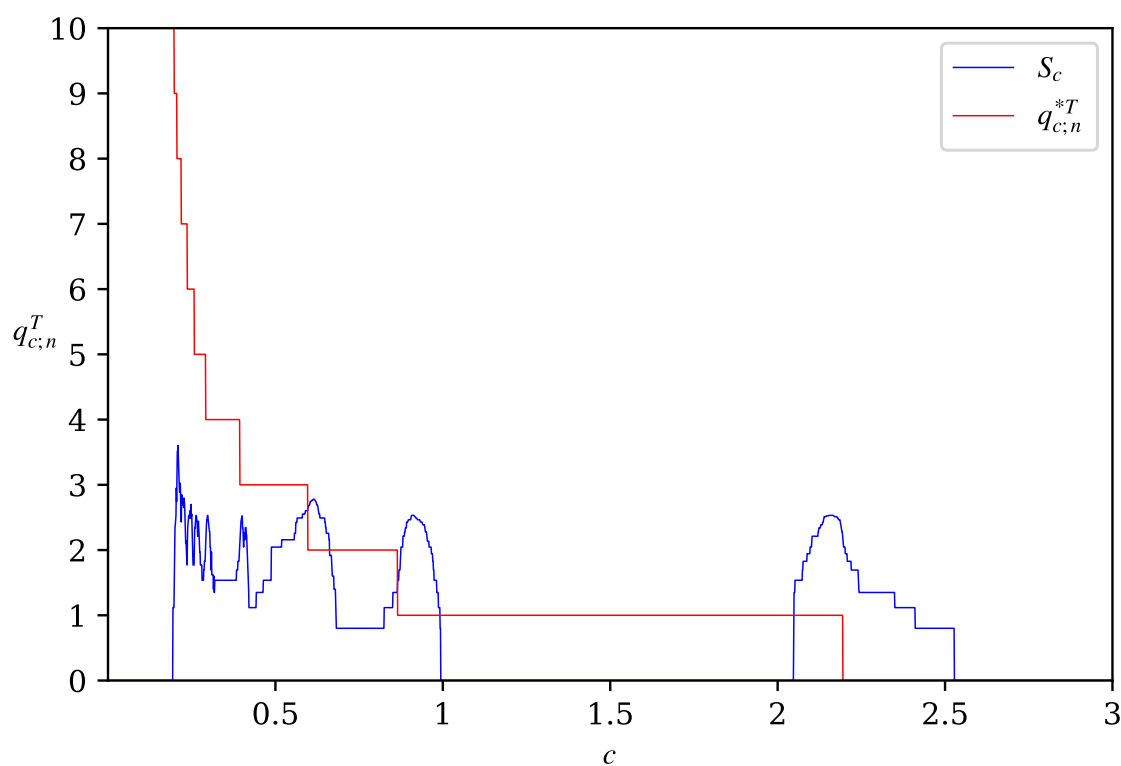
Additional information extracted from the heatmap at figure 3.7 which represents connectedness in the full sample period, will be discussed base on figures 3.7(b) and 3.7(c). First, in figure 3.7(b), the first 10 banks of the financial sector (order matches Table 3.1): Aegon (Netherlands), Generali (Germany), Aviva (Italy), AXA (UK), Hannover Rueck (France), Munich RE (Germany), Swiss RE (Germany), Zurich Insurance (Switzerland), Dexia (Switzerland), and BNP Paribas (Belgium), are estimated to be strongly connected

to each other during the full-sample period. Second, the financial sector seems to have idiosyncratic components that are strongly connected to each other overall. Secondly, in figure 3.7(b), the estimated connectedness from and to the idiosyncratic components of financial/sovereign entities and their corresponding financial/sovereign block factors is strong (see the bottom two lines and the last two columns on the right hand side). Thirdly, in figure 3.7(c), more than 16% of Austria's, France's and Germany's 10-step forecast error variance (FEV) in sovereign level comes from an exogenous shock to either of the following sovereigns, Austria, France or Germany (assuming a shock of their own affects their own FEV variance by zero). Fourthly, Italy, Portugal, Spain, Belgium and the UK affect each others FEV by significant percentages. Finally, the block factors are strongly connected to each other especially those belonging to the non-financial sector.

From figure 3.7(c), it is useful to keep the following spillover effects for the full-sample period 2006-2022. For the *non-financial* sector, around 12.5%, 6% and 15% of its 10-step forecast error variance (FEV) comes from an exogenous common shock to the financial sector, the sovereign sector, and any of the following non-financial sub-sectors (Automobile, Consumers, Energy, Telecommunications), respectively. For the *financial* sector around 9% and 5% of its 10-step forecast error variance (FEV) comes from an exogenous common shock to the non-financial sector, and the sovereigns sector, respectively. For the *sovereigns* sector around 7% and 8% of its 10-step forecast error variance (FEV) comes from an exogenous common shock to the non-financial sector, and the financial sector, respectively.

In addition, based on the last block of the connectedness at figure 3.7(c), in the full sample period, exogenous common shocks originating from the financial and the non-financial

sector affect the respective 10-day FEV of the sovereign sector $1.6(= 8/5)$ and $1.16(= 7/6)$ more proportionally. Also, exogenous common shocks originating from the financial sector affect the 10-day FEV of the non-financial sector around 1.3 more proportionally. Both findings uncover a higher directional connectedness and thus higher transmission of risk from the financial sector towards the non-financial and the sovereign sectors in the full-sample period. This makes sense to the extent that the economic distortions in 2007-2008 started from the financial sector which was in trouble and then spread to the rest economic sectors.

Figure 3.1: Hallin and Liska (2007) IC_2 criterion

Note: The Hallin and Liska (2007) IC_2 criterion suggests the number of common factors to be used in a dynamic factor model. This figure presents the $q_{c;n}^T$ and S_c as functions of c , where $q_{c;n}^T$ comes from the penalty function $p(n, T) = (M_T^{-2} + M_T^{0.5}T^{-0.5} + n^{-1}) \log(\min[n, M_T^2, M_T^{-0.5}T^{0.5}])$. S_c equals zero in three intervals called “stability intervals”, for $c \in \{[0, 0.21], [0.99, 2.12], [2.49, 2.99]\}$. Hallin and Liska (2007) suggest to use the indicated number of factors from the second stability interval, which in this case yields $q_{c;n}^T = 1$, i.e. one global common factor.

Table 3.1: List of CDS entities in the panel dataset

Entity Name	Sector	Sub-Sector	Country	Name Code
Adecco	Non-financial	Autos & Industrials	Switzerland	ADE
Volvo	Non-financial	Autos & Industrials	Sweden	VOL
Akzo Nobel	Non-financial	Autos & Industrials	Netherlands	AKN
Alstom	Non-financial	Autos & Industrials	France	ALS
Anglo American	Non-financial	Autos & Industrials	UK	ANA
Astrazeneca	Non-financial	Autos & Industrials	UK	ASZ
Atlantia	Non-financial	Autos & Industrials	Italy	ATL
Bae Systems	Non-financial	Autos & Industrials	UK	BAE
BASF	Non-financial	Autos & Industrials	Germany	BAS
Bayer	Non-financial	Autos & Industrials	Germany	BAY
BMW	Non-financial	Autos & Industrials	Germany	BMW
Bouygues	Non-financial	Autos & Industrials	France	BOU
Clariant	Non-financial	Autos & Industrials	Switzerland	CLA
Saint-Gobain	Non-financial	Autos & Industrials	France	SAG
Michelin	Non-financial	Autos & Industrials	Switzerland	MIC
Continental	Non-financial	Autos & Industrials	Germany	CON
Daimler	Non-financial	Autos & Industrials	Germany	DAI
Deutsche Post	Non-financial	Autos & Industrials	Germany	DPO
Evonik	Non-financial	Autos & Industrials	Germany	EVO
Finmeccanica	Non-financial	Autos & Industrials	Italy	FME
GKN Holding	Non-financial	Autos & Industrials	UK	GKN
Glencore	Non-financial	Autos & Industrials	Switzerland	GLC
Koninklijke DSM	Non-financial	Autos & Industrials	Netherlands	DSM
Air Liquide	Non-financial	Autos & Industrials	France	AIR
Lanxess	Non-financial	Autos & Industrials	Germany	LAX
Linde	Non-financial	Autos & Industrials	Germany	LIN
Peugeot	Non-financial	Autos & Industrials	France	PEU
Renault	Non-financial	Autos & Industrials	France	REN
Rentokil Initial	Non-financial	Autos & Industrials	UK	REI
Rolls-Royce	Non-financial	Autos & Industrials	UK	ROR
Sanofi-Aventis	Non-financial	Autos & Industrials	France	SAA
Siemens	Non-financial	Autos & Industrials	Germany	SIE
Stora Enso Oyj	Non-financial	Autos & Industrials	Finland	SEO
Solvay	Non-financial	Autos & Industrials	Belgium	SOL
ThyssenKrupp	Non-financial	Autos & Industrials	Germany	THK
UPM-Kymmene Oyj	Non-financial	Autos & Industrials	Finland	UPM
Valeo	Non-financial	Autos & Industrials	France	VAL
Vinci	Non-financial	Autos & Industrials	France	VIN
Volkswagen	Non-financial	Autos & Industrials	Germany	VOL
Wendel	Non-financial	Autos & Industrials	France	WEN
Accor	Non-financial	Consumers	France	ACC
Electrolux	Non-financial	Consumers	Sweden	ELE
Auchan	Non-financial	Consumers	France	AUC
Alliance Boots	Non-financial	Consumers	UK	ALL
Carrefour	Non-financial	Consumers	France	CAR
Casino Guichard	Non-financial	Consumers	France	CAG
Compass	Non-financial	Consumers	UK	COM
Danone	Non-financial	Consumers	France	DAN
Lufthansa	Non-financial	Consumers	Germany	LUF
Diageo	Non-financial	Consumers	UK	DIA
Experian Finance	Non-financial	Consumers	UK	EXF

(Table 3.1 continued)

Entity Name	Sector	Sub-Sector	Country	Name Code
Henkel	Non-financial	Consumers	Germany	HEN
Ladbrokes	Non-financial	Consumers	UK	LAD
Imperial Brands	Non-financial	Consumers	UK	IMB
ISS Global	Non-financial	Consumers	Denmark	ISS
J Sainsbury	Non-financial	Consumers	UK	JSA
Kering	Non-financial	Consumers	France	KER
Kingfisher	Non-financial	Consumers	UK	KIN
Koninklijke Ahold Delhaize	Non-financial	Consumers	Netherlands	AHO
Koninklijke Philips	Non-financial	Consumers	Netherlands	PHI
LVMH	Non-financial	Consumers	France	LVM
Marks & Spencer	Non-financial	Consumers	UK	M&S
Metro	Non-financial	Consumers	Germany	MET
Nestlé	Non-financial	Consumers	Switzerland	NES
Next	Non-financial	Consumers	UK	NEX
PernodRicard	Non-financial	Consumers	France	PER
Safeway	Non-financial	Consumers	UK	SAF
Svenska Cellulosa	Non-financial	Consumers	Sweden	SCE
Swedish Match	Non-financial	Consumers	Sweden	SWM
Tate & Lyle	Non-financial	Consumers	UK	T&L
Tesco	Non-financial	Consumers	UK	TES
Unilever	Non-financial	Consumers	UK	UNI
BP	Non-financial	Energy	UK	BP
Centrica	Non-financial	Energy	UK	CEN
EON	Non-financial	Energy	Germany	EON
Edison	Non-financial	Energy	Italy	EDI
Energias de Portugal	Non-financial	Energy	Portugal	EDP
Electricité de France	Non-financial	Energy	France	EDF
ENBW	Non-financial	Energy	Germany	ENB
ENEL	Non-financial	Energy	Italy	ENE
ENGIE	Non-financial	Energy	France	ENG
Fortum OYJ	Non-financial	Energy	Finland	FOY
Gas Natural SDG	Non-financial	Energy	Spain	SDG
Iberdrola	Non-financial	Energy	Spain	IBE
National Grid	Non-financial	Energy	UK	NGR
Royal Dutch Shell	Non-financial	Energy	Netherlands	RDS
RWE	Non-financial	Energy	Germany	RWE
Statoil	Non-financial	Energy	Norway	STA
Total	Non-financial	Energy	France	TOT
United Utilities	Non-financial	Energy	UK	UNU
British Telecom	Non-financial	TMT	UK	BTE
Deutsche Telekom	Non-financial	TMT	Germany	DTE
Hellenic Telecom	Non-financial	TMT	Greece	HTE
ITV	Non-financial	TMT	UK	ITV
Nokia	Non-financial	TMT	Finland	NOK
Orange	Non-financial	TMT	France	ORA
Pearson	Non-financial	TMT	UK	PEA
Publicis	Non-financial	TMT	France	PUB
Relx	Non-financial	TMT	UK	REL
St Microelectronics	Non-financial	TMT	Switzerland	STM
Ericsson	Non-financial	TMT	Sweden	ERI
Telefonica	Non-financial	TMT	Spain	TEF
Telekom Austria	Non-financial	TMT	Austria	TEA

(Table 3.1 continued)

Entity Name	Sector	Sub-Sector	Country	Name Code
Telenor	Non-financial	TMT	Norway	TEL
Telia	Non-financial	TMT	Sweden	TEI
Vivendi	Non-financial	TMT	France	VIV
Vodafone	Non-financial	TMT	UK	VOD
Wolters	Non-financial	TMT	Netherlands	WOL
WPP	Non-financial	TMT	UK	WPP
Aegon	Financial		Netherlands	AEG
Generali	Financial		Germany	ALL
Aviva	Financial		Italy	GEN
AXA	Financial		UK	AVI
Hannover Rueck	Financial		France	AXA
Munich RE	Financial		Germany	HRE
Swiss RE	Financial		Germany	MRE
Zurich Insurance	Financial		Switzerland	SRE
Dexia	Financial		Switzerland	ZIN
BNP Paribas	Financial		Belgium	DEX
Crédit Agricole	Financial		France	BNP
Société Générale	Financial		France	CAG
Deutsche Bank	Financial		France	SOG
Commerzbank	Financial		Germany	DBA
Bank of Ireland	Financial		Germany	COB
Intesa Sanpaolo	Financial		Ireland	BOI
Banca Monte Di Paschi	Financial		Italy	BMP
Banca Popolare	Financial		Italy	BPO
Unicredit	Financial		Italy	UNI
Mediobanca	Financial		Italy	MED
ING	Financial		Netherlands	ING
Rabobank	Financial		Netherlands	RAB
Banco Comercial Port.	Financial		Portugal	BCP
Santander	Financial		Spain	SAN
BBVA	Financial		Spain	BBV
Royal Bank of Scot.	Financial		UK	RBS
HSBC Bank	Financial		UK	HSB
Barclays Bank	Financial		UK	BAB
Lloyds Bank	Financial		UK	LLB
Standard Chartered	Financial		UK	SCH
UBS	Financial		Switzerland	UBS
Credit Suisse	Financial		Switzerland	CSU
Austria	Sovereign		Austria	AUT
Belgium	Sovereign		Belgium	BEL
France	Sovereign		France	FRA
Germany	Sovereign		Germany	GER
Ireland	Sovereign		Ireland	IRE
Italy	Sovereign		Italy	ITA
Netherlands	Sovereign		Netherlands	NED
Portugal	Sovereign		Portugal	POR
Spain	Sovereign		Spain	ESP
UK	Sovereign		UK	UK

Figure 3.2: Evolution of the *global* common factor over the full-sample period ranging from October 23, 2006 up to May 19, 2022. The global common factor X_t is estimated using the Dynamic Hierarchical Factor model by [Moench, Ng and Potter \(2013\)](#).

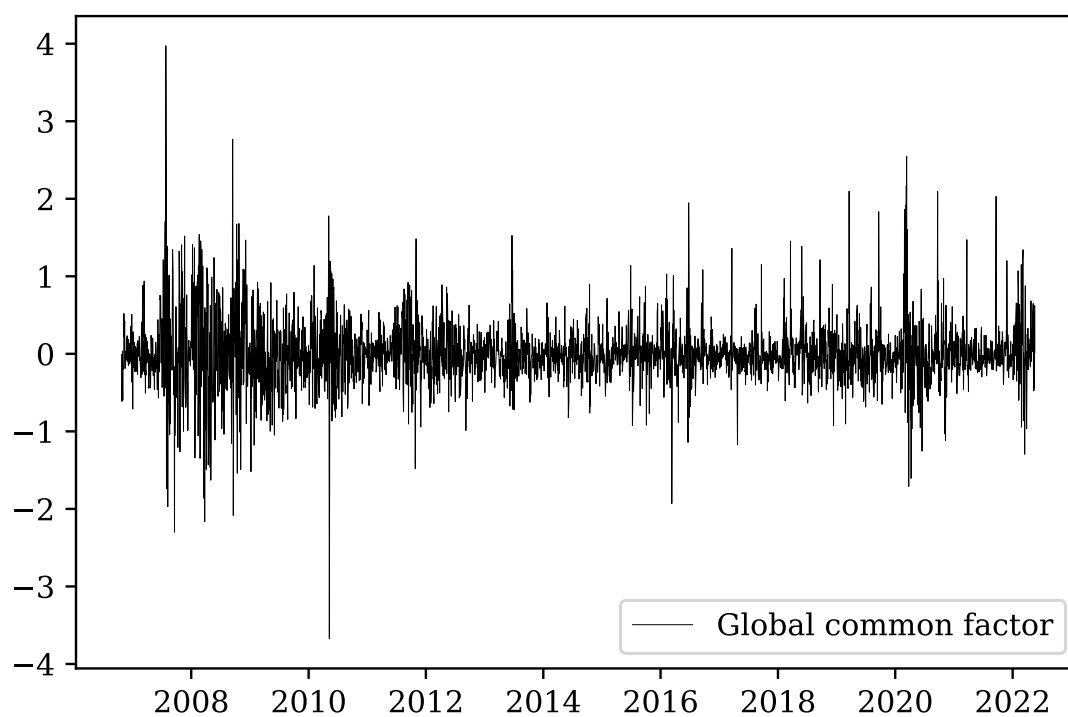


Figure 3.3: Evolution of the *block-specific* common factors over the full-sample period ranging from October 23, 2006 up to May 19, 2022. The block-specific common factors are estimated using the Dynamic Hierarchical Factor model by [Moench, Ng and Potter \(2013\)](#).

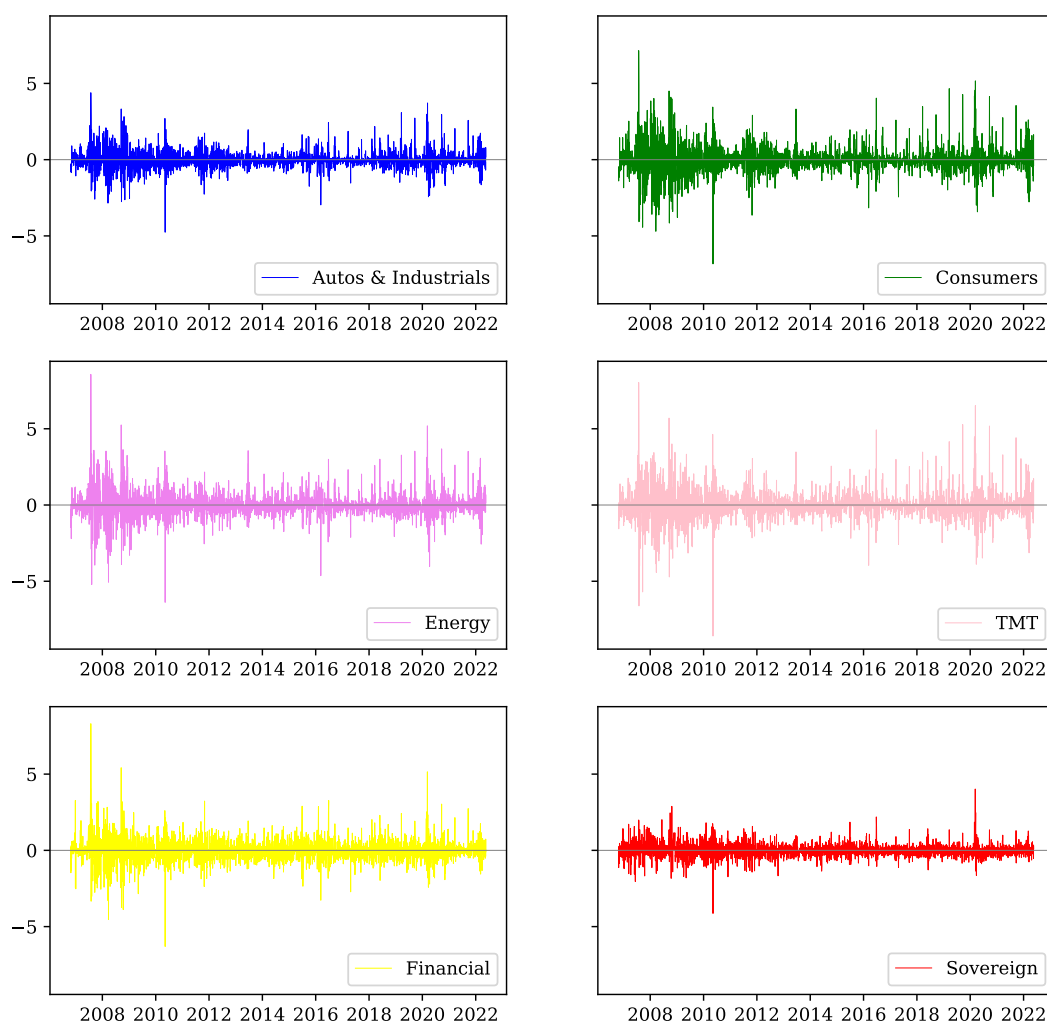


Table 3.2: Explanatory power R^2 of the estimated common factors

R^2	Subsectors						
	Autos & In- dustrials	Consumers	Energy	TMT	Financial	Sovereign	All CDS
R^2 of $F_{AUT,t}$	0.533	0.441	0.442	0.476	0.369	0.103	0.318
R^2 of $F_{CON,t}$	0.470	0.501	0.426	0.482	0.356	0.093	0.308
R^2 of $F_{NRG,t}$	0.429	0.387	0.555	0.440	0.379	0.096	0.305
R^2 of $F_{TMT,t}$	0.442	0.420	0.423	0.575	0.359	0.095	0.303
R^2 of $F_{FIN,t}$	0.357	0.313	0.371	0.360	0.573	0.115	0.345
R^2 of $F_{SOV,t}$	0.199	0.169	0.197	0.198	0.232	0.280	0.234
R^2 of X_t	0.475	0.447	0.477	0.513	0.429	0.115	0.339

Note: This Table presents the explanatory power R^2 of the global and the block-specific common factors for individual CDS spreads averaged by sub-sector.

Table 3.3: Summary statistics of CDS data by country and by sector

Panel A: CDS non-financial corporations									
Countries	Entities	Raw returns				Idiosyncratic returns			
		Mean	Std. dev.	Min	Max	Mean	Std. dev.	Min	Max
Austria	1	0.0	1.0	-8.02	8.14	-0.0	0.64	-5.13	5.82
Belgium	1	-0.0	1.0	-7.92	8.67	-0.0	0.67	-4.30	8.82
Denmark	1	-0.0	1.0	-26.92	12.31	-0.0	0.91	-26.94	10.81
Finland	4	-0.0	1.0	-23.16	11.31	-0.0	0.75	-23.38	11.75
France	24	-0.0	1.0	-18.18	18.08	-0.0	0.70	-18.34	17.48
Germany	19	-0.0	1.0	-10.26	27.40	-0.0	0.71	-9.39	27.33
Greece	1	-0.0	1.0	-7.64	12.54	-0.0	0.79	-6.08	10.59
Italy	4	0.0	1.0	-15.42	20.33	-0.0	0.76	-15.10	20.16
Netherlands	6	-0.0	1.0	-21.43	22.19	-0.0	0.72	-22.36	21.88
Norway	2	0.0	1.0	-9.50	11.27	-0.0	0.77	-6.05	10.41
Portugal	1	-0.0	1.0	-10.77	8.08	-0.0	0.68	-8.30	5.63
Spain	3	0.0	1.0	-11.77	7.93	-0.0	0.65	-6.35	8.75
Sweden	6	-0.0	1.0	-10.06	17.50	-0.0	0.72	-8.76	17.55
Switzerland	6	0.0	1.0	-11.80	13.01	-0.0	0.74	-10.46	11.62
UK	30	0.0	1.0	-29.36	42.70	-0.0	0.73	-30.07	42.59
Panel B: CDS financial institutions									
Countries	Entities	Raw returns				Idiosyncratic returns			
		Mean	Std. dev.	Min	Max	Mean	Std. dev.	Min	Max
Belgium	1	-0.0	1.0	-24.95	20.58	-0.0	0.97	-24.95	20.57
France	4	0.0	1.0	-9.60	15.00	-0.0	0.70	-4.87	9.50
Germany	5	-0.0	1.0	-10.83	13.01	-0.0	0.70	-8.76	9.06
Ireland	1	-0.0	1.0	-17.78	12.35	-0.0	0.97	-17.76	12.22
Italy	6	0.0	1.0	-12.99	14.99	-0.0	0.76	-12.57	12.03
Netherlands	3	0.0	1.0	-9.80	17.47	-0.0	0.79	-8.29	16.14
Portugal	1	0.0	1.0	-9.34	10.68	-0.0	0.84	-8.48	13.04
Spain	2	-0.0	1.0	-9.37	6.95	-0.0	0.74	-6.49	7.62
Switzerland	4	-0.0	1.0	-9.26	13.14	-0.0	0.70	-7.44	7.81
UK	6	0.0	1.0	-15.52	14.17	-0.0	0.75	-13.25	12.65
Panel C: CDS sovereigns									
Countries	Entities	Raw returns				Idiosyncratic returns			
		Mean	Std. dev.	Min	Max	Mean	Std. dev.	Min	Max
Austria	1	0.0	1.0	-22.66	17.33	0.0	0.98	-22.34	17.41
Belgium	1	-0.0	1.0	-6.75	16.36	-0.0	0.90	-6.57	13.95
France	1	-0.0	1.0	-23.04	17.62	-0.0	0.98	-22.75	17.72
Germany	1	-0.0	1.0	-16.42	18.94	0.0	0.98	-16.39	18.99
Ireland	1	0.0	1.0	-15.32	15.20	-0.0	0.99	-15.27	15.28
Italy	1	-0.0	1.0	-9.45	8.44	-0.0	0.86	-9.17	8.41
Netherlands	1	0.0	1.0	-11.89	11.87	-0.0	0.98	-11.68	12.65
Portugal	1	0.0	1.0	-11.98	7.49	-0.0	0.88	-8.31	5.72
Spain	1	0.0	1.0	-11.20	11.18	-0.0	0.91	-11.56	11.12
UK	1	0.0	1.0	-15.27	22.75	-0.0	0.95	-14.55	22.58

Note: The table shows the descriptive statistics of the standardized raw panel of 152 CDS spreads and the estimated idiosyncratic returns arranged by country and by sector.

Table 3.4: Out-of-sample forecast results

	Autos & Industri- als	Consumers	Energy	TMT	Financial	Sovereign	Block Fac- tors	Total
Optimal Elastic Net	5.380	5.222	5.211	4.698	5.517	8.268	4.617	5.429
Constant mean	5.223	5.233	4.878	4.873	5.685	8.766	5.116	5.460
AR(1)	5.275	5.438	5.246	4.755	5.759	8.966	5.207	5.574
Ridge	6.248	6.137	6.111	5.982	6.132	10.526	5.210	6.385
Constant Elastic Net	5.078	5.212	5.227	4.476	5.932	9.473	4.787	5.495

Note: The in-sample period is 10/23/2006 - 12/31/2019, the out-of-sample period corresponds to 01/01/2020-05/19/2022. The table shows the mean squared error (MSE) of the chosen estimation penalization method of optimal elastic net by sector and compares it to constant mean, AR(1), Ridge regression and Constant elastic net models. The optimal elastic net model chooses the optimal mixing parameter $\alpha \in \{[0.1, 0.2, 0.3, 0.4, 0.5, 0.6, 0.7, 0.8, 0.9, 1]\}$ and the penalty tuning parameter λ jointly in the shrinkage and selection process. The constant mean model uses the in-sample mean of each variable as forecasts. The AR(1) model conducts forecasts based on the fitted values from a persistent process. Ridge regression applies shrinkage in the VAR with $\alpha = 1$ and constant elastic net uses $\alpha = 0.5$ and chooses only the optimal λ in the penalty function.

Table 3.5: Ranking of largest senders and receivers of credit risk for the full-sample period 2006-2022

(a) Financial \rightarrow Non-Financial

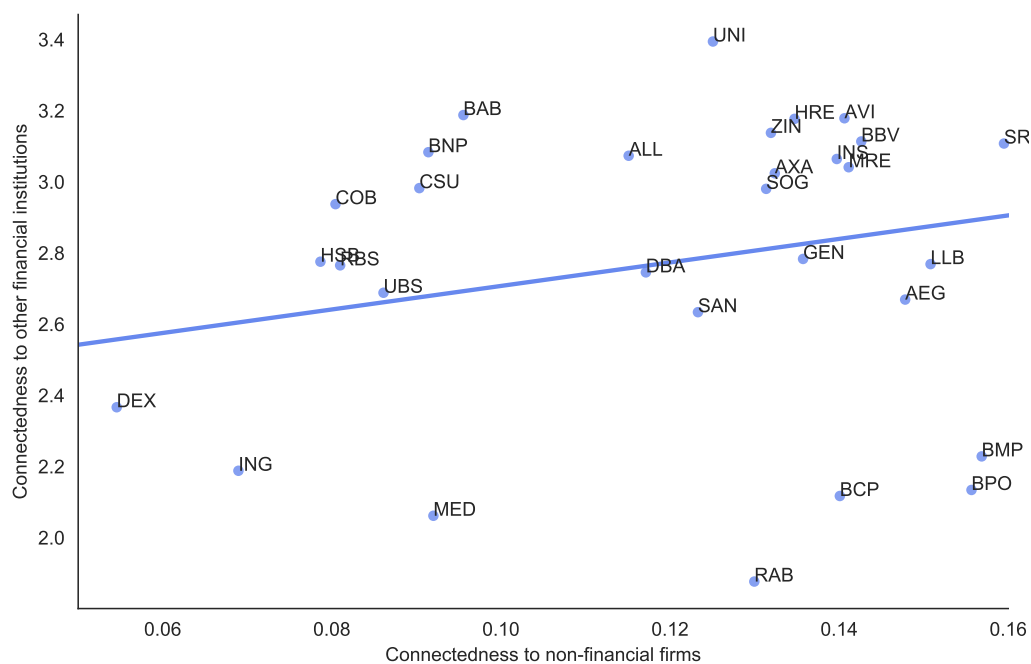
Sender			Receiver		
Rank	Name	Connectedness "To"	Rank	Name	Connectedness "From"
1	Credit Agricole	0.16	1	Wendel	0.74
2	Swiss RE	0.16	2	Royal Dutch Shell	0.32
3	Banca Monte Di Paschi	0.16	3	Energias de Portugal	0.32
4	Banca Popolare	0.16	4	Relx	0.27
5	Lloyds Bank	0.15	5	Edison	0.26
6	Aegon	0.15	6	Henkel	0.25
7	BBVA	0.14	7	ENEL	0.24
8	Munich RE	0.14	8	WPP	0.24
9	Aviva	0.14	9	British Telecom	0.24
10	Banco Commercial Port.	0.14	10	Hellenic Telecom	0.23
⋮	⋮	⋮	⋮	⋮	⋮
29	HSBC Bank	0.08	105	BMW	0.03
30	ING	0.07	106	Daimler	0.02
31	Dexia	0.05	107	Renault	0.02
32	Bank of Ireland	0.05	108	Solvay	0.02
33	Standard Chartered	0.03	109	Volkswagen	0.02

(b) Sovereign \rightarrow Non-Financial

Sender			Receiver		
Rank	Name	Connectedness "To"	Rank	Name	Connectedness "From"
1	Italy	0.18	1	Hellenic Telecom	0.35
2	Spain	0.12	2	ENEL	0.29
3	Portugal	0.10	3	Energias de Portugal	0.27
4	Belgium	0.08	4	Telefonica	0.20
5	UK	0.07	5	Iberdrola	0.19
6	Netherlands	0.05	6	Orange	0.18
7	Austria	0.04	7	Wendel	0.17
8	France	0.03	8	EON	0.17
9	Ireland	0.03	9	Anglo American	0.17
10	Germany	0.03	10	Gas Natural SDG	0.16
			⋮	⋮	⋮
			105	Solvay	0.02
			106	Edison	0.01
			107	Daimler	0.01
			108	Continental	0.01
			109	BMW	0.01

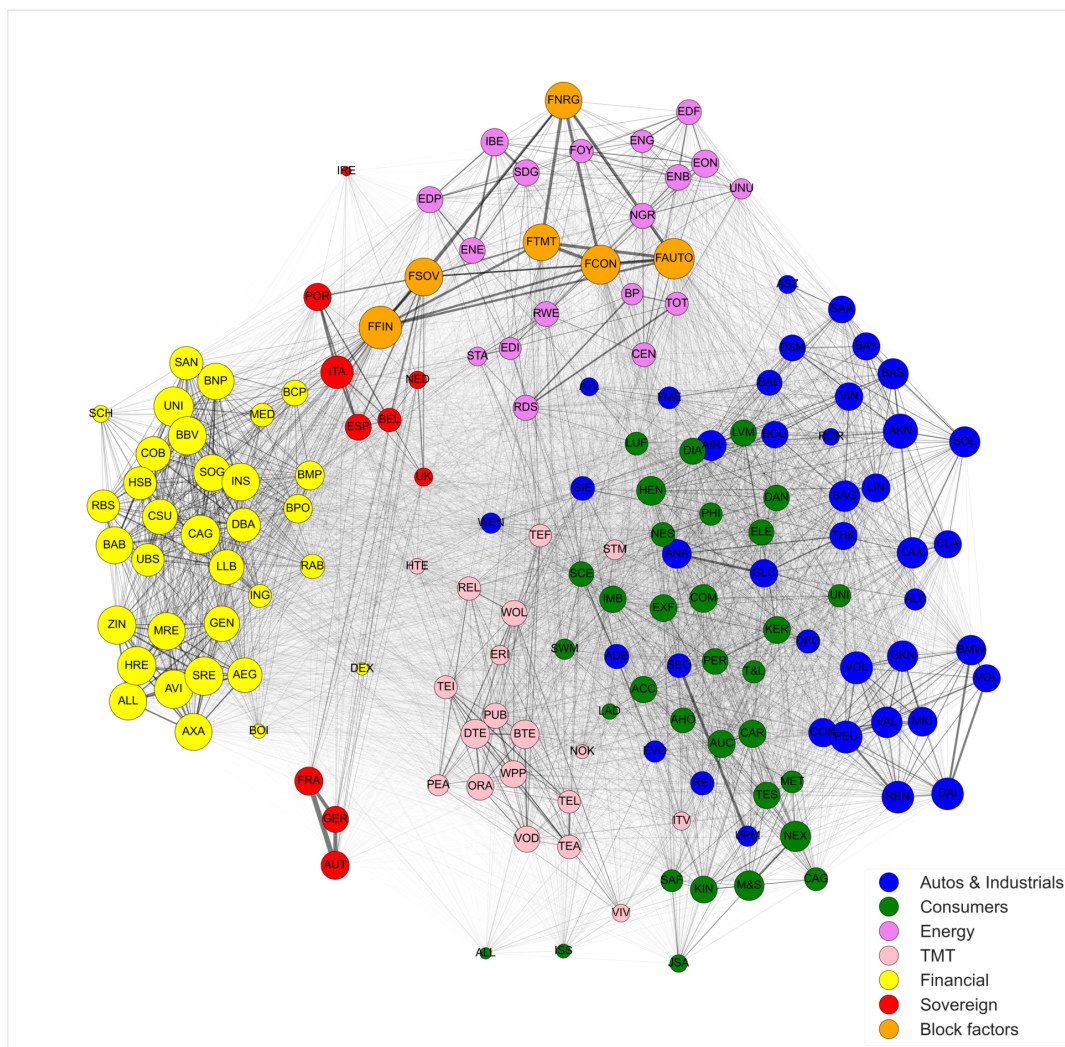
Note: The tables ranks senders and receivers according to the strength of their incoming or outgoing connections to others are. The table represents connectedness by taking into account the total number of entities, therefore the displayed connectedness is the average value per entity.

Figure 3.4: Individual senders of financial risk for the full-sample period (2006-2022)



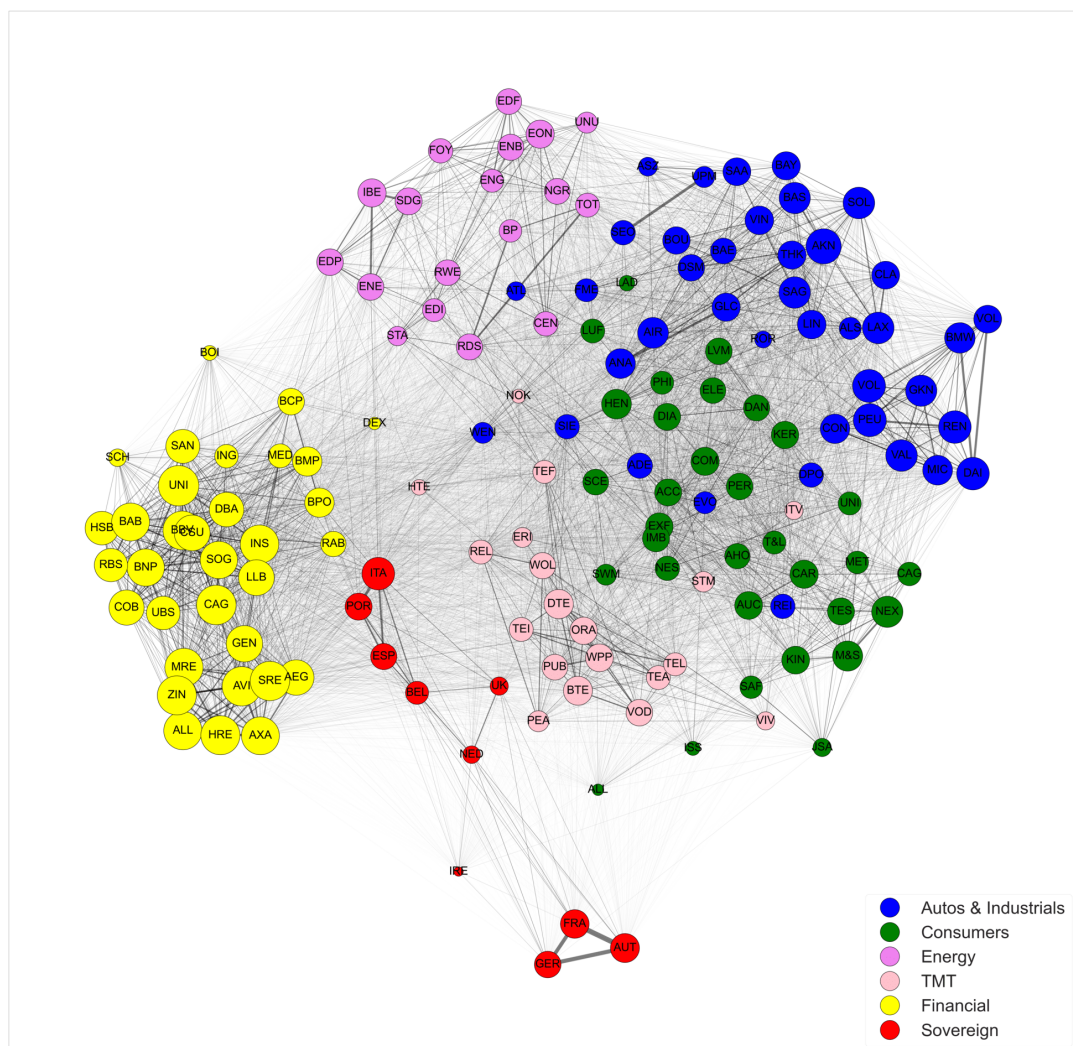
Note: The figure shows the financial entities' total connectedness to other financial institutions versus other non-financial firms. Total connectedness' definition used here is borrowed from [Gross and Siklos \(2020\)](#). The financial entities appear with their Name Code, see Table 3.1.

Figure 3.5: CDS network graph for the full-sample period (2006-2022)



Note: The network's nodes are the CDS individual institutions colored by sub-sector and named according to the institutions' corresponding *Name Code* in Table 3.1. Their size represents the number and strength of outgoing connections they have, the bigger the size the more the risk they transmit to others. They are positioned based on the force-directed algorithm of [Fruchterman and Reingold \(1991\)](#), which places nodes close to each other according to how strongly they are connected. The connections are estimated using $h = 10$ -step forecast error variance decompositions. The number of common factors used is equal to one and comes from applying the [Hallin and Liška \(2007\)](#) IC_2 criterion.

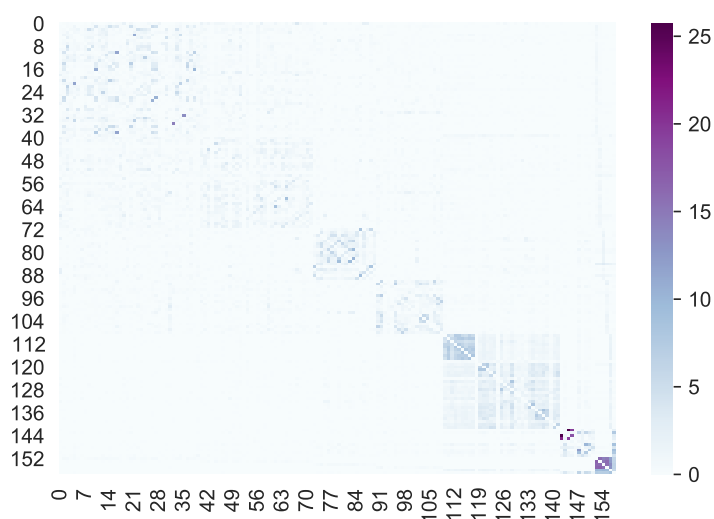
Figure 3.6: CDS network graph for the full-sample period (2006-2022) with only the idiosyncratic component in the estimated VAR, i.e. no block-specific factors are included in the panel VAR



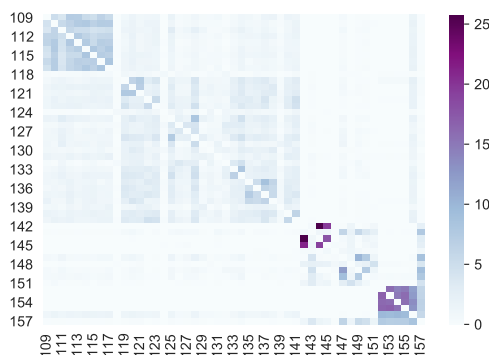
Note: The network's nodes are the CDS individual institutions colored by sub-sector and named according to the institutions' corresponding *Name Code* in Table 3.1. Their size represents the number and strength of outgoing connections they have, the bigger the size the more the risk they transmit to others. They are positioned based on the force-directed algorithm of [Fruchterman and Reingold \(1991\)](#), which places nodes close to each other according to how strongly they are connected. The connections are estimated using $h = 10$ -step forecast error variance decompositions. The number of common factors used is equal to one and comes from applying the [Hallin and Liška \(2007\)](#) IC_2 criterion.

Figure 3.7: CDS variance decomposition heatmap for the full-sample period (2006-2022)

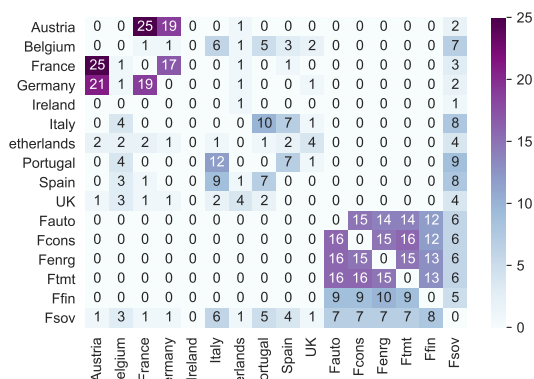
(a) The whole heatmap including all 152 idiosyncratic CDS and the 6 block-specific factors. Indices start from 0 up to 157 for the 158 CDS ordered as in Tables 3.1 and 3.2, respectively.



(b) Bottom right corner of whole heatmap zoomed in to the last 49 CDS: 33 financial entities, 10 sovereigns and 6 block-specific factors heatmap



(c) Bottom right corner of whole heatmap zoomed in to the last 16 CDS: 10 sovereigns and 6 block-specific factors heatmap



3.4.2 Sub-sample Results

In this sub-sample analysis, the same methodology steps followed for the full-sample analysis, are repeated for as many as the periods considered. Initially, I consider three periods: period 1 from 10/23/2006 up to 12/31/2009 covering the financial crisis period of 2007-2008, period 2 from 01/01/2010 up to 12/31/2015 covering the sovereign crisis of 2010, and period 3 from 01/01/2016 up to 05/19/2022 covering both 2016 a year of challenges for the EU, such as the Chinese stock market fall, OPEC's production cut, and 'Brexit', and the 2020 pandemic crisis.

In these three period analysis, I run the DHFM and get for each period, one *global* common factor and the *block-specific* common factors which are 6 as many as the sub-sectors. Increased volatility in the factors appears to be coinciding with major global and european level events overtime. The DHFM model for each period is run very similarly as the full-sample. The output factors can be found in figures 3.8, 3.9, 3.10 and 3.11.

Next, I estimate connectedness for each period, see also sections 3.3.2 and 3.4.1. I find the connectedness measures for each period 1, 2, and 3 and I represent them in heatmap form, see figures 3.12, 3.13, and 3.14. From the heatmaps, attention goes immediately to the block factors connectedness to each other across the three periods. In period 1, one can see very a low but significant connectedness around 3% across the non-financial and financial block factors, while the sovereign factor seems to be a receiver of connecteness and therefore risk at period 1. To verify that, one can see the last column at figure 3.12(c) versus the last row. Also, in period 1, the strongest connections appear to be among idiosyncratic entities and among idiosyncratic entities and block factors.

In period 2 and figure 3.13, it seems that the formation of risk exchanges in the previous period has increased the risk exchanges across the block factors from around 3% in previous period to 16% in the current period. Also, idiosyncratic entity exchanges among each other seem to be weaker in this period compared to the previous. Similarly, the connections from the idiosyncratic entities to the block factors and vice versa, are weaker too. This behavior verifies what authors have been discussing on *pure contagion effect*, a domino effect that starts from a number of individual entities (period 1) spreading to the whole system (period 2).

In period 3 and figure 3.14, one can spot similarities to period 2's heatmap. One difference is that the risk from and to the sovereign block factor is around 2% less in period 3 comparing to the previous period.

The connectedness measures depicted as heatmaps in figures 3.12, 3.13, and 3.14 are represented as network graphs in figures 3.15, 3.16 and 3.17. In network plot for period 1, figure 3.15, the major holders of risk being in the center of the network are the non-financial and the financial sector, by noticing the block factors' position. In the periphery the sovereigns are connected closely with the sovereign factor which is connected weakly with the rest factors. The size of the non-financial and financial factors is big indicating that in the current period not only they are the major holders of risk based on their positions, but they also transmit big amounts of risk to the rest network entities.

In periods 2 and 3, one can notice how far away from the idiosyncratic network the block-specific factors have moved. This means that the big bubbles of factors of the previous period have 'exploded' by transmitting risk to others and now they still hold risk sharing it

mainly to each other, but barely to other idiosyncratic entities. Comparing periods 2 and 3, one can notice the factors holding even weaker connections to the rest of the idiosyncratic network.

To understand this network behavior from a policy standpoint, it would be useful to create even smaller periods between periods 1 and 2. This would give a better intuition on when the movement, size and role of block factors in the network structure. For this purpose, periods I, II, III, and IV are studied. Period I is from 10/23/2006 up to 08/08/2007 right before the BNP Paribas announcement about freezing \$2.2 billion of funds due to the subprime mortgage sector. Period II is from 08/09/2007 up to 09/14/2008, right before the Lehman Brothers bankruptcy. Period III is from 09/15/2008 up to 04/01/2009, before the G20's decision to finance the financial sector. Period IV is from 04/02/2009 up to 05/08/2010, the period just before the Eurozone's decision to finance certain of its country members.

In period I, one can see its estimated connectedness heatmap 3.18 and network plot 3.22. In the network plot one can see how close to the rest entities the block factors lie having a small size. This means that they are strongly connected to other idiosyncratic entities and not necessary to each other as the orange block factor nodes are not all close to each other, with the exception of the non-financial factor which all express one sector. This is also quite clear in the connectedness heatmap where one can notice idiosyncratic connectedness mostly sectoral but most importantly connectedness from idiosyncratic entities towards the common factors, see the bottom of the heatmap at figure 3.18. In other words, an idiosyncratic shock affecting one entity could potentially emerge to a common shock to entire sectors. Notice

that in figure 3.18, more than 50% of the sovereigns' common factor 10-day forecast error variance comes from exogenous shocks to Austria and Germany combined.

In the next periods II, III and IV, one can see their estimated connectedness heatmaps 3.19, 3.20, 3.21 and network plots 3.23, 3.24, 3.25. In all these periods the block factors have moved away from the rest idiosyncratic entities, holding stronger connections than in period I. To illustrate the difference accross all periods consider the following: (a) exogenous common shocks originating from the financial and the non-financial sector affect the FEV of the sovereign sector $\{-, 5/2, 9/8, 14/10\}$ and $\{-, 5/2, 10/7, 11/8\}$ more proportionally for each period I, II, III and IV, (b) exogenous common shocks originating from the financial sector affect the FEV of the non-financial sector around $\{-, 16/17, 11/13, 15/15\}$ more proportionally for each period I, II, III and IV.

From the sub-sample analysis' findings, the policy maker can identify an upcoming economic crisis studying the behavior of the idiosyncratic and the block factors. When the block factors are close topologically to the rest of the network the researcher could look into the reason of this appealing force. If this force is due to idiosyncratic entities transmitting risk to the block factors this signals the contagion effect's onset.

Figure 3.8: Global common factor evolution in periods 1, 2, and 3

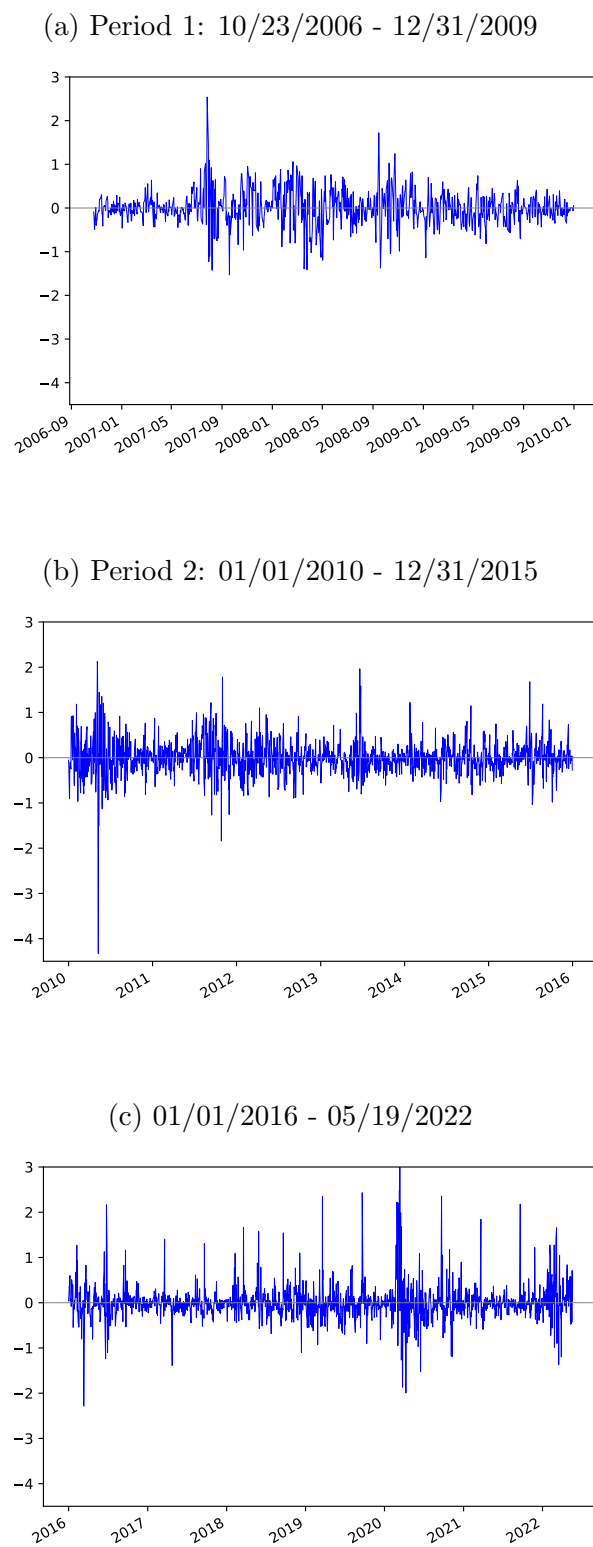


Figure 3.9: Evolution of the block-specific common factors over period 1 ranging from October 23, 2006 up to December 31, 2009. The block-specific common factors are estimated using the Dynamic Hierarchical Factor model by [Moench, Ng and Potter \(2013\)](#).

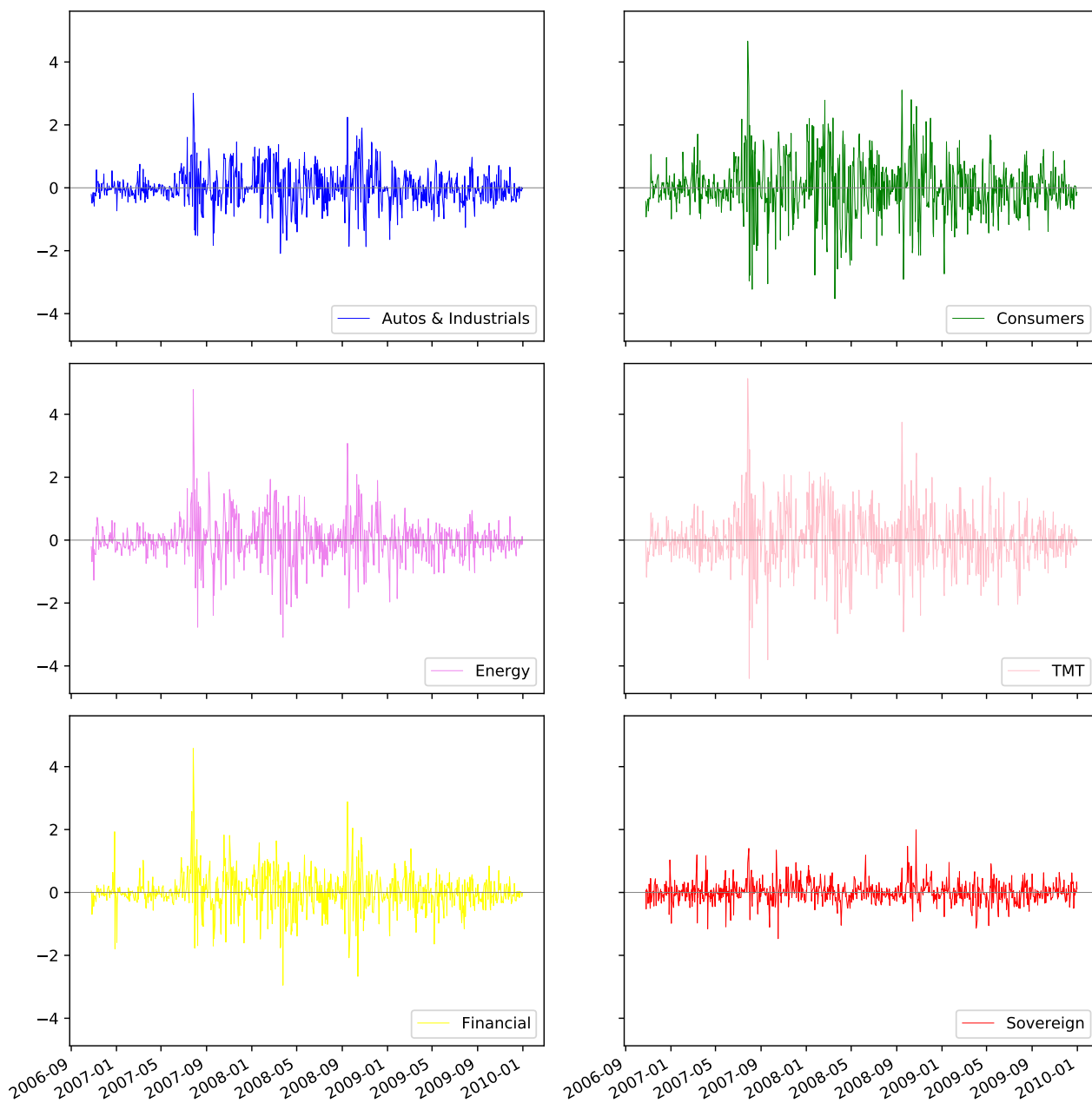


Figure 3.10: Evolution of the block-specific common factors over period 2 ranging from January 1, 2010 up to December 31, 2015. The block-specific common factors are estimated using the Dynamic Hierarchical Factor model by [Moench, Ng and Potter \(2013\)](#).

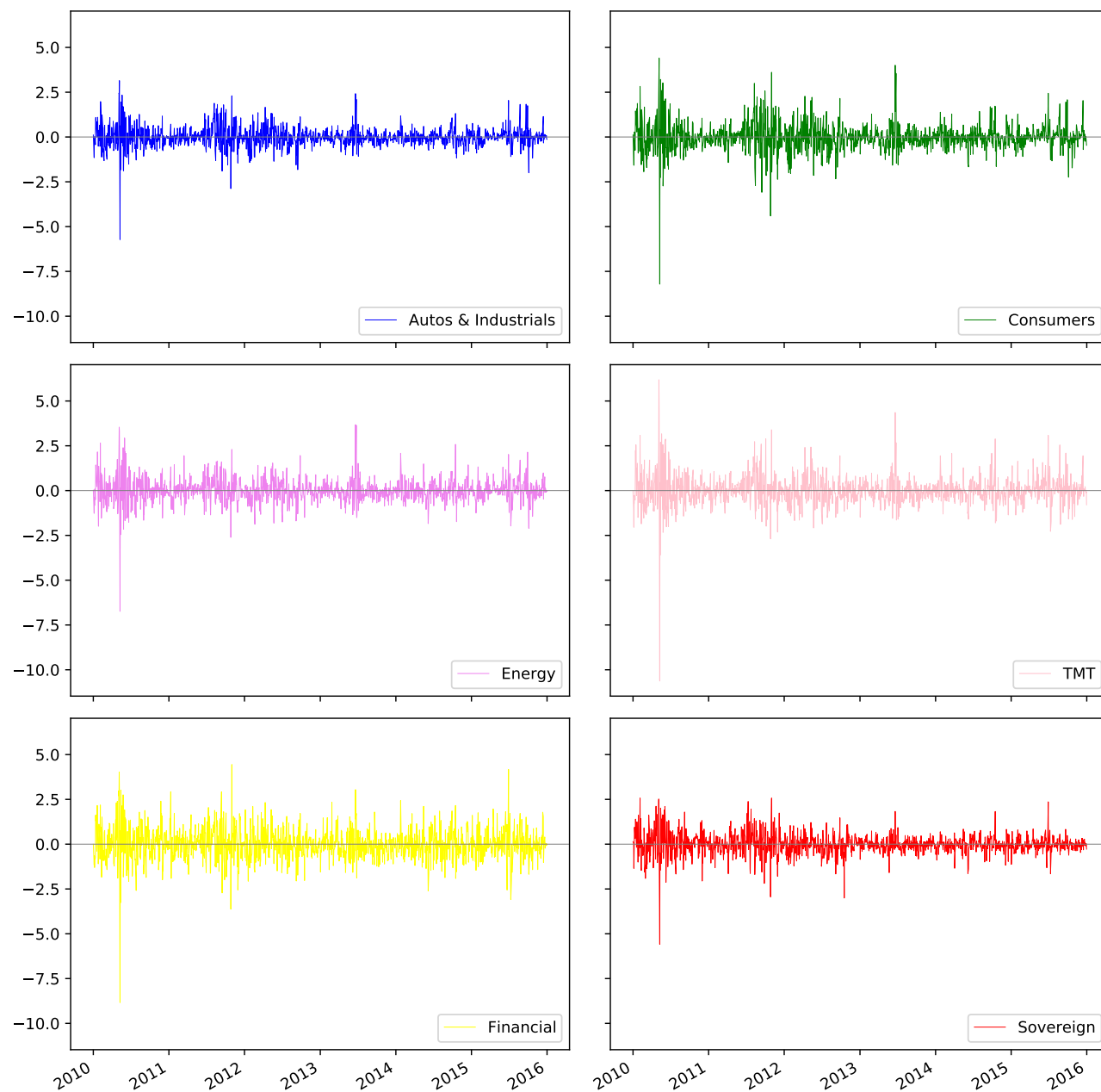


Figure 3.11: Evolution of the block-specific common factors over period 3 ranging from January 1, 2016 up to May 19, 2022. The block-specific common factors are estimated using the Dynamic Hierarchical Factor model by [Moench, Ng and Potter \(2013\)](#).

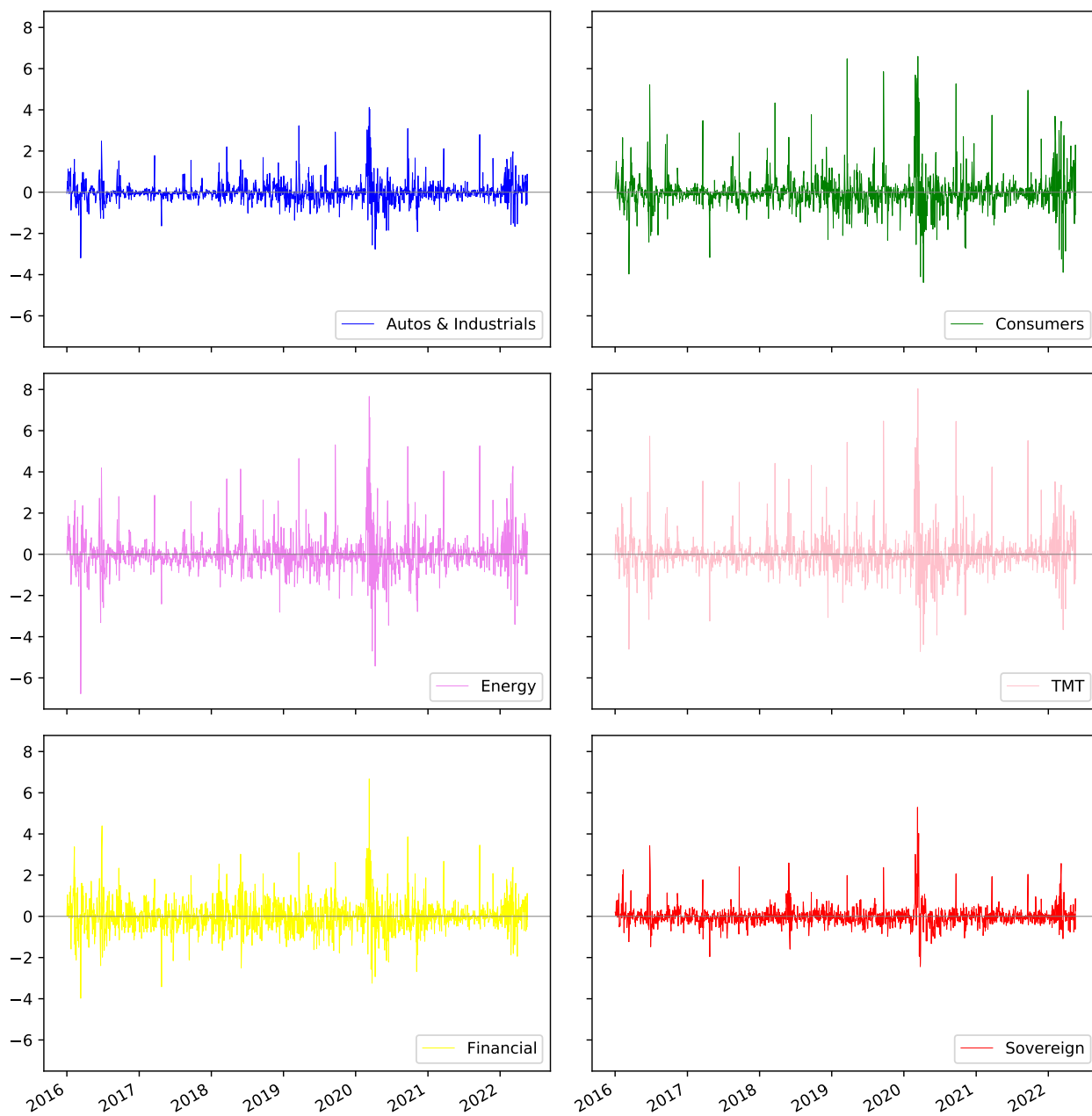
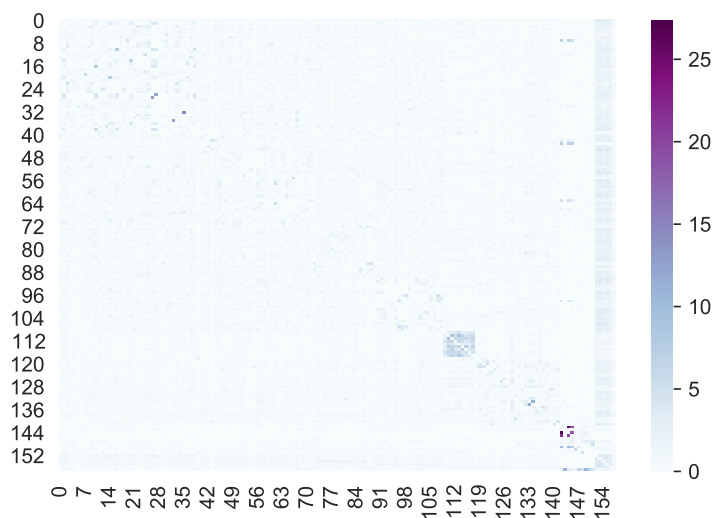
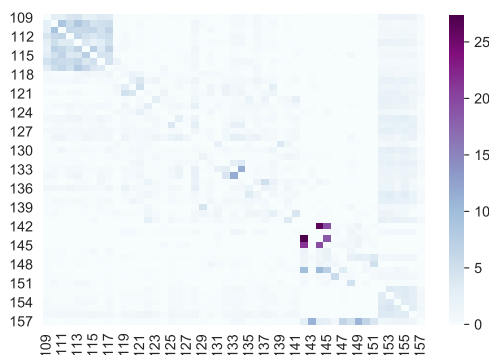


Figure 3.12: CDS heatmap for the sample period 1: 10/23/2006 - 12/31/2009

(a) The whole heatmap including all 152 idiosyncratic CDS and the 6 block-specific factors. Indices start from 0 up to 157 for the 158 CDS ordered as in Tables 3.1 and 3.2, respectively.



(b) Bottom right corner of whole heatmap zoomed in to the last 49 CDS: 33 financial entities, 10 sovereigns and 6 block-specific factors heatmap



(c) Bottom right corner of whole heatmap zoomed in to the last 16 CDS: 10 sovereigns and 6 block-specific factors heatmap

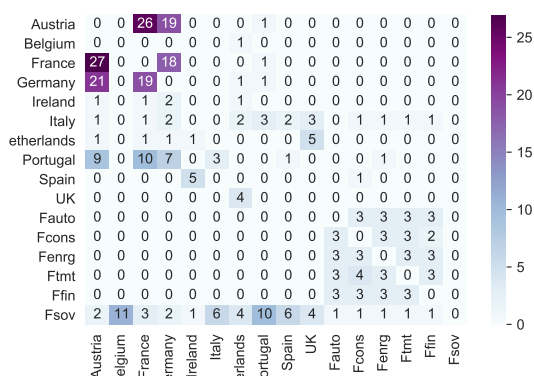
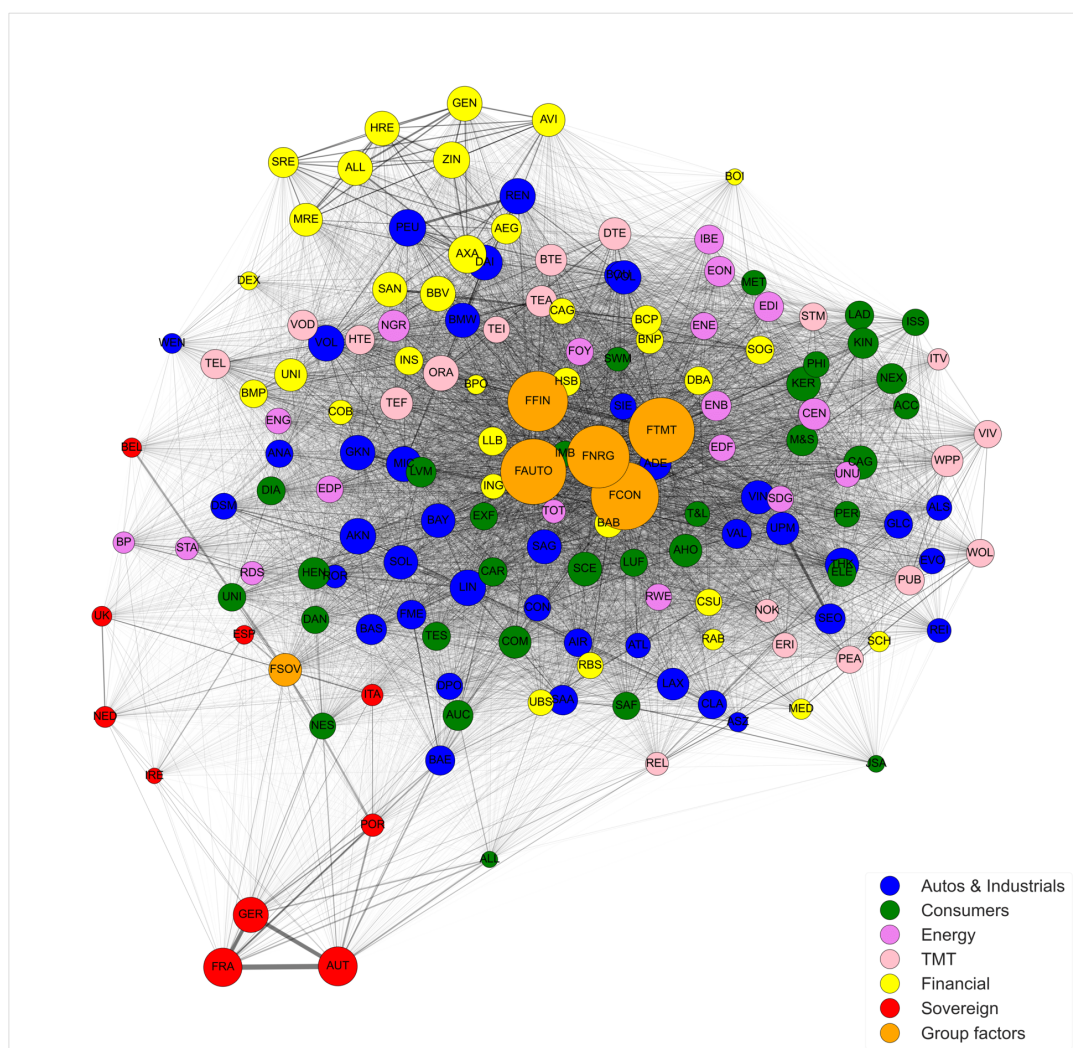
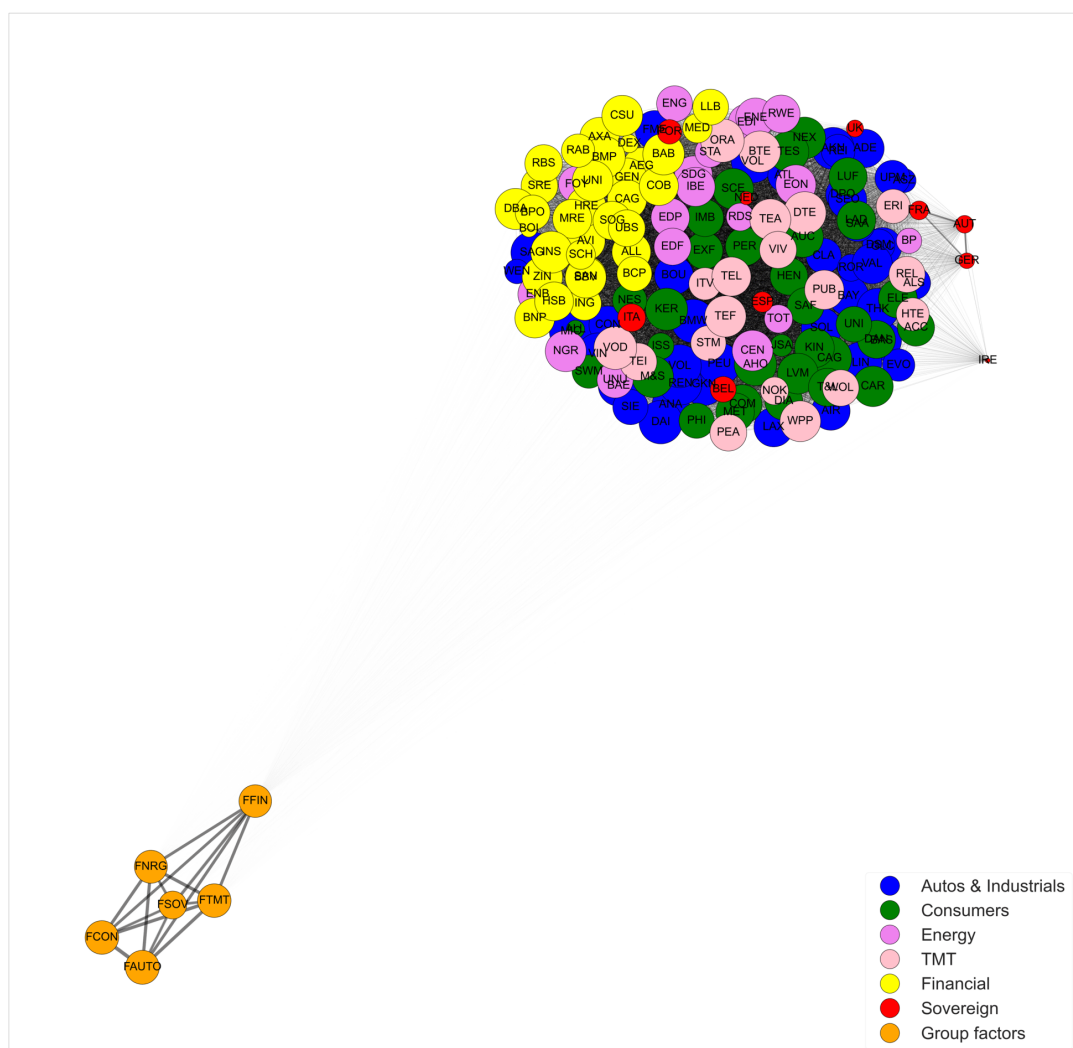


Figure 3.15: CDS network graph for the sample period 1: 10/23/2006 - 12/31/2009



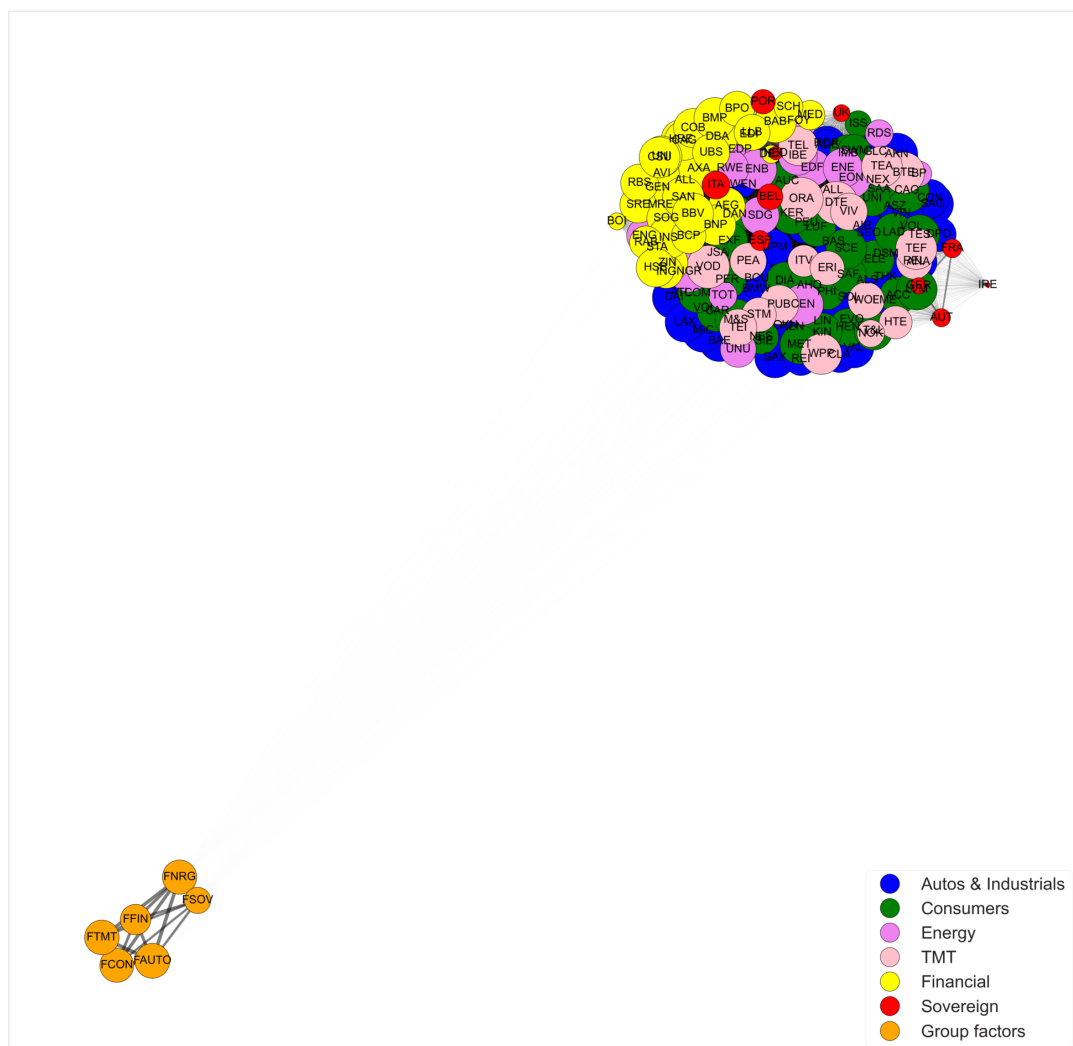
Note: The network's nodes are the CDS individual institutions colored by sub-sector and named according to the institutions' corresponding *Name Code* in Table 3.1. Their size represents the number and strength of outgoing connections they have, the bigger the size the more the risk they transmit to others. They are positioned based on the force-directed algorithm of [Fruchterman and Reingold \(1991\)](#), which places nodes close to each other according to how strongly they are connected. The connections are estimated using $h = 10$ -step forecast error variance decompositions. The number of common factors used is equal to one and comes from applying the [Hallin and Liška \(2007\)](#) IC_2 criterion.

Figure 3.16: CDS network graph for the sample period 2: 01.01.2010 - 12.31.2015



Note: The network's nodes are the CDS individual institutions colored by sub-sector and named according to the institutions' corresponding *Name Code* in Table 3.1. Their size represents the number and strength of outgoing connections they have, the bigger the size the more the risk they transmit to others. They are positioned based on the force-directed algorithm of [Fruchterman and Reingold \(1991\)](#), which places nodes close to each other according to how strongly they are connected. The connections are estimated using $h = 10$ -step forecast error variance decompositions. The number of common factors used is equal to one and comes from applying the [Hallin and Liška \(2007\)](#) IC_2 criterion.

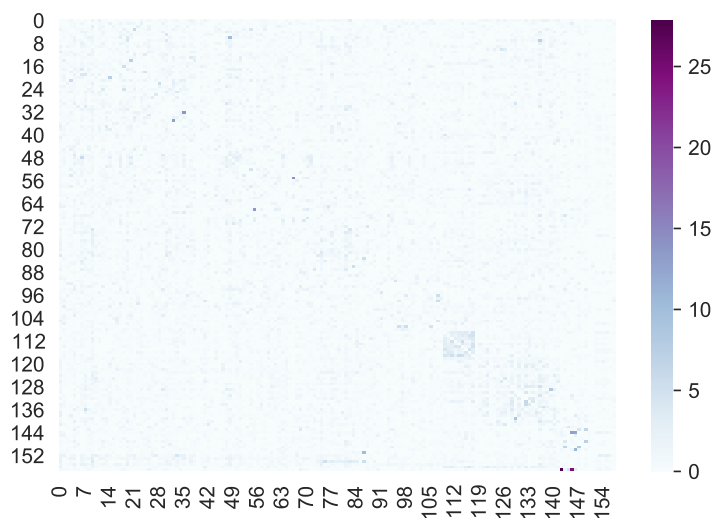
Figure 3.17: CDS network graph for the sample period 3: 01.01.2016 - 05.19.2022



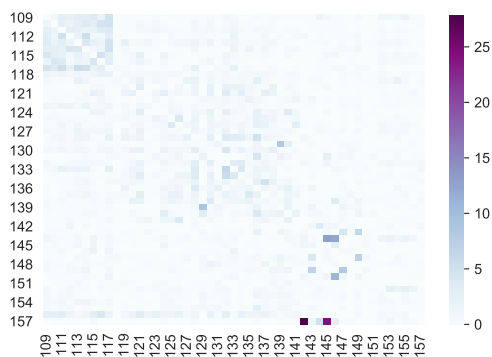
Note: The network's nodes are the CDS individual institutions colored by sub-sector and named according to the institutions' corresponding *Name Code* in Table 3.1. Their size represents the number and strength of outgoing connections they have, the bigger the size the more the risk they transmit to others. They are positioned based on the force-directed algorithm of [Fruchterman and Reingold \(1991\)](#), which places nodes close to each other according to how strongly they are connected. The connections are estimated using $h = 10$ -step forecast error variance decompositions. The number of common factors used is equal to one and comes from applying the [Hallin and Liška \(2007\)](#) IC_2 criterion.

Figure 3.18: CDS heatmap for the sample period I: 10/23/2006 - 08/08/2007

(a) The whole heatmap including all 152 idiosyncratic CDS and the 6 block-specific factors. Indices start from 0 up to 157 for the 158 CDS ordered as in Tables 3.1 and 3.2, respectively.



(b) Bottom right corner of whole heatmap zoomed in to the last 49 CDS: 33 financial entities, 10 sovereigns and 6 block-specific factors heatmap



(c) Bottom right corner of whole heatmap zoomed in to the last 16 CDS: 10 sovereigns and 6 block-specific factors heatmap

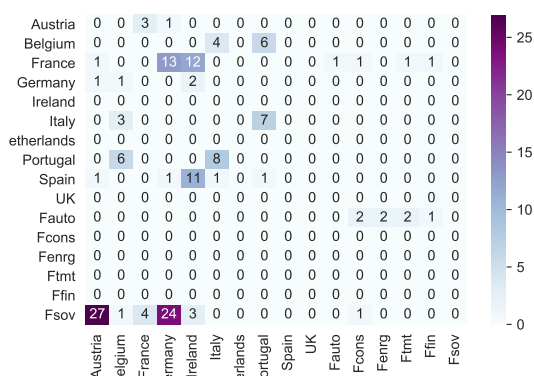
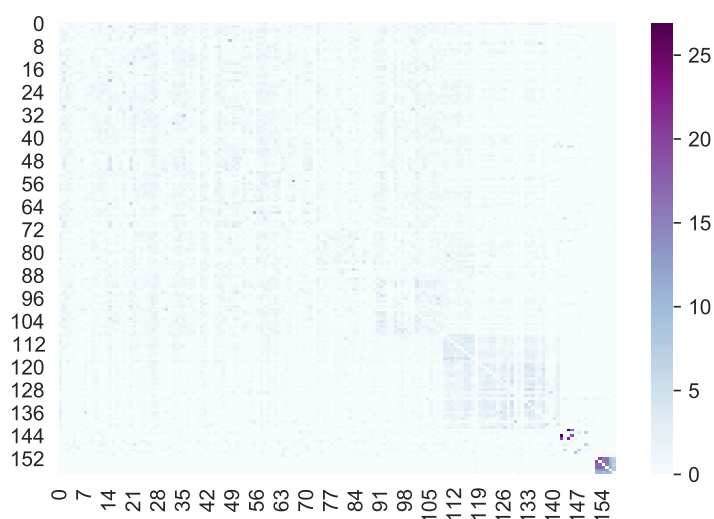
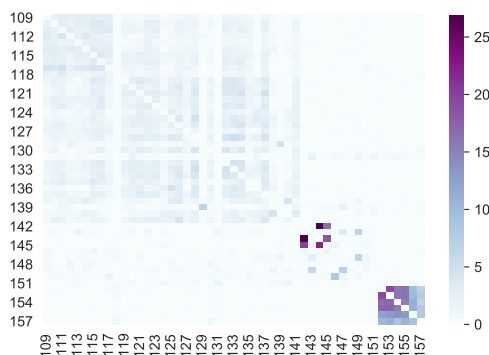


Figure 3.20: CDS heatmap for the sample period III: 09/15/2008 - 04/01/2009

(a) The whole heatmap including all 152 idiosyncratic CDS and the 6 block-specific factors. Indices start from 0 up to 157 for the 158 CDS ordered as in Tables 3.1 and 3.2, respectively.



(b) Bottom right corner of whole heatmap zoomed in to the last 49 CDS: 33 financial entities, 10 sovereigns and 6 block-specific factors heatmap



(c) Bottom right corner of whole heatmap zoomed in to the last 16 CDS: 10 sovereigns and 6 block-specific factors heatmap

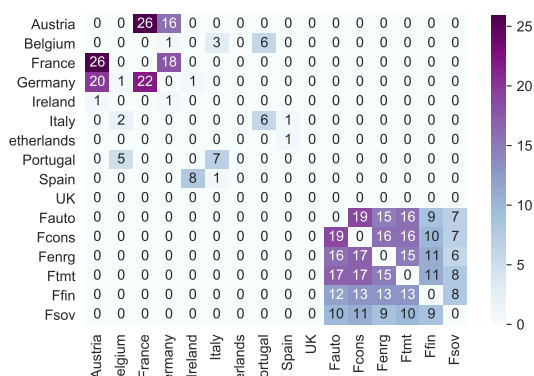
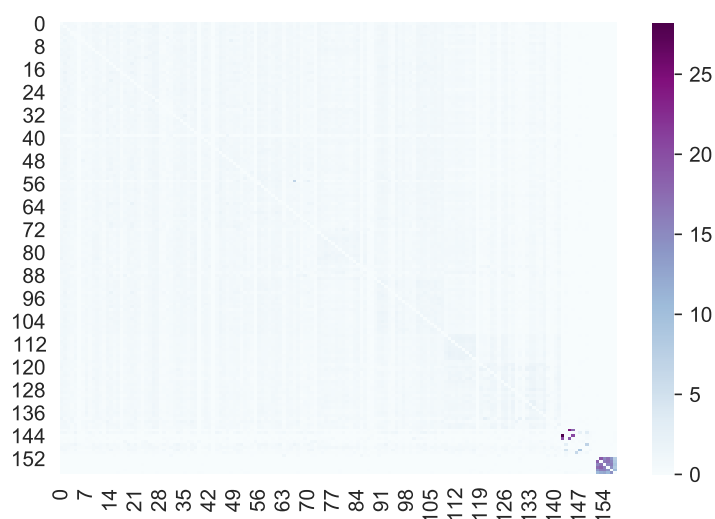
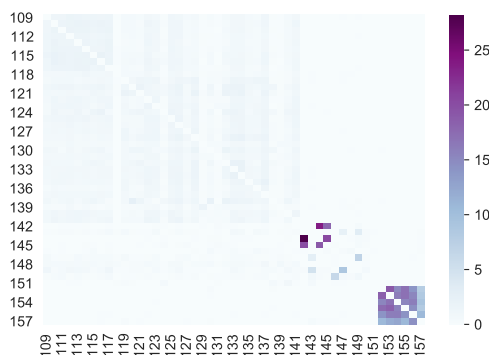


Figure 3.21: CDS heatmap for the sample period IV: 04/02/2009 - 05/08/2010

(a) The whole heatmap including all 152 idiosyncratic CDS and the 6 block-specific factors. Indices start from 0 up to 157 for the 158 CDS ordered as in Tables 3.1 and 3.2, respectively.



(b) Bottom right corner of whole heatmap zoomed in to the last 49 CDS: 33 financial entities, 10 sovereigns and 6 block-specific factors heatmap



(c) Bottom right corner of whole heatmap zoomed in to the last 16 CDS: 10 sovereigns and 6 block-specific factors heatmap

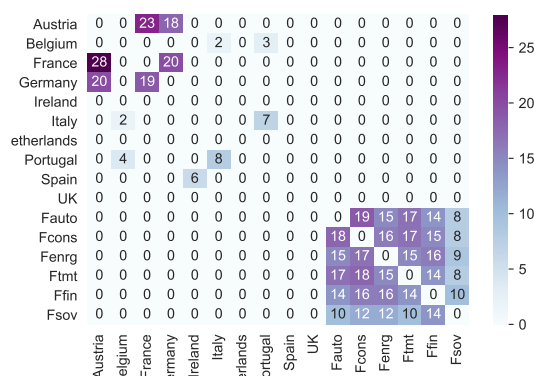
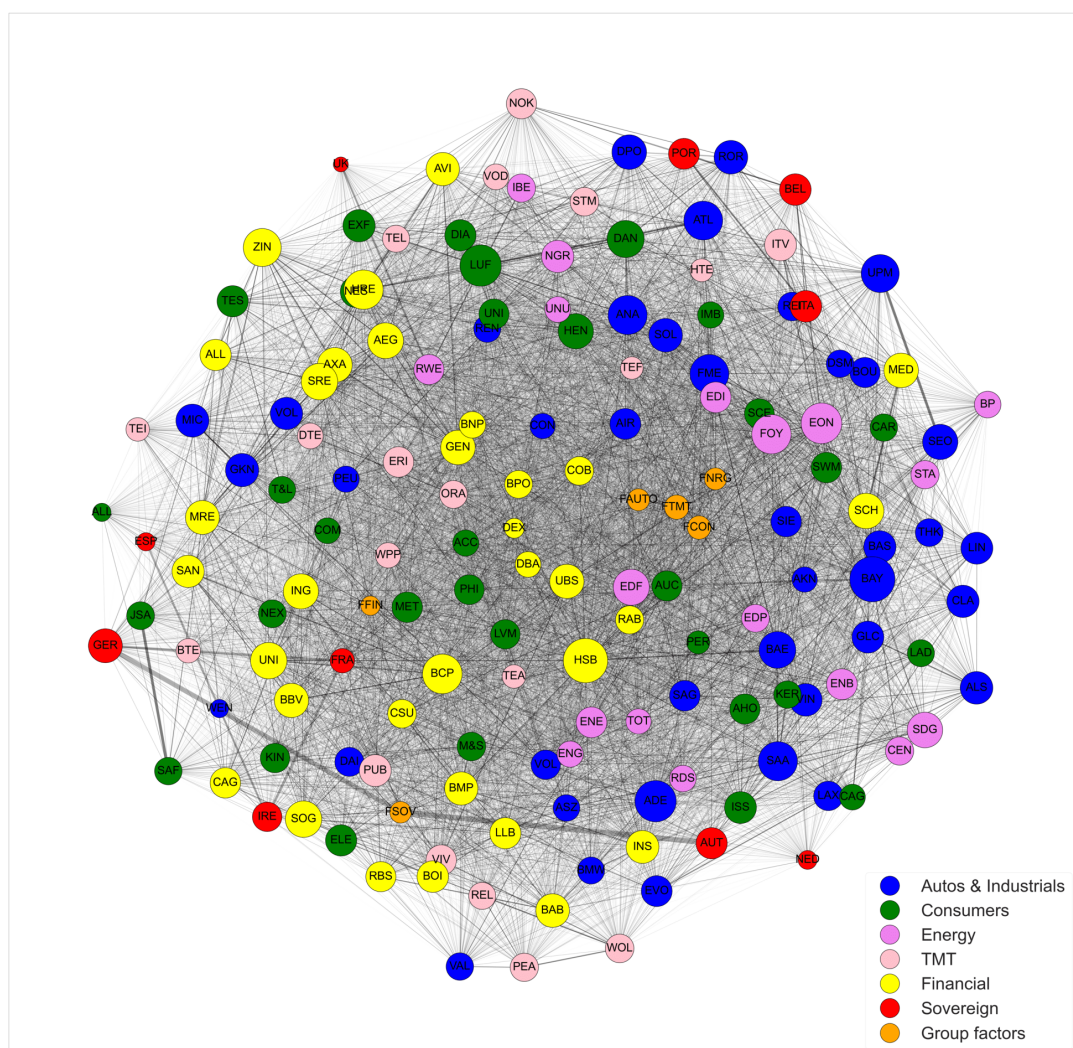
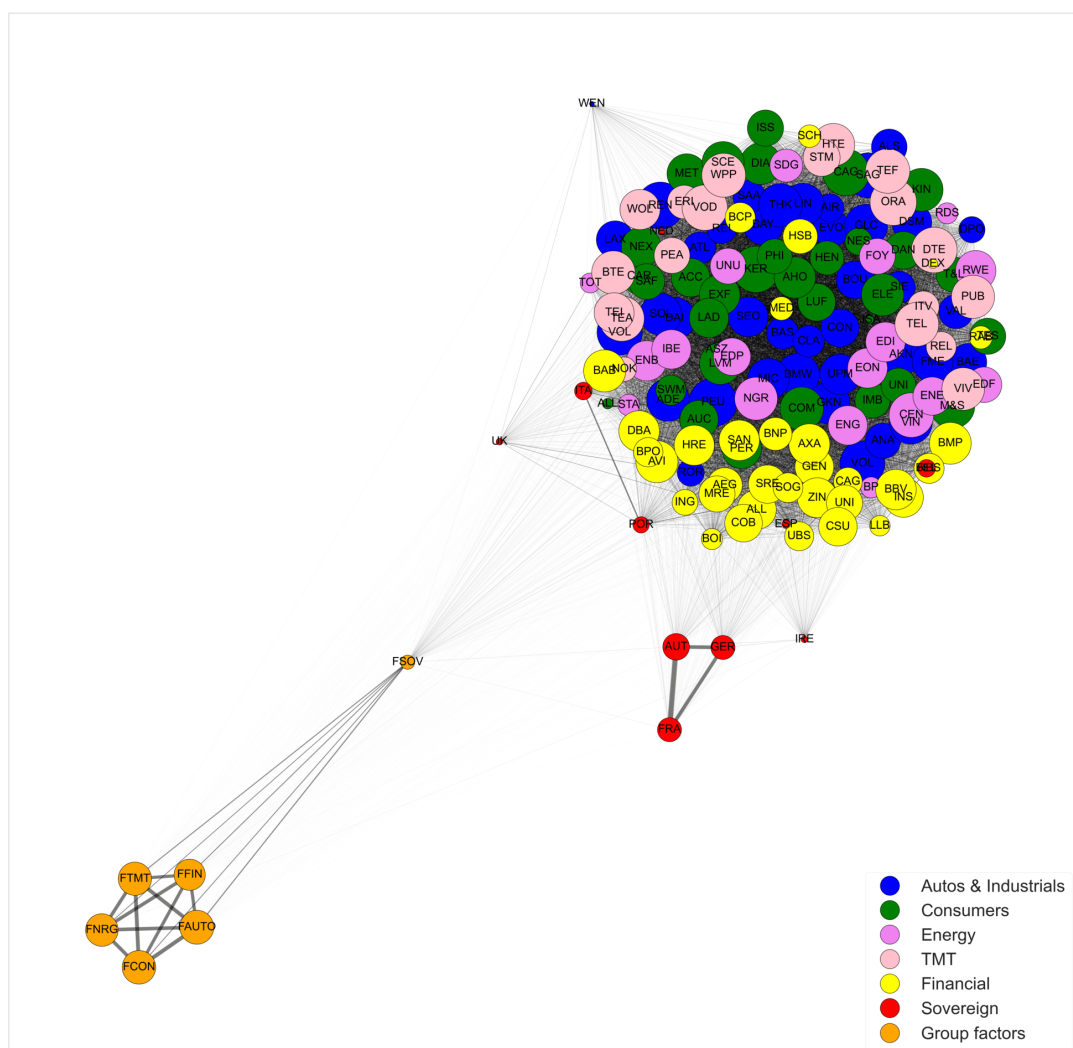


Figure 3.22: CDS network graph for the sample period I: 10/23/2006- 08/08/2007



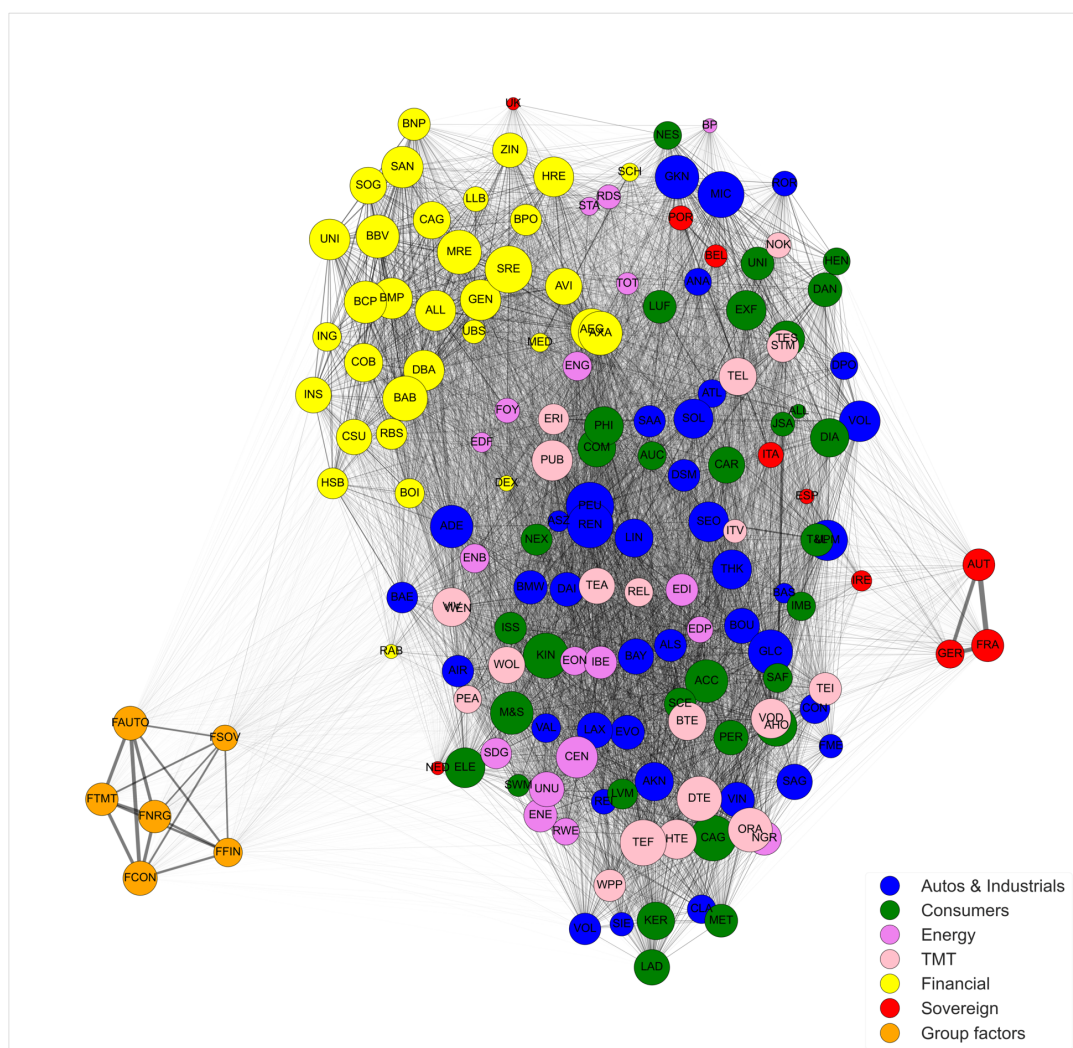
Note: The network's nodes are the CDS individual institutions colored by sub-sector and named according to the institutions' corresponding *Name Code* in Table 3.1. Their size represents the number and strength of outgoing connections they have, the bigger the size the more the risk they transmit to others. They are positioned based on the force-directed algorithm of [Fruchterman and Reingold \(1991\)](#), which places nodes close to each other according to how strongly they are connected. The connections are estimated using $h = 10$ -step forecast error variance decompositions. The number of common factors used is equal to one and comes from applying the [Hallin and Liška \(2007\)](#) IC_2 criterion.

Figure 3.23: CDS network graph for the sample period II: 08/09/2007 - 09/14/2008



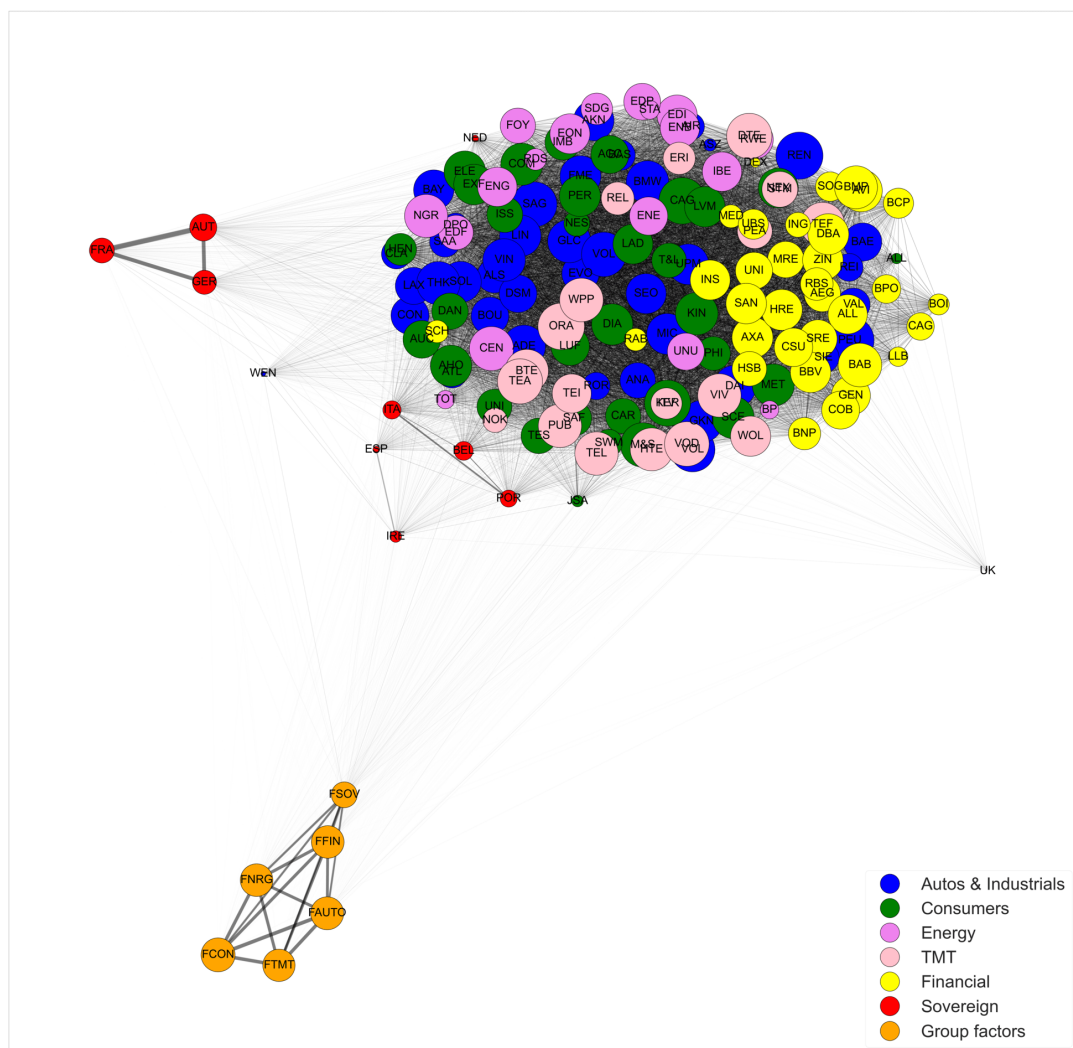
Note: The network's nodes are the CDS individual institutions colored by sub-sector and named according to the institutions' corresponding *Name Code* in Table 3.1. Their size represents the number and strength of outgoing connections they have, the bigger the size the more the risk they transmit to others. They are positioned based on the force-directed algorithm of [Fruchterman and Reingold \(1991\)](#), which places nodes close to each other according to how strongly they are connected. The connections are estimated using $h = 10$ -step forecast error variance decompositions. The number of common factors used is equal to one and comes from applying the [Hallin and Liška \(2007\)](#) IC_2 criterion.

Figure 3.24: CDS network graph for the sample period III: 09/15/2008 - 04/01/2009



Note: The network's nodes are the CDS individual institutions colored by sub-sector and named according to the institutions' corresponding *Name Code* in Table 3.1. Their size represents the number and strength of outgoing connections they have, the bigger the size the more the risk they transmit to others. They are positioned based on the force-directed algorithm of Fruchterman and Reingold (1991), which places nodes close to each other according to how strongly they are connected. The connections are estimated using $h = 10$ -step forecast error variance decompositions. The number of common factors used is equal to one and comes from applying the Hallin and Liška (2007) IC_2 criterion.

Figure 3.25: CDS network graph for the sample period IV: 04/02/2009 - 05/08/2010



Note: The network's nodes are the CDS individual institutions colored by sub-sector and named according to the institutions' corresponding *Name Code* in Table 3.1. Their size represents the number and strength of outgoing connections they have, the bigger the size the more the risk they transmit to others. They are positioned based on the force-directed algorithm of [Fruchterman and Reingold \(1991\)](#), which places nodes close to each other according to how strongly they are connected. The connections are estimated using $h = 10$ -step forecast error variance decompositions. The number of common factors used is equal to one and comes from applying the [Hallin and Liška \(2007\)](#) IC_2 criterion.

3.5 Conclusion

This paper studies risk connectedness among European economic entities during 2006-2022. The findings show that the inclusion in the full and sub-sample analysis of the block factors reveals the contagion effect and its implications during the onset of the global financial crisis of 2008. The methodology followed including the network graphical representations it allows for, could be of particular utility for future analysis on the status of an economy consisting of a large number of entities.

The full-sample 2006-2022 findings suggest that for the *non-financial* sector, around 12.5%, 6% and 15% of its 10-day forecast error variance (FEV) comes from an exogenous common shock to the financial sector, the sovereign sector, and any of the following non-financial sub-sectors (Automobile, Consumers, Energy, Telecommunications), respectively. For the *financial* sector around 9% and 5% of its 10-day forecast error variance (FEV) comes from an exogenous common shock to the non-financial sector, and the sovereigns sector, respectively. For the *sovereigns* sector around 7% and 8% of its 10-day forecast error variance (FEV) comes from an exogenous common shock to the non-financial sector, and the financial sector, respectively.

In addition, in the full-sample period, exogenous common shocks originating from the financial and the non-financial sector affect the respective 10-day FEV of the sovereign sector 1.6 and 1.16 more proportionally. Also, exogenous common shocks originating from the financial sector affect the 10-day FEV of the non-financial sector around 1.3 more proportionally. Both these findings uncover a higher directional connectedness and thus higher transmission of risk from the financial sector towards the non-financial and the sovereign

sectors in the full-sample period. This makes sense to the extent that the economic distortions in 2007-2008 started from the financial sector which was in trouble and then spread to the rest economic sectors.

From the sub-sample analysis' findings, a policy maker can identify an upcoming economic crisis studying the behavior of the idiosyncratic and the block factors. When the block factors are close topologically to the rest of the network the researcher could look into the reason of this appealing force. If this force is due to idiosyncratic entities transmitting risk to the block factors this signals the contagion effect's onset.

3.6 Appendix: Assumed zero correlations under the DHFM

From section 3.3.2 notice that the idiosyncratic component $E_t = \{E_{b\eta t}, \forall b, \eta\} = f(e_{F_{bt}}, e_{Y_{b\eta t}})$ $\forall b, \eta$ and from section 3.3.1 see equations (3.1) and (3.2). For $N_{F_b} = 1, \forall b$, we have that

$$Y_{b\eta t} = \lambda_{F_b}^\eta(L)F_{bt} + e_{Y_{b\eta t}},$$

$$F_{bt} = \lambda_{X_b}(L)X_t + e_{F_{bt}}.$$

This implies,

$$Y_{b\eta t} = \lambda_{F_b}^\eta(L) (\lambda_{X_b}(L)X_t + e_{F_{bt}}) + e_{Y_{b\eta t}}$$

$$Y_{b\eta t} = \lambda_{F_b}^\eta(L)\lambda_{X_b}(L)X_t + \underbrace{\lambda_{F_b}^\eta(L)e_{F_{bt}} + e_{Y_{b\eta t}}}_{E_{b\eta t}}.$$

Correlation between i and j variables of E_t

Any two variables i and j of E_t , $i \neq j$, that belong to (a) the same block can be correlated because of $e_{F_{bt}}$ or $e_{Y_{b\eta t}}$, or both, (b) different blocks can be correlated because of $e_{Y_{b\eta t}}$ even though $b \neq b'$. This is because in the VAR part of the methodology, the variables are modeled altogether, not in blocks. Observing higher within-block correlation does not necessarily mean that we assume zero *correlation between i and j of E_t* that belong to different blocks.

Correlation between variables of F_{bt} and E_t

Since F_{bt} and E_t both depend on $e_{F_{bt}}$, any shock that starts from economic entity i of E_t in block b will affect F_{bt} and any shock that starts from the block-specific common factors F_{bt} will affect block b of E_t . For the same block b , any correlation between E_t and F_{bt} comes via $e_{F_{bt}}$. Basically, $e_{F_{bt}}$ is the only source that makes E_t and F_{bt} able to affect each other (not orthogonal), for $b = 1, \dots, B$.

However, the correlation between variable i in block k of E_t and block-specific factor $F_{k't}$ (assuming each block has one block-specific factor), where blocks $k \neq k'$, is assumed to be zero by the construction of the estimated DHFM. For instance, let variable i of block 1 of $E_{i1t} = e_{F_{1t}} + e_{Y_{1it}}$ and the block-specific factor $F_{2t} = X_t + e_{F_{2t}}$. We have that E_{i1t} and F_{2t} are uncorrelated by construction in the DHFM. More specifically, block-specific factors (F_{1t}, F_{2t}) can be correlated only through X_t by the DHFM, thus it is assumed that $\text{Corr}(e_{F_{1t}}, e_{F_{2t}}) = 0$.

Correlation between block-specific factors F_{bt}

Block-specific factors F_{1t}, \dots, F_{Bt} are correlated with each other because of the global common factors X_t .

Zero correlations Table

Below, a Table that describes exactly the assumed zero correlations is provided. For simplicity, in the Table it is assumed that the number of blocks in the model is $B = 3$.

Table 3.6: Summarizing the assumed zero correlations of the DHFM model

	E_{1t}	E_{2t}	E_{3t}	F_{1t}	F_{2t}	F_{3t}
E_{1t}	x	x	x	x	0	0
E_{2t}	x	x	x	0	x	0
E_{3t}	x	x	x	0	0	x
F_{1t}	x	0	0	x	x	x
F_{2t}	0	x	0	x	x	x
F_{3t}	0	0	x	x	x	x

Note: Summarizing the assumed zero correlations when $B = 3$, where the zeros represent the assumed zero correlations and the x's the existence of correlation.

Bibliography

- Agarwal S, Mikhed V, Scholnick B. 2019. Peers' income and financial distress: Evidence from lottery winners and neighboring bankruptcies. *The Review of Financial Studies* **33**: 433–472.
- Alter A, Beyer A. 2014. The dynamics of spillover effects during the european sovereign debt turmoil. *Journal of Banking & Finance* **42**: 134–153.
- Badinger H, Egger P. 2011. Estimation of higher-order spatial autoregressive cross-section models with heteroscedastic disturbances. *Papers in Regional Science* **90**: 213–235.
- Barigozzi M, Hallin M. 2016. Generalized dynamic factor models and volatilities: recovering the market volatility shocks.
- Barigozzi M, Hallin M. 2017. A network analysis of the volatility of high dimensional financial series. *Journal of the Royal Statistical Society: Series C (Applied Statistics)* **66**: 581–605.
- Bertrand M, Morse A. 2016. Trickle-down consumption. *Review of Economics and Statistics* **98**: 863–879.
- Bhutta N, Keys BJ. 2016. Interest rates and equity extraction during the housing boom. *American Economic Review* **106**: 1742–74.
URL <https://www.aeaweb.org/articles?id=10.1257/aer.20140040>
- Claeys P, Vašíček B. 2014. Measuring bilateral spillover and testing contagion on sovereign bond markets in europe. *Journal of Banking & Finance* **46**: 151–165.
- Constancio V, et al. 2012. Contagion and the european debt crisis. *Financial Stability Review* **16**: 109–121.
- De Bandt O, Hartmann P. 2000. Systemic risk: a survey. *Available at SSRN 258430* .

- De Bandt O, Hartmann P, Peydro JL. 2009. Systemic risk in banking: An update. *Berger, A., MP, Wilson, J.(Eds.), Oxford Handbook of Banking. Oxford University Press, Oxford* .
- de Paula Á. 2017. *Econometrics of Network Models*, volume 1 of *Econometric Society Monographs*. Cambridge University Press, 268–323.
- Dell’Ariccia MG, Ferreira C, Jenkinson N, Laeven ML, Martin A, Minoiu MC, Popov A. 2018. Managing the sovereign-bank nexus. *ECB working paper* .
- Demirer M, Diebold FX, Liu L, Yilmaz K. 2018. Estimating global bank network connectedness. *Journal of Applied Econometrics* **33**: 1–15.
- Diebold FX, Yilmaz K. 2009. Measuring financial asset return and volatility spillovers, with application to global equity markets. *The Economic Journal* **119**: 158–171.
- Diebold FX, Yilmaz K. 2014. On the network topology of variance decompositions: Measuring the connectedness of financial firms. *Journal of econometrics* **182**: 119–134.
- Dornbusch R, Park YC, Claessens S. 2000. Contagion: understanding how it spreads. *The World Bank Research Observer* **15**: 177–197.
- Erdős P, Rényi A. 1959. On random graphs. *Publicationes Mathematicae (Debrecen)* **6**:: 290–297.
- Forbes KJ, Rigobon R. 2002. No contagion, only interdependence: measuring stock market comovements. *The journal of Finance* **57**: 2223–2261.
- Fruchterman TM, Reingold EM. 1991. Graph drawing by force-directed placement. *Software: Practice and experience* **21**: 1129–1164.
- Galariotis EC, Makrichoriti P, Spyrou S. 2016. Sovereign cds spread determinants and spillover effects during financial crisis: A panel var approach. *Journal of Financial Stability* **26**: 62–77.
- Gerschgorin S. 1931. Über die abgrenzung der eigenwerte einer matrix. *Izv. Akad. Nauk. USSR Otd. Fiz.-Mat. Nauk (in German)* : 6: 749–754.
- Giles DE. 1982a. General instrumental variables estimation under stochastic linear restrictions. *Economics Letters* **10**: 269–275.

- Giles DE. 1982b. Instrumental variables estimation with linear restrictions. *Sankhyā: The Indian Journal of Statistics, Series B* : 343–350.
- Goldstein H, Browne W. 2014. Multilevel factor analysis modelling using markov chain monte carlo estimation. In *Latent variable and latent structure models*. Psychology Press, 237–256.
- Gross C, Siklos PL. 2020. Analyzing credit risk transmission to the nonfinancial sector in europe: A network approach. *Journal of Applied Econometrics* **35**: 61–81.
- Gross M, Kok C. 2013. Measuring contagion potential among sovereigns and banks using a mixed-cross-section gvar. *ECB working paper* .
- Hallin M, Liška R. 2007. Determining the number of factors in the general dynamic factor model. *Journal of the American Statistical Association* **102**: 603–617.
- Henry C, Huynh KP, Welte A. 2018. 2017 methods-of-payment survey report. Staff Discussion Paper 2018-17, Bank of Canada.
URL <https://www.bankofcanada.ca/2018/12/staff-discussion-paper-2018-17/>
- Judge GG, Takayama T. 1966. Inequality restrictions in regression analysis. *Journal of the American Statistical Association* **61**: 166–181.
- Kelejian HH, Prucha IR. 1998. A generalized spatial two-stage least squares procedure for estimating a spatial autoregressive model with autoregressive disturbances. *The Journal of Real Estate Finance and Economics* **17**: 99–121.
- Kose MA, Otrok C, Whiteman CH. 2003. International business cycles: World, region, and country-specific factors. *american economic review* **93**: 1216–1239.
- Lee L. 2003. Best spatial two-stage least squares estimators for a spatial autoregressive model with autoregressive disturbances. *Econometric Reviews* **22**: 307–335.
- Liew CK. 1976. Inequality constrained least-squares estimation. *Journal of the American Statistical Association* **71**: 746–751.
- Liu X, Patacchini E, Zenou Y. 2014. Endogenous peer effects: local aggregate or local average? *Journal of Economic Behavior & Organization* **103**: 39–59.
- Lütkepohl H. 2005. *New introduction to multiple time series analysis*. Springer Science & Business Media.

- Manta A, Ho AT, Huynh KP, Jacho-Chávez DT. 2022. Estimating social effects in a multilayered linear-in-means model with network data. *Statistics & Probability Letters* **183**: 109331.
- Melkumova L, Shatskikh SY. 2017. Comparing ridge and lasso estimators for data analysis. *Procedia engineering* **201**: 746–755.
- Moench E, Ng S, Potter S. 2013. Dynamic hierarchical factor models. *Review of Economics and Statistics* **95**: 1811–1817.
- Nițoi M, Pochea MM. 2021. The nexus between bank connectedness and investors' sentiment. *Finance Research Letters* : 102432.
- Nyholm K. 2016. Us-euro area term structure spillovers, implications for central banks. *ECB working paper* .
- Pesaran HH, Shin Y. 1998. Generalized impulse response analysis in linear multivariate models. *Economics letters* **58**: 17–29.
- Wang GJ, Yi S, Xie C, Stanley HE. 2021. Multilayer information spillover networks: measuring interconnectedness of financial institutions. *Quantitative Finance* **21**: 1163–1185.
- Yang J, Tong M, Yu Z. 2021. Housing market spillovers through the lens of transaction volume: A new spillover index approach. *Journal of Empirical Finance* **64**: 351–378.
- Yuan M, Lin Y. 2006. Model selection and estimation in regression with grouped variables. *Journal of the Royal Statistical Society: Series B (Statistical Methodology)* **68**: 49–67.
- Zou H. 2006. The adaptive lasso and its oracle properties. *Journal of the American statistical association* **101**: 1418–1429.
- Zou H, Hastie T. 2005. Regularization and variable selection via the elastic net. *Journal of the royal statistical society: series B (statistical methodology)* **67**: 301–320.